Experimental Investigation and Numerical Modeling of Corrosion Induced Expansive Pressure on Concrete Cover in Reinforced Concrete

by

Sheikh Shakib

A thesis submitted to the Department of Civil Engineering, Khulna University of Engineering & Technology in partial fulfillment of the requirements for the degree of Master of Science in Civil Engineering
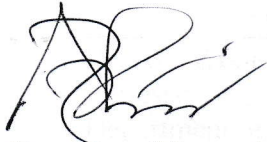
Khulna University of Engineering & Technology

Khulna 9203, Bangladesh

November 2018

Declaration

This is to certify that the thesis work entitled *"Experimental Investigation and Numerical Modeling of Corrosion Induced Expansive Pressure on Concrete Cover in Reinforced Concrete"* has been carried out by Sheikh Shakib in the Department of Civil Engineering, Khulna University of Engineering & Technology, Khulna, Bangladesh. The above thesis work or any part of this work has not been submitted anywhere for the award of any degree or diploma.

Signature of Supervisor

Signature of Candidate

Approval

This is to certify that the thesis work submitted by Sheikh Shakib entitled *Experimental Investigation and Numerical Modeling of Corrosion Induced Expansive Pressure on Concrete Cover in Reinforced Concrete* has been approved by the board of examiners for the partial fulfillment of the requirements for the degree of Master of Science in Civil Engineering in the Department of Civil Engineering, Khulna University of Engineering & Technology, Khulna, Bangladesh in 2018.
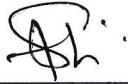
BOARD OF EXAMINERS

08. 11. 2018

Chairman
(Supervisor)

Dr. Abu Zakir Morshed
Professor
Department of Civil Engineering
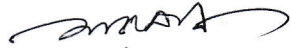Khulna University of Engineering & Technology

Member

Head of the Department
Department of Civil Engineering
Khulna University of Engineering & Technology

Member

Dr. Muhammad Harunur Rashid
Professor
Department of Civil Engineering
Khulna University of Engineering & Technology

Member

Dr. Md. Mahfuzur Rahman
Assistant Professor
Department of Civil Engineering
Khulna University of Engineering & Technology

Member
(External)

Dr. Raquib Ahsan
Professor
Department of Civil Engineering
Bangladesh University of Engineering & Technology

Acknowledgement

I would like to express my gratitude to my supervisor Prof. Dr. Abu Zakir Morshed as without his continuous support, expertise and motivation, this thesis would not become in reality. While performing this research, his guidance and support, while still allowing me the freedom to learn first-hand, proved to be technical in the advancement of my work. His high standards and commitment to research set a strong example for me in my time in the work, and provides me with the motivation necessary to perform the required tasks. He has passionately inspired me throughout this research. I am really thankful for his great mentorship, time, and support throughout the thesis work over the last two and half a year. I would also like to thank my committee members, Prof. Dr. Muhammad Harunur Rashid and Dr. Md. Mahfuzur Rahman for their crucial suggestion on my research projects, and my external examiner Prof. Dr. Raquib Ahsan for his time to read and critique my thesis.

I would also like to thank my respective teachers, and colleagues in the Department of Civil Engineering, Khulna University of Engineering & Technology for their valuable supports.

Finally, I would like to express my deepest love, respect and appreciation to my parents, wife and brother, for their consistent and unconditional love and support. I am very much indebted to my parents and wife for their motivation which has sustained me throughout the long journey of my academic life.

Abstract

Corrosion of reinforcement is an important durability concern for the structures exposed to adverse weather conditions especially in coastal regions. The volume of corrosion products are much higher than the original volume of the corroding reinforcement, which exerts an expansive pressure on the surrounding concrete and results in cracking of the concrete cover. In this research an investigation was carried out through numerical modeling and experimentation to explore the mechanism of concrete cover cracking due to that expansive pressure. It was aimed that structural health monitoring in terms of level of corrosion might be possible through monitoring the crack width and crack propagation in the cover concrete. In addition a convenient means of corrosion protection was investigated by using zinc as sacrificial anode. A numerical model was developed using a commercial finite element modeling software ABAQUS 6.14 to evaluate the cracking pressure, crack initiation, crack propagation and radial deformation for different cover thicknesses and bar locations. The model was also used to determine the effect of bar diameter on cracking pressure and the patterns of crack for different number of bars. Numerical results were validated by experimental investigation.

The cracking pressure was simulated experimentally by applying hydraulic pressure through a hole in the specimens having similar diameter as of the reinforcement. 150 mm cube specimens for three different grades of concrete with various clear cover and location of bar were used for the simulation. Impressed current technique was used to accelerate the corrosion of reinforcement. Characterization of impressed current technique involved determination of optimum chloride content and minimum immersion time of specimens for which the application of Faraday's law could be efficient. To obtain optimum chloride content, the electrolytes in the corrosion cell were prepared similar to that of concrete pore solutions. Concrete cubes of 50 mm were used to determine the optimum immersion time for saturation. It was found that the optimum chloride content was 3.5% by mass of water and the minimum immersion time for saturation was 24 hours. Concrete prisms of 250 mm x 250 mm x 300 mm with 12 mm-Ø grade 60 plain mild steel bars were used to simulate RCC beams with various cover thicknesses of 20 mm, 37.5 mm, 50 mm and 75 mm, respectively, to observe the mechanism of crack initiation, propagation and level of corrosion with respect to the width of surface crack. Level of corrosion was measured in

mg/cm^2 following Faraday's law and by gravimetric loss method, and width of crack was measured by image analysis.

From numerical modeling it was found that, with the increase of cover thickness the pressure as well as the radial expansion needed to initiate crack was increased. The same pattern was found for both corner bar and side bar. A lower cracking pressure was required for corner bar with respect to side bar. On the other hand, with the increase in bar diameter, a decrease in cracking pressure was observed. It was also found that the crack was initiated from outer surface and propagated towards the steel concrete interface for a cover thickness of 20 mm as well as 37.5 mm. This result was accomplished due to heaving of cover concrete and crack initiated when bending stress exceeded the tensile strength of concrete. Whereas for a cover thickness of 50 mm as well as 75 mm, crack was initiated at the steel-concrete interface and propagated towards the cover surface. These observations were further confirmed through experimental investigation. From the experimental simulation of cracking pressure, it was found that the cracking pressure varied linearly with the increase in concrete cover-to-diameter ratio (c/d). The pressure requirement to initiate crack was also higher with higher grades of concrete. For corner bars with cover thickness 37.5 mm, the critical pressure was 6-10 MPa and it increased up to 17 MPa for cover thickness of 64 mm for different grades of concrete. On the other hand, for other bar location with cover thickness of 37.5 mm and 64 mm, the pressure required to initiate crack was about 7.6 MPa and 14.8 MPa, respectively, for C20 grade concrete. A linear relationship was found between crack width and level of corrosion. For cover thicknesses of 20 mm and 37.5 mm, the critical corrosion amount (CCA) needed to initiate crack was about 22 mg/cm^2. However, a sudden increase in CCA was noticed when the cover thickness was over 44 mm. For cover thicknesses of 50 mm and 75 mm the CCA values were 129 and 211 mg/cm^2, respectively. Cathodic protection of reinforcement corrosion was investigated by using zinc as sacrificial anode in the accelerated corrosion cell with two environments- (i) synthesized solutions similar to concrete pore solution and, (ii) concrete. It was found that up to 65% of the corrosion current could be diverted through the sacrificial anode.

It is concluded that level of corrosion could be predicted by monitoring the surface crack width with reasonable accuracy, a minimum of 50 mm concrete cover should be provided in the corrosion prone environment and zinc as sacrificial anode could reduce as much as two-thirds of corrosion hazard to prolong the service life of reinforced concrete structures.

Contents

List of Tables

List of Figures

CHAPTER 1
INTRODUCTION

1.1 Introduction

Bangladesh is a deltaic country with total area of 147,570 square km. The coastal region covers almost 29,000 square km i.e., about 20% of the country. The deterioration caused by corrosion of reinforcing steel ("rebars") in concrete structures has been recognized as one of the greatest maintenance challenges in Bangladesh, especially, in coastal regions. Concrete has its own self-defense mechanism to resist corrosion by formation of a layer of passivation, a surface film of iron oxide, owing to its highly alkaline pore solution. However, this passive layer is disrupted due to either chlorination or carbonation (Bazant, 1979). If the chloride ions present beyond a threshold value, the passive layer is destroyed and steel spontaneously corrodes. On the other hand, corrosion may also occur due to the reaction of carbon dioxide (CO_2) with cement in concrete, which is termed as carbonation (Nossoni & Harichandran, 2012). In coastal regions, the marine structures are mostly affected by the high concentration of chlorides from the saline water. Some of the major factors that affect the rate of corrosion are chloride concentration, temperature, relative humidity, cover thickness, concrete quality and etc. As the reinforcement corrodes, the transformation of metallic iron to oxides can result in an increase in volume of up to 600%, depending on the final oxide form (Liu & Weyers, 1998). This expansion causes cracking and spalling of concrete thus adversely affects the serviceability of reinforced concrete structures by reducing the strength and durability of concrete.

Operation and maintenance of a structure is a challenging issue especially for marine structures like bridge, culvert, buildings in coastal region etc. Now-a-days structural Health Monitoring (SHM) has become an effective system to monitor the health of structures and assess the risk of failure (He et al., 2016; Kulkarni & Achenbach, 2008). For most environmental hazards, crack propagation due to corrosion of reinforcement is one of the major failure mechanisms and the damage due to corrosion is dependent on the amount of mass loss of steel. In reality, direct measurement of mass loss of corroding steel, which is embedded in concrete, is very difficult to measure. Thus indirect measurement for corrosion prediction is a more practicable approach for SHM. Width of crack at the surface of concrete could be one of such important parameter

to predict the amount of corrosion. This prediction may help a lot to assess the risk of failure due to corrosion.

Besides corrosion prediction through crack width monitoring a protection system is also needed to prolong the life of marine structures or a prevention system is needed where the structures are already affected before it becomes a significant problem. Cathodic protection is a widely used method to inhibit the corrosion process nowadays. There are two approaches to cathodic protection have been investigated in the past (Vrable & B., 1977)- Sacrificial anodes and Impressed current system. In sacrificial anode methods of cathodic protection, a metal having more electromotive force than steel in electrochemical series is employed.

1.2 Objectives of the Research Work

The overall objectives of this research are as follows:

i) Characterization of accelerated corrosion test to find out the optimum chloride content and time of immersion before starting test for full efficiency of current;

ii) Experimental investigation of the growth of corrosion products and the mechanism of crack initiation due to corrosion induced pressure and to establish a correlation between the crack width and level of corrosion;

iii) Experimental simulation of the critical pressure for cover cracking for various concrete cover thicknesses;

iv) Development of a numerical model to simulate cracking pressure and crack propagation and to compare those with the experimental results;

v) Development of a sacrificial anode system for corrosion protection using zinc and to investigate its effectiveness.

1.3 Scope of the Research

In this research an investigation was carried out through numerical modeling and experimentation to explore the mechanism of concrete cover cracking due to the expansive pressure induced by corrosion of reinforcement. It was also investigated to monitor the level of corrosion aimed that structural health monitoring in terms of might be possible through monitoring the crack width and crack propagation in the cover concrete. In addition a convenient means of corrosion protection was investigated by using zinc as sacrificial anode.

Many investigations have contributed to a better understanding of the corrosion process, however, the study on corrosion induced expansive pressure and associated cover cracking is

still very limited (Allan & Cherry, 1992; Maaddawy & Soudki, 2003; Williamson & Clark, 2000a). Researchers' use different methodologies to test corrosion induced cracking (Ahmed et al., 2007) and loss of steel (Alonso et al., 1998a; Nossoni & Harichandran, 2012). Impressed current system is a commonly used methodology to accelerate the corrosion. In impressed current system Faradays law is used to calculate the mass loss of steel. The accuracy of using Faradays law to predict the mass loss in concrete environment is dependent on the amount of chloride ions present in electrolyte and amount of current supplied. So an investigation is needed to characterize the accelerated corrosion technique for further use. In this research an investigation was done to depict the efficiency of the use of Faradays law to predict the mass loss of reinforcement in accelerated corrosion technique.

Few investigation is done to predict the crack width in relation with the corrosion penetration (Alonso et al., 1998a; Andrade et al., 1993; Vu et al., 2005) as well as with the mass loss (Tran et al., 2011) similar to the present study but attention was not paid to those paper to relating the crack initiation mechanism having a variable cover thickness. Relation between the amount of corrosion and the width of cover cracking with the variation of clear cover is still challenging in a sense that there are no consistency of the results showed in those paper. This research would give an explanation of the mechanism of initiation of cracks for different clear cover which create a new thinking in the fracture mechanics and establish a definite relation between the crack width and mass loss. This outcome would help a lot to the companies which are working for SHM consequences expanding the life of structures, reduction in cost of repairing and cost of time.

There are lacking of guidelines in design of durable reinforced concrete structures exposed to marine environment. The structure will be more durable when the cover concrete sustains more expansive pressure induced by expansion due to the corrosion products. So there is a need for investigation of accumulation of corrosion products around the reinforcement, corrosion induced expansive pressure as well as expansion behavior for different concrete quality, cover thickness as well as bar diameter. Nevertheless experimental studies are time consuming. Numerical modeling is a key tool to avoid the time consumption. Regarding this, a numerical model is developed which would be validated by experimental study. This numerical model would predict the accumulation capacity and the pressure for which the concrete cover cracks, different critical pressure for different cover thickness and various bar diameter. This may finally lead to a proper selection of clear cover as well as rebar diameter.

In addition, several research works are found on cathodic protection in reinforced concrete structures (Das et al., 2015), however only a few of them paid attention on the effectiveness of using sacrificial anode in terms of mass loss. In this research, an investigation would be executed to evaluate the efficiency of zinc as sacrificial anode so that it could be incorporated for corrosion protection even in the projects of small budget.

1.4 Organization of the Thesis

The overall work of this study is presented into seven chapters because of the multidisciplinary nature of the work. The relevant background is incorporated in each section to provide a better understanding of the work.

Chapter 1 presents an introduction of this research work along with the objectives, significance and organization of the research.

Chapter 2 incorporates a detailed literature review on experimental and finite element studies relevant to the corrosion of reinforcing steel in concrete. This chapter also includes the literature on cathodic protection system. The literature review mainly focuses on the areas related to the research objectives; the electrochemical concepts of steel in both alkaline and concrete media, the rate of corrosion and factors affecting the rate of corrosion, and concrete cracking model.

Chapter 3 summaries the experimental characterization of accelerated corrosion technique and application of the Faraday's law to evaluate the amount of mass loss due to corrosion.

Chapter 4 focuses on detailed description of the experiments, conducted to measure the mechanism of crack initiation, width of surface crack, and the level of corrosion, Thickness of corrosion products as a function of time and current density up to the time of cracking of the concrete.

Chapter 5 describes the development of a finite element model considering the uniform corrosion of reinforcement and also an experimental procedure to simulate the pressure causing the cover cracking. The critical pressure obtained through the finite element model was validated with the experimental ones.

Chapter 6 comprises the experimental study to evaluate the effectiveness of zinc metal for using as sacrificial anode cathodic protection system.

Chapter 7 includes the conclusions and limitations of the study along with the recommendations for the further studies.

CHAPTER 2
LITERATURE REVIEW

2.1 Introduction

Over the last several decades, studies on the corrosion of reinforcing steel in reinforced concrete structures have been widely reported in the literature. Corrosion is one of the major durability problems in concrete structures, mainly when the rebar is exposed to chlorides from the surrounding corrosive environment. Carbonation of the concrete due to the penetration of acidic gasses into the concrete is the other major cause of reinforcement corrosion. Beside these, there are other factors that affect rebar corrosion, some related to the concrete quality (such as water cement ratio, cement content, impurities in concrete ingredients, presence of surface cracks), and others related to the external environment (such as moisture, oxygen, temperature, and bacterial attack). The effect and assessment of these factors are carried out by different experimental program, and electrochemical models. In this chapter comprehensive literature review is presented on many aspects of corrosion of steel rebars in concrete and some existing durability models for predicting the time for cracking of the concrete cover.

2.2 Corrosion Mechanism

Corrosion is a natural process, which converts refined metal to their more stable oxide. It is the gradual destruction of materials by chemical reaction with their environment. Most of the common metals and their alloys are attached by ordinary environments such as atmospheric water or aqueous solution to form compound of metals. The chemical attack of all environments upon any metal results in the oxidation of metal and form corrosion products. The usual corrosion products are oxide, hydroxide, carbonate, sulfide etc. In the most cases the corrosion products are insoluble in the environment and form a separate phase on or adjacent to the metal.

2.2.1 Corrosion Reaction

Although iron can corrode by chemical attack, the most common form of corrosion in an aqueous medium is electrochemical. The corrosion process is similar to the action which takes place in a flashlight battery. In the anode, an electrochemical oxidation takes place and in the cathode an electrochemical reduction occurs in the presence of electrolytes. Any metal surface on which corrosion is taking place, a composite of anodes and cathodes forms by electrically

connected through the body of metals itself. Reaction of anodes and cathodes are broadly referred to as "half-cell reaction". Five essential components are involved in a basic corrosion cell (Nossoni, 2010)

Anode: The anode usually corrodes by losing electrons and dissolution of the metal. The anodic reaction depends on the pH of the pore solution of the concrete, presence of aggressive ions, and the potential at the surface (Nossoni, 2010). The general anodic reaction for steel corrosion is:

$$Fe = Fe^{2+} + 2e^- \; ; E_0 = -0.440V \text{ (Standard Redox Potential)}...............(2.1)$$

The standard redox potential is the potential generated when the metal is connected to a hydrogen electrode and is one method of expressing electromotive forces.

Cathode: The cathodic reaction must consume the electrons produced at the anode and the exact reaction depends on the availability of oxygen and the pH of the solution. The following reduction process occurs in concrete:

$$H_2O + 1/2 \; O_2 + 2e^- = 2OH^- \; ; E_0 = 0.401V \text{ (Standard Redox Potential)} ....(2.2)$$

Electrolyte: The solution that conducts electricity.

Metallic path: Metallic connection between the anode and cathode which allows the current to flow.

Current: Electrons those are produced due to the anodic reaction, flow through the rebar from the anode to the cathode, and the rate of flow is conventionally measured as current. The current is related to the rate of the anodic and cathodic reactions. The current will reach its limit when one of the reactions reaches its maximum rate due to the limitation in availability of a required species. The corroding iron piece has an open circuit potential, related to Standard Redox Potentials of the above reactions to the composition, the temperature, and to the "polarizations" of these half cells.

For corrosion of steel in concrete, the steel acts both as the anode and the cathode and the pore solution acts as the electrolyte.
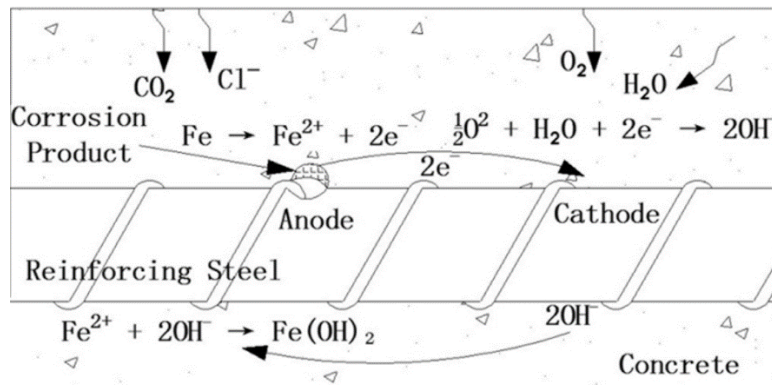
Figure 2.1: Corrosion process on steel bar surface (Zhao et al., 2011)

The actual mass loss due to corrosion is due to the reaction that takes place at the anode. The iron atoms ionize to Fe^{2+} ions according to Equation 2.1 and are dissolved in the pore solution around the steel bar. The electrons are deposited on the rebar surface and raise its electrochemical potential. The electrons then flow through and along the steel to a lower potential region (cathode) as shown in Figure 2.1. The free electrons are consumed in the cathodic reaction as shown in Equation 2.2. The electrochemical character of the corrosion process is demonstrated by the flow of current in the closed loop as shown in Figure 2.1. The rate of electron flow within the steel bar results from the difference in potential and determines the rate of corrosion.

2.2.2 Pourbaix Diagram

Pourbaix, (1976) produced a diagram based on thermodynamic data for Iron-Water system, which shows the equilibrium between potential (against standard hydrogen electrode, SHE) and pH of the system. The pourbaix diagram is shown in figure 2.2.
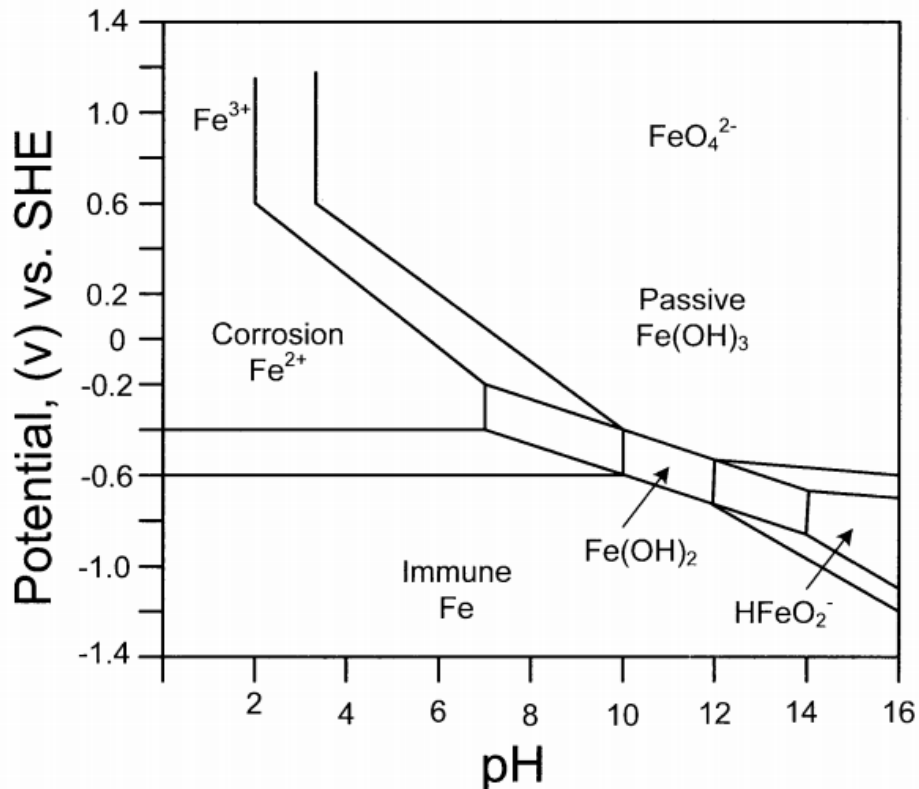
Figure 2.2: Pourbaix diagram for iron at 25^0c (Nossoni, 2010))

There are three regions in the diagram, the first one is "immunity" region which describes the region of stability of the base metal (Fe) and in this region no corrosion will occur. Second one is passive region, where one could expect to see a stable coating of an oxide (Fe_3O_4) or other salt on the surface of steel, a non-protective form of corroded steel. And the third one is corrosion region where general corrosion occurs. Steel's nature is tending to undergo corrosion reactions but the alkaline environment of concrete (pH of >12) provides both physical and chemical protection to reinforcing steels by its cover and high pH environment. At the high pH, a thin oxide layer in the range of 10-100 nm (Ouglova et al., 2006) known as passive film, forms on the steel and prevents steel from dissolving. This passive film does not stop corrosion, it reduces the corrosion rate even 1000 times from that of in passive state (Zhang & Poursaee, 2014)). This film breakdown when the pH value goes below 10. In the range of pH about 9.5-13 in corrosion region, the most stable iron oxide, $Fe(OH)_2$ (known as 'blue rust' or 'green rust', a rarely encountered and highly soluble form of corroded iron) is formed. Insoluble products are formed in acidic and highly alkaline conditions.

2.3 Corrosion of Steel in Concrete

Concrete is a composite material, consisting of cement, fine aggregate and coarse aggregate. Concrete is weak in tension so to resist the tension, steel reinforcement is incorporated in the concrete. It is essential that every concrete structure should sustain for a long period maintaining its strength and serviceability. Corrosion of reinforcing steel become a vital mechanism of deterioration of reinforced structures. The main causes of steel corrosion in concrete are carbonation and chloride attack. They do not affect any harm on the integrity of concrete rather the aggressive ions attack the steel reinforcement.

Solution in the pore spaces of the concrete is highly alkaline due to the products of cement hydration. On the other hand, in the process of hydration of cement, 25-50% $Ca(OH)_2$ by weight of cement produces which causes a pH of minimum 12.5. Carbon dioxide from the atmosphere, react with the $Ca(OH)_2$ forming calcium carbonate. Fully carbonated solution attains a pH of 7.0, so that the High alkalinity neutralizes due to the CO_2.

$$CO_2 + H_2O = H_2CO_3 \dots\dots\dots\dots\dots\dots\dots\dots\dots\dots\dots\dots\dots\dots\dots\dots\dots\dots\dots\dots\dots\dots(2.3)$$

$$Ca(OH)_2 + H_2CO_3 = CaCO_3 + 2H_2O\dots\dots\dots\dots\dots\dots\dots\dots\dots\dots\dots\dots\dots\dots(2.4)$$

This process begins from the surface of the concrete and moves gradually to the inner zone and when the whole concrete has carbonated, at the neutralized environment there is no longer existence of passive film. So if there is enough supply of H_2O, local cells are formed and corrosion takes place.

Due to carbonation, there is a formation of discolored zone. The color varies from light gray to strong orange. Carbonation can be detected in the field by Phenolphthalein indicator. Phenolphthalein is a white or pale yellow crystalline material. The indicator is dissolved in a suitable solvent such as isopropyl alcohol (isopropanol) in a 1% solution. The phenolphthalein indicator solution is applied to a fresh fracture surface of concrete. If the indicator turns purple, the pH is above 8.6. Where the solution remains colorless, the pH of the concrete is below 8.6, suggesting carbonation. A fully-carbonated paste has a pH of about 8.4. In practice, a pH of 8.6 may only give a faintly discernible slightly pink color. A strong, immediate, color change to purple suggests a pH that is higher, perhaps pH 9 or 10.

On the other hand, the chloride ions does not affect the products of hydration. They ingresses through the pores of concrete and attack the passive film. So that there is no change in pH of concrete pore solution.

$$Fe^{2+} + 2Cl^- + 4H_2O = FeCl_2. 4H2O \dots\dots\dots\dots\dots\dots\dots\dots\dots\dots\dots\dots\dots\dots\dots\dots\dots.(2.5)$$

$$FeCl_2. 4H_2O = Fe(OH)_2 + 2Cl^- + 2H^+ + 2H_2O \dots\dots\dots\dots\dots\dots\dots\dots\dots\dots\dots\dots.(2.6)$$
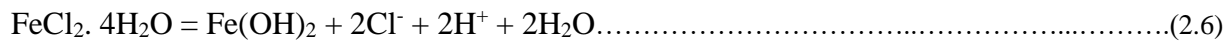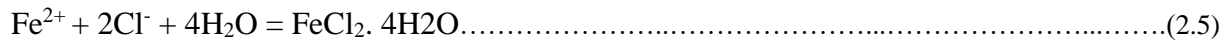
When a certain area of the passive film of bar surface is destroyed, chloride ions acts as catalysts. From the reactions it is clear that the chlorides are reproduced. So that the chloride ions affect the rate at which the process of corrosion occurs. The concentration of the hydroxide ions in the pore solution of the concrete in contact with the steel is usually sufficiently high to maintain this passivation film (Zhao & Jin, 2016). When the concentration of chloride ions reaches a threshold value, then the depassivation occurs.

2.3.1 Threshold Value of Chlorides

All the chloride ions present in the pore solution do not take part in corrosion. Some chlorides react with the C_3A of cement to form calcium chloroaluminates and removed from the solution (ACI 222R-01). The fraction of chlorides which take part in corrosion is dependent on the C_3A and C_4AF content, pH, w/c ratio, and whether the chloride ions were mixed with mixture or penetrated into the hardened concrete (ACI 222R-01).
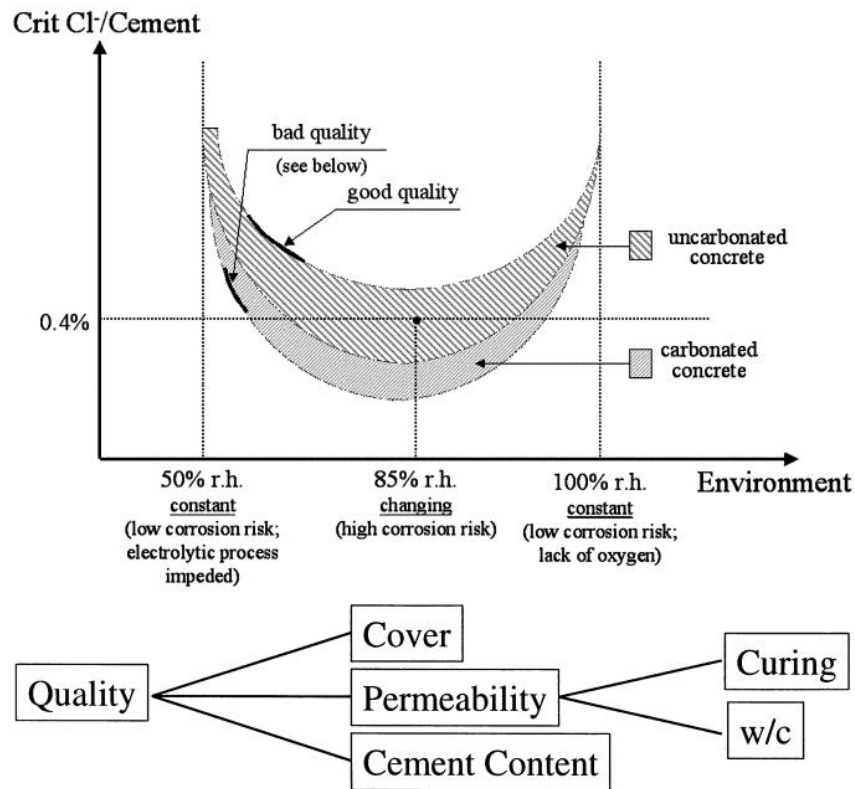
Figure 2.3: The critical chloride content (taken from ACI 222R)

Figure 2.3 shows that, with the increase of relative humidity, a higher chloride content is needed to initiate corrosion. With the increase of pH the threshold value increases to a great extent. The threshold value was assumed to 0.4% (1.4 kg/m^3 of concrete) by mass of cement (CEB) where the US uses this value as 0.6-0.9 kg/m^3 (ACI 222R). Corrosion can be observed as a threshold level of 0.2% chloride by weight of cement if the water and oxygen are available or up to 1.0% or more (Broomfield, 2006). Mindess et al., (2003) reported that corrosion will start when [Cl-]/[OH-] reaches 0.6. Whereas ACI 222R suggested this value as 0.29 at pH =12.6 and 0.3 at pH = 13.3.

2.3.2 Concrete Pore Solution

There are several types of pores present in the concrete namely entrapped air, capillary pores, gel pores, and entrained air, if present. These pores contains a certain amount of water depends on the humidity of the surrounding environment. In these liquid several ions produced by hydration of cement are dissolved. The chemical composition of the solution in pores of hydrated cement paste depends on the composition of the concrete, mainly on the type of cement, but also on the exposure conditions, e. g. it changes due to carbonation or penetration of salts. Bertolini et al. (2013) studied the chemical composition of pore solution which is shown

in table 2.1. The pore solution mainly consists of NaOH and KOH. Other ions like Ca^{2+}, SO_4^{2-} are very low in concentrations. The pH calculated for OPC was 13.4 to 13.9.

Table 2.1: Ionic concentration (mmol/L) measured in pore solution (n. a. = concentration not available)

Cement	Age (days)	Sample	[OH^-]	[Na^+]	[K^+]	[Ca^{2+}]	[Cl^-]	[SO_4^{2-}]
OPC	28	Paste	470	130	380	1	n. a.	n. a.
OPC	28	Mortar	391	90	288	<1	3	<0.3
OPC	28	Paste	834	271	629	1	n. a.	31
OPC	192	Mortar	251	38	241	<1	n. a.	8
OPC	--	Paste	288	85	228	n. a.	1	n. a.
OPC	84	Paste	589	n. a.	n. a.	n. a.	2	n. a.
OPC	84	Paste	479	n. a.	n. a.	n. a.	3	n. a.

The water content in the pore spaces of concrete is dependent on the relative humidity of the surrounding environment which is shown in figure 2.4.
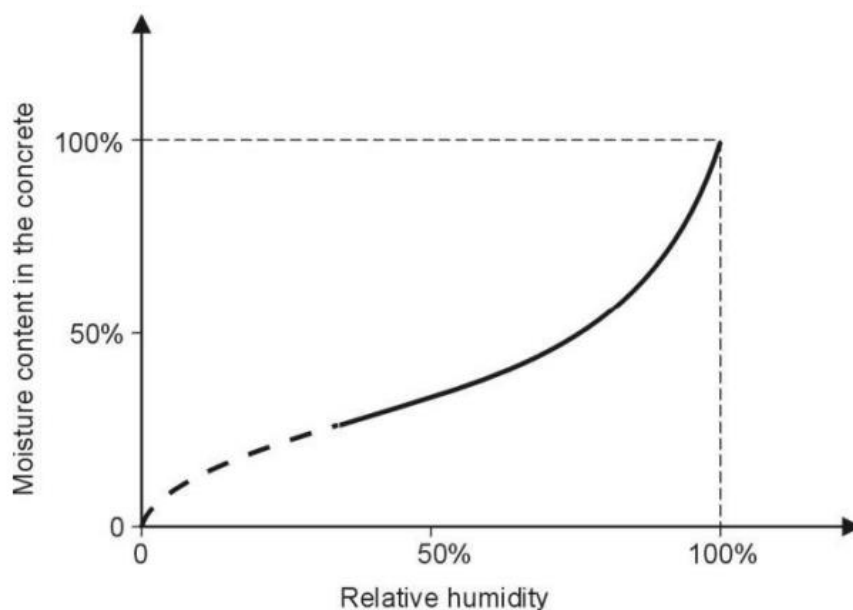
Figure 2.4: Variation of water content in the pores of concrete with respect to relative humidity (Bertolini et al., 2013)

The diffusion of oxygen is largely dependent on the water content in the pore solution because the diffusion of oxygen through air is much higher than that in water. So when pore spaces are partially filled with water the availability is higher than that for saturated concrete. Honda et al. (1992) reported that when the moisture content of concrete is lowered from 80% to 40%, the

value of the oxygen diffusion coefficient increases by a factor of 15. So, the corrosion rate is very low when the structure is in fully submerged conditions.

2.3.3 Corrosion Products

Corrosion of steel is an electrochemical process in which a varieties of oxides and hydroxides are formed. These oxides are commonly found in nature. The name and general properties is shown in table 2.2. Among them Fe_2O_3 and α-FeOOH are the most stable iron oxides. Different types of iron oxides transform in to these stable formation under different environmental conditions.

Table 2.2: Different types of corrosion products (Y. Zhao & Jin, 2016)

Corrosion products	Chemical formula	Density (gm/cm3)	color
Wűstite	FeO	4.26	Yellow-Brown
Magnetite	Fe_3O_4	5.18	Black
Hematite	α-Fe_2O_3	5.26	Red
Maghemite	γ-Fe_2O_3	4.87	Reddish brown
Feroxyhyte	δ-FeOOH	4.20	Red-brown
Akaganeite	β-FeOOH	3.56	Yellow-brown
Lepidocrocite	γ-FeOOH	4.09	Orange
Goethite	α-FeOOH	4.26	Yellow-brown
--	$Fe(OH)_2$	--	--
Bernalite	$Fe(OH)_3$	--	--
--	$Fe_2O_3.3H_2O$	--	--

The volume of these products occupies larger volume than the virgin iron. Corrosion products are thus formed on the reinforcing steels which are expansive in nature, as shown in Figure 2.5. From the figure it shows that the expansion may occur 1.7 to 6.15 times. Due to this expansion, radially outward pressure is induces on the concrete around the steel surface consequences the cracking, spalling even delamination.
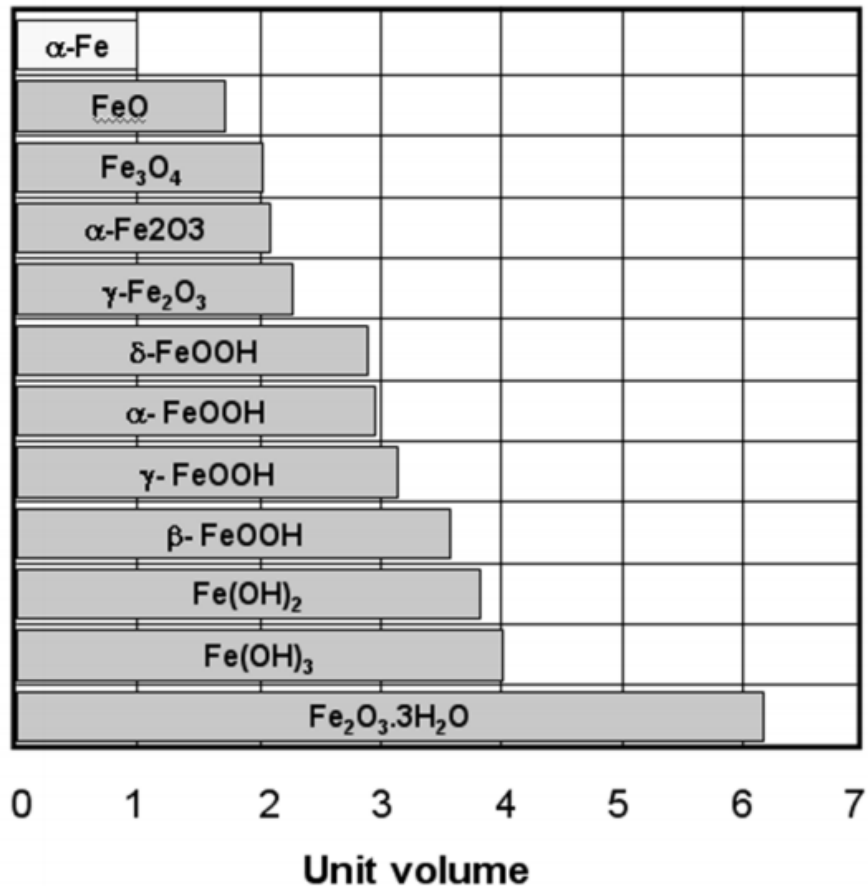
Figure 2.5: Unit volume of corrosion products of steel (Zhang & Poursaee, 2014)

2.4 Rate of Corrosion and Rate Monitoring Techniques

In the electrochemical process of corrosion, it can be seen that there is an accumulation of positive and negative ions. Water diffuses towards the anode as hydroxide ions taking the electrons liberated from anode (iron) and causes formation of oxides. These anodic and cathodic processes neutralize the electrons if there is no external source of electrons. So that the rate of oxidation at the anode and the rate of reduction at the cathode must be equal, and this equality controls the corrosion rate.

One important factor controlling the rate of corrosion is the availability of dissolved oxygen surrounding the cathodic areas because, in the cathodic reaction oxygen is consumed to form hydroxide ions. If the supply of dissolved oxygen can be stopped then the corrosion reaction may be restricted to a great extent. Cover of concrete in reinforced concrete, slows the diffusion of oxygen from the surrounding environment. Due to the controlled diffusion of oxygen through the cover concrete, a significant reduction occurs in the potential difference between the anodic

and cathodic areas. This effect is called a "polarizing effect" and the process is called "polarization" (Zhao & Jin, 2016).

The other important factor in the corrosion process of steel in concrete is the limitation of the ionic current flow through the pores of the concrete surrounding the steel. If the flow rate of the charge-carrying ions is slow, then the corrosion reactions can proceed only at a slow rate. This happens when the electrical resistance of the concrete surrounding the steel between the anode and the cathode is high. In practice, the phenomenon of steel corrosion does not easily occur in dry concrete due to the high electrical resistance of the dry concrete cover. Therefore, the measurement of the electrical resistance of concrete cover can sometimes serve as an indication of how fast the corrosion reactions proceed (Zhao & Jin, 2016).

2.4.1 Half Cell Potential

The electrochemical process of corrosion causes a potential difference between anode and cathode zone in reinforced concrete structures. ASTM C876 presents a procedures regarding the measurement of potential of reinforcing steel by a half cell which is shown in figure 2.6. The numeric magnitude does not indicate the corrosion rate of the steel except under certain specific conditions. This method only provides an indications of whether corrosion occurring or not. The potential measured is dependent on various factors like type of half-cell used, concrete is saturated or not, concrete is carbonated or not etc. The potential was interpreted according to table 2.3.

Table 2.3: Guidance for interpretation of results from Half-cell surveying

E_{corr} (Cu/CuSO4)	Probability of Corrosion
less negative than -0.20 V	Greater than 90% probability of no corrosion
-0.20 V$> E_{corr}>$ -0.35 V	Corrosion activity uncertain
More negative than -0.35 V	Greater than 90% probability of active corrosion
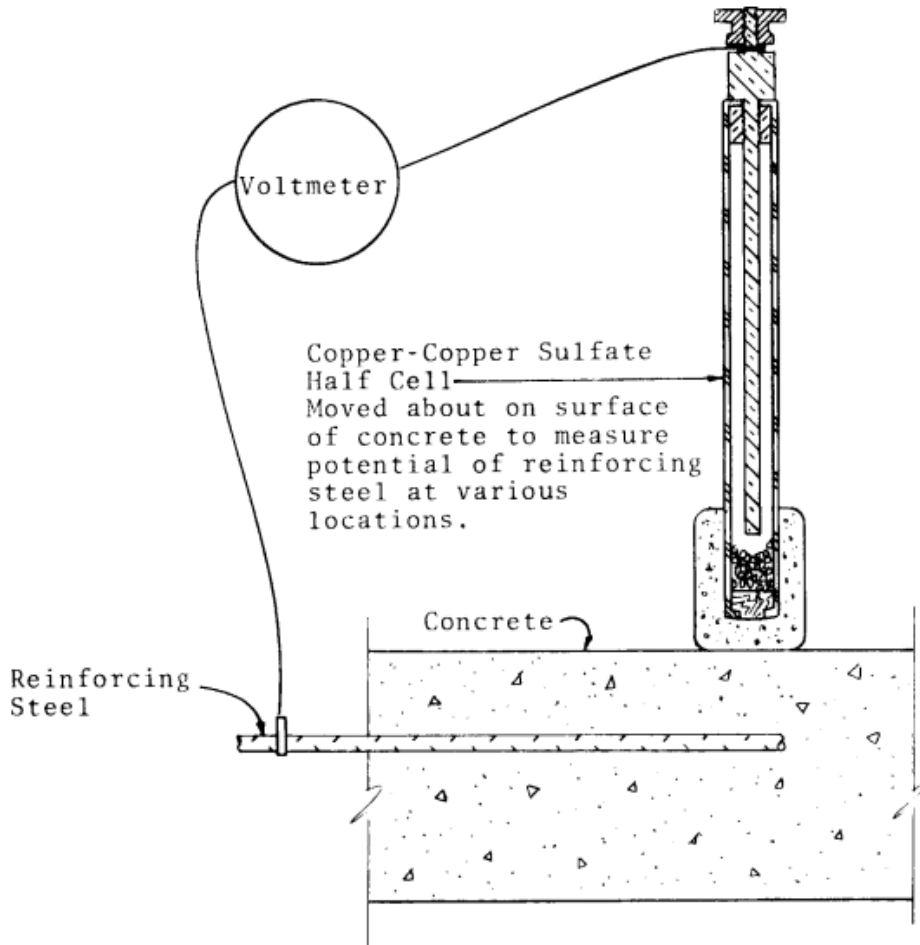
Figure 2.6: Copper-copper sulfate Half-cell circuit (taken from ASTM C876)

2.4.2 Linear Polarization Technique

Linear Polarization resistance has become a well-established method of determining the instantaneous corrosion rate measurement of reinforcing steel in concrete. In this method a small portion of concrete cover is to be broken up to connect an electrical circuit to the reinforcing steel. It is the technique in which an accurate assessment of the condition of reinforced concrete structures are possible. This method provides an information from which the rate of corrosion can be calculated accurately. There are two ways of measuring the rate of corrosion, one is measuring the amount of change of current ΔI due to change of potential of reinforcing steel by ΔE for a fixed time. And the other one is measuring the amount of change of potential ΔE due to apply of current to the reinforcing steel by ΔI for a certain time. The polarization resistance, Rp of steel then calculated as

$Rp = \Delta E/ \Delta I$.…………………………………………………….…...…………………...…….(2.7)

From which the rate of corrosion is calculated as

$$\text{Icorr} = \frac{\beta_a \beta_c}{2.3 Rp (\beta_a \beta_c)} \dots \dots \dots \dots \dots \dots \dots \dots \dots \dots \dots \dots \dots \dots .(2.8)$$

Where βa and βc are the anodic and cathodic Tafel slopes. As shown in Figure 2.7, the polarization curve for iron is divided into active, passive and transpassive regions. The linear part of the curve (active region) is called the Tafel region where the steel corrodes.
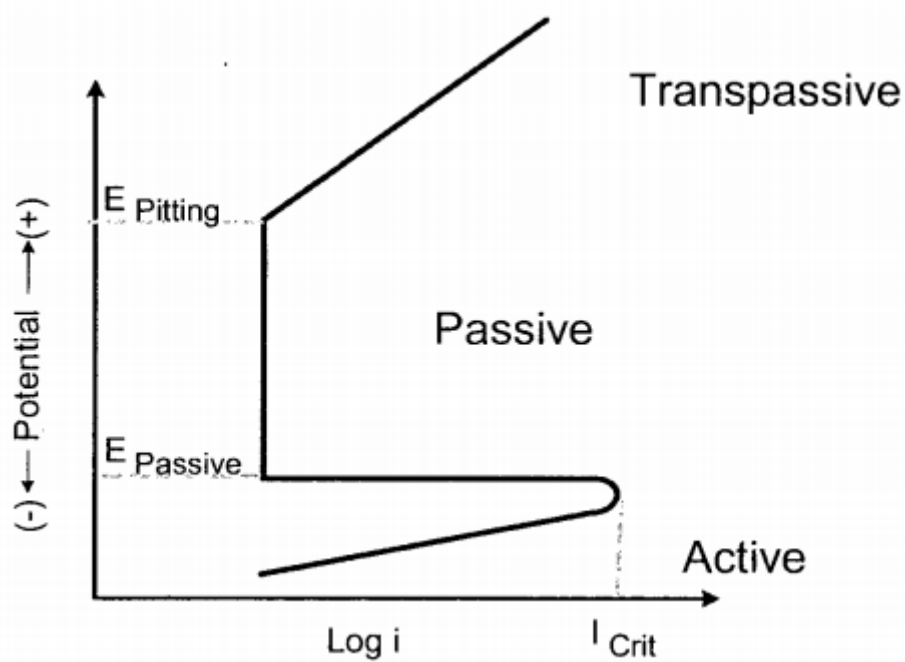
Figure 2.7: General polarization curve for steel (Nossoni & Harichandran, 2012)

Tafel equation for this region is

$$\eta = \beta \log(i/i_0) \dots \dots \dots \dots \dots \dots \dots \dots \dots \dots \dots \dots \dots \dots \dots \dots .(2.9)$$

Where η is the potential, β is the Tafel constant, and i_0 is the exchange current density. The plot is linear up to critical current i_{crit} and then the passive region starts. The passive state is reached due to the formation of a thin layer of oxides at a certain pH. The passive region continues until E_{pit} where the trans passive region starts. This region is also linear in the semi-logarithmic plot. From the polarization curve it is possible to evaluate the passivation current and pitting corrosion current.

The present residual strength and, by extrapolation, the remaining service life of the structure can then be estimated. In a conventional LPR test, the current is applied from an auxiliary electrode on the concrete surface. The method is illustrated in figure 2.8
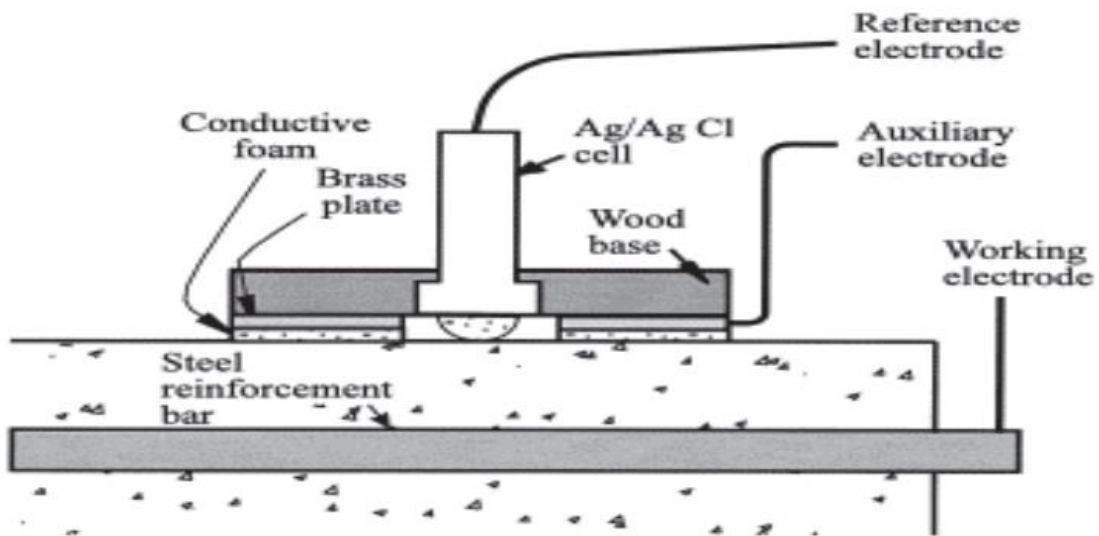
Figure 2.8: Linear polarization resistance measurement (Song & Saraswathy, 2007))

The interpretation of the results obtained by LPR method according to table 2.4

Table 2.4: Corrosion current vs. condition of the rebar

Corrosion current, Icorr ($\mu A/cm^2$)	Condition of the steel
<0.2	No corrosion expected
0.2-1.0	Damage possible in 10 15 years (low corrosion)
1.0-10.0	Damage possible in 2-10 years (moderate)
>10.0	Damage possible in less than 2 years (high corrosion)

2.4.3 Gravimetric Loss Method

This method is only for laboratory works and it is time consuming in a sense the mass loss is measured by the difference of masses steel before and after corrosion. On the basis of total mass loss, the rate of corrosion is calculated by the equation

$$\text{Corrosion rate} = \frac{K\Delta m}{Atd}$$ ………………………………………………………………....……….(2.10)

Where k is a constant, Δm is the mass loss, A is the surface area, t is the time and d is the density of the corroding steel. Before measuring the mass of the steel after completing test, the corroded steel is cleaned according to ASTM G1. This method gives only the average rate of corrosion.

2.5 Models Predicting the Failure of Concrete due to Corrosion

There are various deterioration models used to predict the service life of concrete structures due to corrosion induced damage (Allan & Cherry, 1992; Bazant, 1979; Bhargava et al., 2006; Maaddawy & Soudki, 2003). Mathematical models (Du et al., 2006; Kassir & Ghosn, 2002), and empirical equations for predicting the time to cracking have also been proposed. Various numerical analysis (Nossoni & Harichandran, 2014; Val et al., 2009) are also used to predict the failure pressure due to corrosion of steel in concrete.

2.5.1 Bazant's Model

Bazant, (1979) proposed a simplified model to calculate the time to crack the cover concrete due to the corrosion of steel. The model was based on the theoretical electrochemistry. According to the model, the time to crack the cover concrete is

$$t_{corr} = \rho_{corr} \frac{D \Delta D}{p J_r} \qquad \qquad (2.11)$$

Where ρ_{corr} is the combined density of steel and rust, D is the diameter of bar, ΔD is the change in diameter of bar, p is the perimeter of the bar and Jr is the instantaneous corrosion rate.

2.5.2 Morinaga's Model

Morinaga developed an empirical model based on field and laboratory data to compute the amount of corrosion, Q_{corr}, which causes the concrete cover to crack. The expression to estimate Q_{corr} is

$$Q_{corr} = 0.602(1+2C_v/D)^{0.85}D \qquad \qquad (2.12)$$

Where Cv is the concrete cover and D is the diameter of bar. The time to cracking is estimated as

$$t_{corr} = Q_{corr}/i_{corr} \qquad \qquad (2.13)$$

Where i_{corr} is the corrosion current and t_{corr} is the corrosion time.

2.5.3 Bhargava et al. Model

Bhargava et al. (2006) developed a mathematical model for cracking of the concrete. The problem was modeled as a boundary value problem wherein the governing equations are expressed in terms of the radial displacement and the analytical solutions are presented considering a simple two-zone model for the cover concrete that may be cracked or uncracked. Firstly, porous zone is assumed to exist around the steel reinforcement and the surrounding concrete is not subjected to any pressure until the porous zone fills up with rust products. The model assumes that this porous zone takes care of the problem of evenly applied pressure on the concrete cover, and the cracking occurs when the hoop stress exceeds the tensile strength of the concrete. A bilinear model was used for the tensile strength of concrete and the effect of softening due to opening of cracks. The internal pressure and corrosion current were considered and an equation to predict the cracking time was presented.

2.6 Corrosion Protection

Damage of concrete due to corrosion of reinforcing steel is a vital and very costly problem in terms of its financial implications and also for its structures safety. So it is necessary to develop methods to increase the service live of the structures. A general method is to design the concrete properly which can prevent ingression of the aggressive ions. Dense concrete is a very good barrier of the aggressive ions because of having low permeability. On the other hand, use of thicker concrete cover will provide a long distance for aggressive agents to reach the reinforcing steel. In recent years there have been rapid development of various materials and methods which can be used for increasing the service life of concrete structure subjected to chloride attack. The use of some materials such as stainless steel can increase the corrosion resistance. Various techniques can be used to minimize the effect of rebar corrosion such as protective coatings, cathodic protection and corrosion inhibitors. The use of cathodic protection is probably more attractive from structural point of view and ease of application.

CHAPTER 3
EXPERIMENTAL CHARACTERIZATION OF
ACCELERATED CORROSION TEST

3.1 Introduction

This chapter focuses on the experimental investigation of steel bar corrosion both in concrete and in alkaline solution, with the use of impressed current to accelerate the corrosion process. The experiment was set up in alkaline solution because the solution in pore space of concrete is highly alkaline. In addition, the Faraday's Law was employed to calculate the mass loss in the accelerated corrosion tests.

Corrosion of steel in reinforced concrete is a long term process over the serviceable life. It might take many years before reinforced concrete specimens starts to corrode, and studying the effect of the corroded rebar on the structural member might take even decades. To understand the corrosion process, an accelerated corrosion test using impressed current was utilized in this research to increase the corrosion rate so as to study the effect of corrosion damage on concrete members in a short period of time.

Accelerated corrosion test had been used simultaneously (Andrade et al., 1993; Alonso et al., 1998b; Val et al., 2009, Tran et al., 2011) but still there was no certain standard test procedure. Gravimetric method was used to measure the real mass loss of the bars and the result was compared with the theoretical result calculated from the Faraday's Law. This chapter incorporates the results of a comprehensive study on the accelerated corrosion testing of steel bars under different environmental conditions to determine the conditions under which Faraday's Law would give the most accurate results. This environmental condition was used to investigate the growth of the corrosion products, pressure induced by corrosion products and cracking of cover concrete due to the pressure.

3.2 Electrochemical Concepts and Principle of Faraday's Law

Corrosion is an electrochemical process in which a microcell is formed. If a potential difference is created, an oxidation-reduction reaction occurs where the metal acts as an anode. In accelerated corrosion test, a constant DC power supply is used to apply current through the steel rebar. In the presence of Chloride and water, the steel bar acts as an anode. In this experiment,

the applied voltage across each specimen was kept controlled during the test with constant current from the DC power supply. Faraday's Law was employed to evaluate the overall mass loss of the anodic steel bar which was directly related to current and time. The typical schematic diagram of the accelerated corrosion test set-up is shown in Figure 3.1.
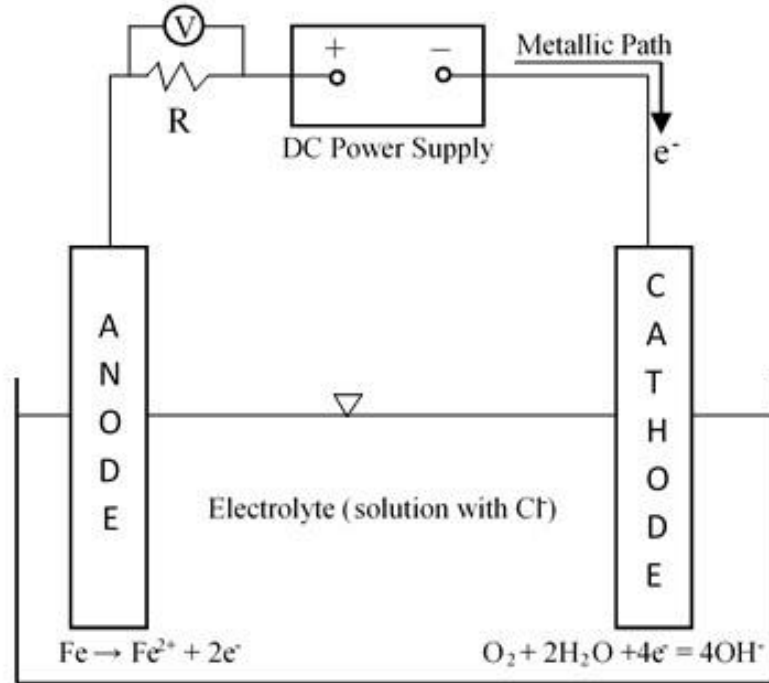
Figure 3.1: Schematic Diagram of Accelerated Corrosion Test Setup

As shown in Figure 3.1, the anodic reaction is the oxidation of iron to ferrous ions according to:

$$Fe = Fe^{2+} + 2e^- \quad\text{...(3.1)}$$

The cathodic reaction is the reduction of oxygen to hydroxide ions according to:

$$O_2 + 2H_2O + 4e^- = 4OH^- \quad\text{...(3.2)}$$

Corrosion is induced by applying an electrochemical potential between the reinforcing steel anode and cathode. A constant voltage was applied by the controlled DC supply and the current was recorded to calculate an estimated corrosion-induced steel loss using Faraday's law

$$m_F = \frac{MIT}{ZF} \quad\text{..(3.3)}$$

Where, m_F = the mass loss of steel bars (gm), M = atomic weight of metal (For Fe, M = 56), I = current (amperes), t = time (seconds), Z = ionic charge (for Fe, Z = 2), F = Faraday's constant = 96,500 amperes/second.

3.3 Current Density

Various researchers used different current density and different test environments. El Maaddawy et al., (2015) summarized the effectiveness of impressed current technique in inducing corrosion of steel reinforcement in concrete which was shown in Table A1. The previous experimental results showed that the accelerated corrosion by the impressed current technique was effective in inducing corrosion of steel in reinforced concrete. Theoretical mass loss was calculated in this technique by Faraday's law. But the measured corroded mass loss of the steel rebar based on gravimetric mass loss was not always in good agreement with the theoretical mass loss calculated from Faraday's law. This variation was dependent on the amount of chloride ions present in adjacent to the reinforcement irrespective of current density. Chloride ions in the concrete could present in two ways; one was addition of chlorides during casting and the other was ingression of chlorides through concrete pores. Current density was used to measure the rate of corrosion in impressed current system (Alonso et al., 1998a; Austin et al., 2004; Molina et al., 1993; Nossoni & Harichandran, 2014) and was defined as the current supplied through the circuit per unit active corroding surface area. The amount of current density had no impact on the final crack pattern and the strain induced by the corrosion (Shao, 2016).

3.4 Materials Used

Two 10 mm diameter grade 500W deformed mild steel bars was used as both anode and cathode in this investigation. The length of each bar was 76 mm. The bars were cleaned by steel wire brush. Pallets of NaOH, $Ca(OH)_2$, and KOH were used to prepare the high pH solution. The pH of prepared solutions were 13.7, 13.9, and 13.5 respectively. The high pH solutions were similar to that of concrete pore solution (Nossoni & Harichandran, 2012). The concrete used in this experiment was made with ordinary Portland cement with w/c of 0.45. The mix was designed according to the ACI 211.1 for a C30 grade concrete considering the requirements for corrosion protection of reinforcements in concrete exposed to corrosive environment. 19 mm downgrade stone chips was used as coarse aggregate and river sand with fineness modulus of 2.8 was used as fine aggregate in concrete. The mix proportion is shown in Table 3.1.

A DC (converted from AC current) power supply was used to supply current through the circuit. The input AC voltage was 200-220V 50/60Hz switchable. Output DC voltage was variable (3-30 V). A resistor of 4.7Ω was used in the circuit and a multi meter was used to measure the voltage drop across the resistor, from which the current flowing through the circuit was

calculated by Ohm's Law (I=V/R), where I is the current (A), V is the Voltage difference (V) and R is the resistance (Ω).

Table 3.1: Mix Proportions for the Concrete

Materials (kg/m^3)					w/c ratio
Water	Cement	Fine Aggregate	Coarse Aggregate	Fresh density	
190	422	677	1056	2345	0.45

3.5 Methodology

The accelerated corrosion test was done both in two environments i) in solution of high pH similar to concrete pore solution and ii) in concrete. The corroding surface area (A=16.0 cm^2) of anode and gap between the electrodes were kept constant in both environments. Chloride ion concentration was varied during the test from 0 to 1000 mMol/L in the solutions. Corrosion of steel is dependent on the amount of chlorides in electrolyte. Optimum chloride content is the concentration of chlorides in electrolytes for which the actual mass loss is equal to the theoretical mass loss. In this study, the optimum chloride content was investigated.

3.5.1 Accelerated Corrosion Test in Solution

Concrete pore solution has a very high pH (pH > 13.0) consisting of NaOH, Ca(OH)$_2$, and KOH (Bertolini et al., 2013). The concentrations of different ingredients is shown in Table A2. The similar solutions as in the concrete pore solutions were prepared. Table 3.2 shows the concentration of the species for the different concrete pore solutions which was also used by Nossoni & Harichandran (2012).

Table 3.2: Solution Properties

	$[OH^-]$ (mMol/L)	$[Na^+]$ (mMol/L)	$[K^+]$ (mMol/L)	$[Ca^{2+}]$ (mMol/L)	Calculated pH
Solution 1	470	130	380	1.0	13.7
Solution 2	834	271	629	1.0	13.9
Solution 3	288	85	228	0	13.5

The test was performed using constant application of voltage and the voltage drop against the fixed resistor was monitored. Two 10 mm dia deformed reinforcing bars were used for both

anode and cathode. Sodium chloride was added to the solution in various proportions as shown in Table 3.3.

Table 3.3: Different Combination of Salt Solution

Sl	[Cl-]/[OH-]	NaCl (mMol)	NaCl (%)
1	0	0	0.0
2	0.05	25.5	0.2
3	0.1	51	0.3
4	0.2	102	0.6
5	0.3	153	0.9
6	0.4	204	1.2
7	0.5	255	1.5
8	0.6	306	1.8
9	0.8	408	2.4
10	1	510	3.0
11	1.5	765	4.5
12	2	1020	6.0

Figure 3.2 showed the setup for test in solution. The anode bar was cleaned by steel wire brush before and after the test. A new solution and anode bar was used for each trial. The actual mass loss was measured from the difference between the weights recorded before and after the test. The actual mass loss was then compared with the theoretical mass loss following Faraday's law and the current efficiency was calculated as

$$\text{Current efficiency} = \frac{Current\ Inducing\ CORROSION}{Total\ Current} = \frac{Actual\ Mass\ Loss}{Theoretical\ Mass\ Loss} = \frac{m_R}{m_F} \quad \ldots\ldots\ldots\ldots\ldots(3.4)$$

A constant 12V current was applied across the circuit. The distance between the anode and cathode was kept constant (20 mm) throughout the test. Each test was continued for 18 hours.
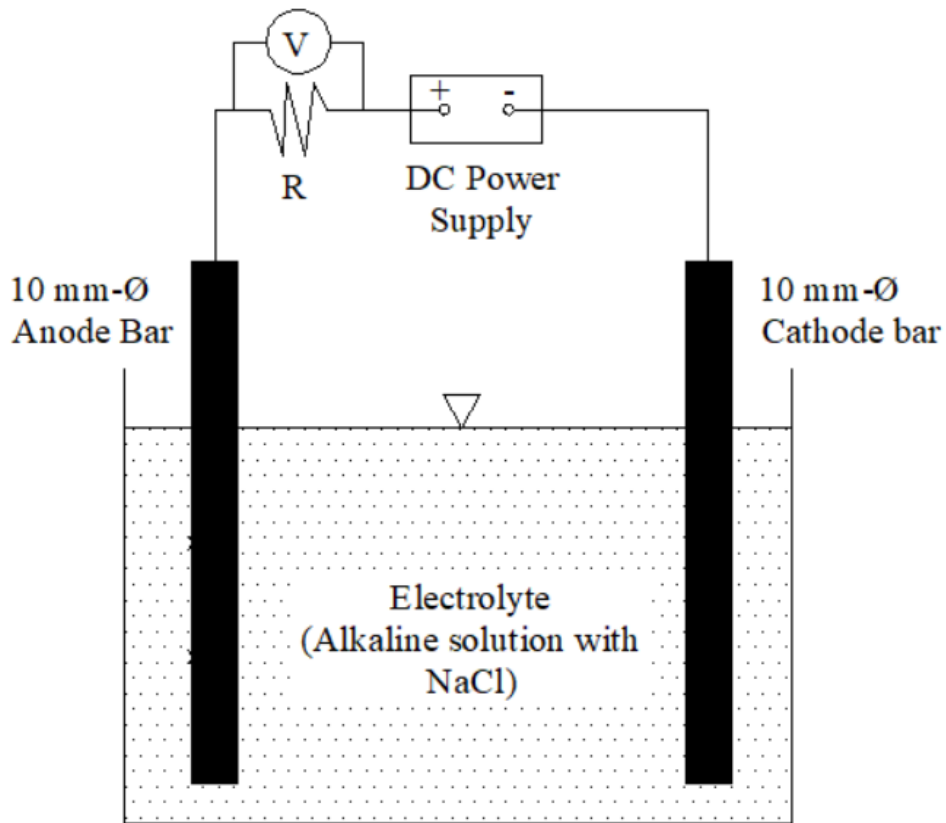
Figure 3.2: Accelerated Corrosion Test Set-Up in Solution

3.5.2 Accelerated Corrosion Test in Concrete

A 51 mm*51 mm*51 mm concrete cube was used to perform the accelerated corrosion test in concrete environment. The corrosion setup is shown in Figure 3.3. In accelerated corrosion test, specimens were wetted with saline water to increase the conductivity of concrete. To obtain the optimum chloride content adjacent to the steel concrete surface, the specimens were needed to wet for a certain period of time before starting the tests. There are no certain guideline regarding this. In this context, the optimum chloride content obtained from the tests in solution was used to wet the specimens. The specimens were immersed in salt solutions with optimum chloride content for different period of time (0 day, 1 day, and 7 day) before conducting the test to investigate the optimum time for which efficiency was 100%. Two 10 mm deformed rebars were used as anode and cathode. A constant distance (20 mm) was kept in between two electrodes to keep similarities with test in solution. A constant voltage of 12V was applied across the circuit. The actual mass loss and theoretical mass loss was measured as stated before and the current efficiency was also calculated.
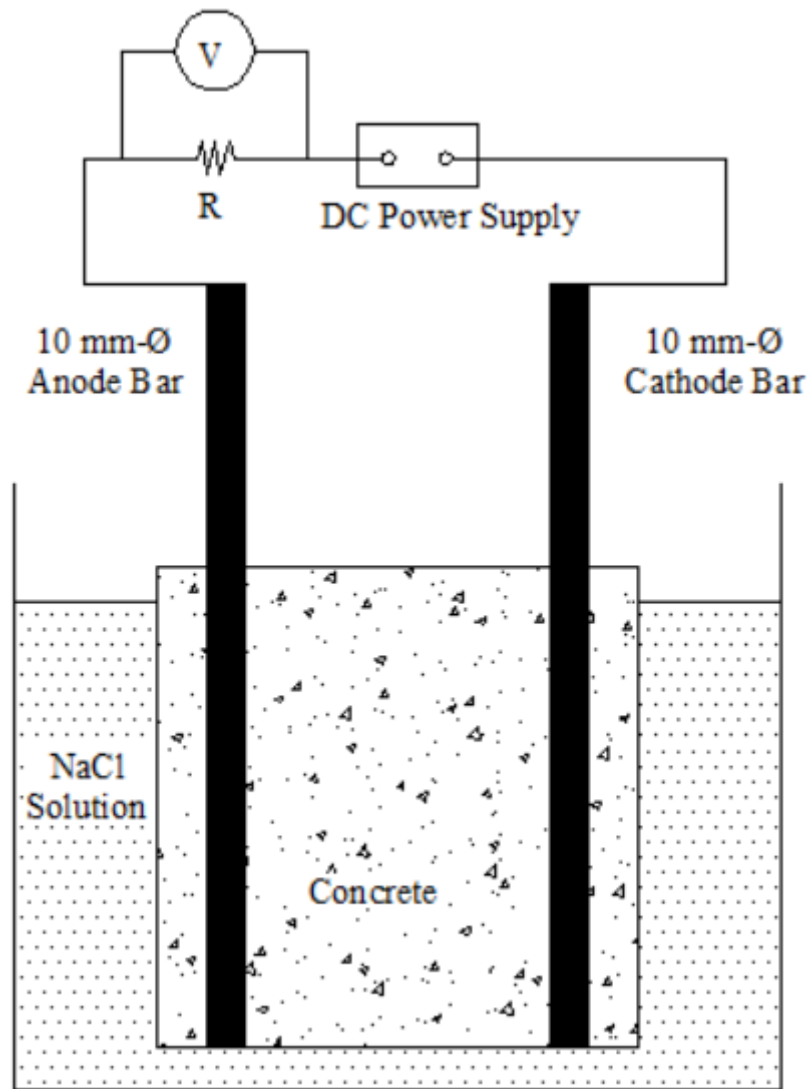
Figure 3.3: Accelerated Corrosion Test Set-Up in Concrete

3.6 Results and Discussion

3.6.1 Tests in Solution

The current efficiency for different chloride concentrations were plotted against the $[Cl^-]/[OH^-]$ in Figure 3.4 for solution 1. The current efficiency for each data point was an average of three set of tests. The graph shows that the efficiency of current is highly dependent on the amount of chloride present in solution. In chloride free solution the oxidation of anode was almost zero and gradually increased with the increase of chloride ions. From Figure 3.4 it is found that the current efficiency reached to 99% at a high chloride concentration $[Cl-]/[OH-]= 1.0$ which represents 3% salt in solution as shown in Table 3.3. The chloride content required to reach 100% current efficiency was dependent on the pH of the solution and current density (Nossoni & Harichandran, 2012). This phenomenon can also be described by the pourbiax diagram for

steel as shown in Figure 3.5. According to pourbiax diagram, when no chloride was present there were two active zones for corrosion: one for pH lower than 9 and another for pH higher than 14. Negligible corrosion occurred when pH of solution was 13.7. But due to addition of chloride content, a pitting zone was found and it became more active with increased chloride content. On the other hand, the more chloride content was needed for oxidation when the pH was higher. Because few different reaction might have occurred in addition to oxidation of steel. Some gases emitted by the reaction which irritated the eyes. They were not chemically identified but the probable reaction might be as (Nossoni & Harichandran, 2012),

Anode: $2OH^- = 1/2O_2 + 2H_2O + 2e^-$

Cathode: $2H_2O + 2e^- = H_2 + 2OH^-$
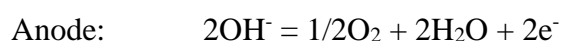
In chloride free solution all the current was used to break the water molecule and produced oxygen gas at anode and hydrogen gas at cathode. In presence of chlorides lower than a certain amount, partial current was used to oxidize the steel and rests was for breaking water molecule. So, for a fixed pH there was a certain chloride content for which a full oxidation of anode occurred. For a solution having pH 13.7, it was found that a 3.0% NaCl by weight was needed for 100% efficiency of current. It was also dependent on the current density applied through the circuit. Previous studies also showed that 1.65% to 3% NaCl was required for 100% efficiency (Nossoni & Harichandran, 2012) depending on the current density. Figure 3.4 showed that a higher ([Cl-]/[OH-] ≈ 1.0) was required for a 100% efficiency when a current density of 100 A/m^2 was applied which was also observed by (Nossoni & Harichandran, 2012) when current density of 170 A/m^2 was applied.
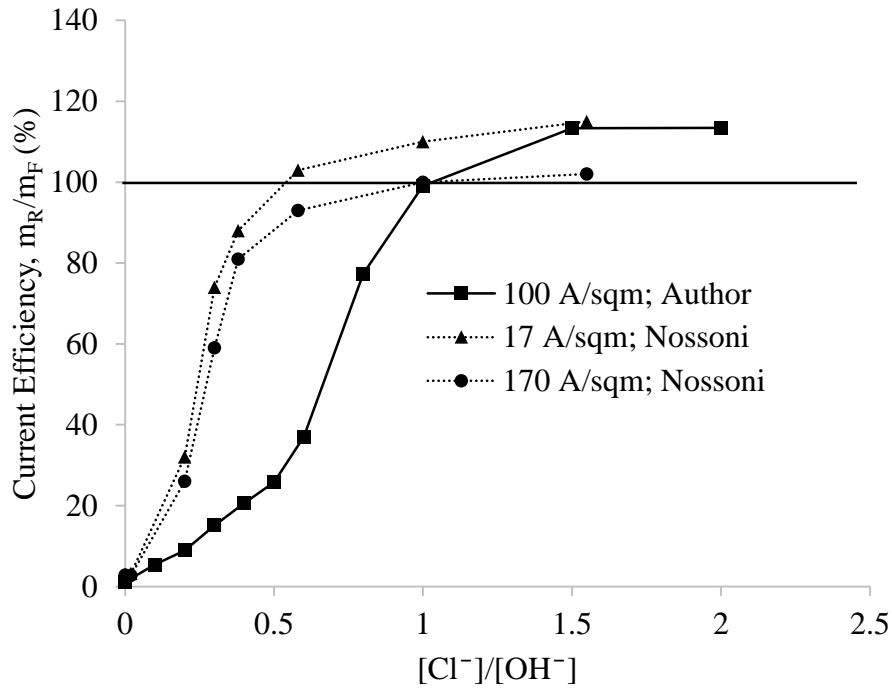
Figure 3.4: Variation of Current Efficiency with respect to Different Chloride Concentration in Solution 1
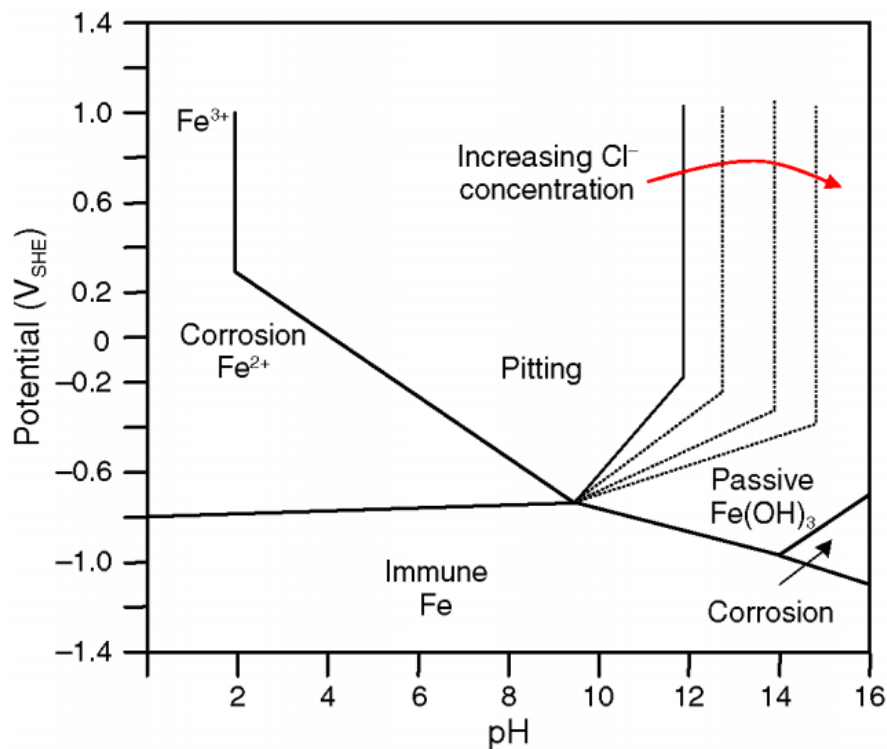
Figure 3.5: Pourbaix Diagram for Iron (Nossoni & Harichandran, 2012)

Since in the previous studies 3-5% NaCl was used, an investigation was done to characterize the optimum chloride content shown in Figure 3.6. It showed that in the solution 1 and 2, over

100% efficiency of current was attained for 3.5% NaCl solution irrespective of current density. Whereas for solution 2 it was about 95% at 3.5% NaCl. The reason for the current efficiency below 100% might be the solution properties or the cleaning problem. So the 3.5% NaCl was applied for tests in concrete environment as optimum chloride content.
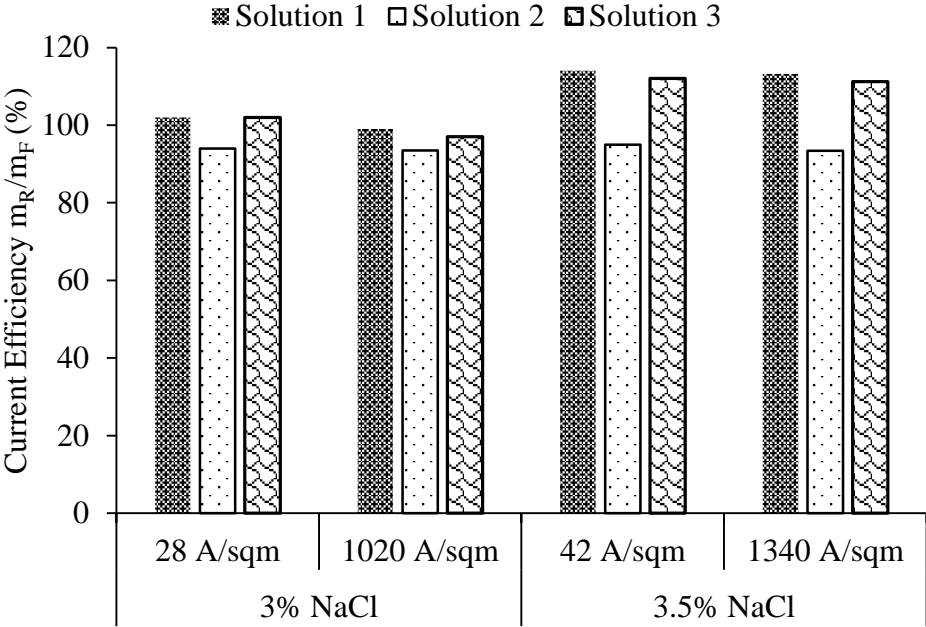
Figure 3.6: Current Efficiency for Different Solutions

3.6.2 Tests in Concrete

The high alkaline environment, attained due to hydration of cement in concrete, forms a passive film on the surface of the embedded steel which normally prevents the steel from corrosion. However, under chloride penetration, the passive film is disrupted or destroyed, and the steel is exposed to the harmful attackers and corroded spontaneously. From the investigation in solutions similar to the concrete pore solutions it was found that a 3.5% NaCl caused a 100% current efficiency. This finding was applied in concrete specimens. The results of the accelerated corrosion tests in concrete are presented in Figure 3.7. The rebars were taken out from the concrete sample and cleaned by steel wire then weight was measured. The actual loss of mass was calculated. Theoretical mass loss as well as current efficiency was calculated. The test of each specimen was continued for 18 hours.
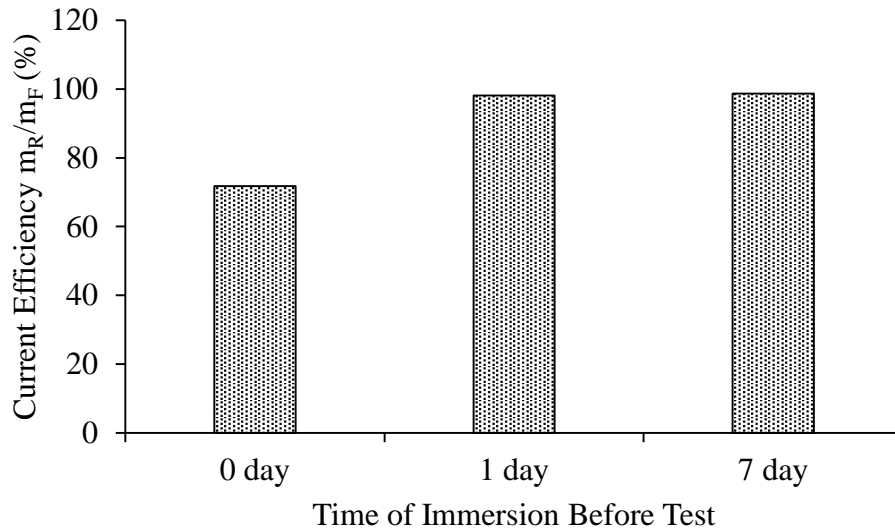
Figure 3.7: Current Efficiency for Different Immersion Time in 3.5% NaCl Solution

The test was continued with a partial immersion in 3.5% NaCl solution. It was obvious that chloride ions were needed to corrode the reinforcement and amount of chlorides was a governing factor for full current efficiency. Amount of chlorides was very much dependent on the time of immersion before test. Researchers used a short time immersion, a twenty four hour immersion as well as over seven days immersion before test to saturate the concrete with chloride ions. Figure 3.7 showed that an accuracy of current of 72% was attained for no immersion time before starting test. This was because a certain time was required to penetrate the chloride ions adjacent to the reinforcement and after that the oxidation was continued. On the other hand, immersion for one day and seven days showed almost similar results and it was about 98%. The ingression of chloride ions through the concrete was very much dependent on the quality of concrete and concrete cover. The results of this investigation was used for further work in this research.

CHAPTER 4

EXPERIMENTAL INVESTIGATION ON PHYSICAL CHANGES OF CORROSION PRODUCTS

4.1 Introduction

Concrete, a common construction material using worldwide, is durable against aggressive ions because of its high alkalinity. This high alkalinity attains due to the hydration of cement in concrete. Steel reinforcement in concrete is passivated due to the formation of a layer of oxides around which is known as layer of passivation (Bazant, 1979). Depassivation of this layer is occurred by chlorination or by an acidification (carbonation) of the environment close to the reinforcing steel (Bazant, 1979). It was reported that a chloride concentration ([Cl-]/[OH-]) of about 0.6 might lead to depassivate the protective layer (Hausmann, 1967; Mindess et al., 2003). However, the value varies from 0.3 to above 3 depending on many factors such as temperature, stress level, pitting potential, experimental conditions, experimental methods etc (Molina et al., 1993).

In marine environment, or in cold regions where salt is used for de-icing, chlorination is a major and alarming issue affecting the durability of concrete. Since the volume of the corrosion products is about six times more than that of the original corroding portion of the reinforcing steel, it exerts pressure on the surrounding concrete. The resultant tensile stress developed due to this pressure is released through the crack formation in the concrete, which is inherently weak to bear tensile stress. A continuous increase in corrosion products causes spalling even delamination of cover concrete.

Due to the expansive nature of corrosion products, an outward pressure was generated on the cover concrete. When the circumferential stress developed due to the outward pressure, exceeds the tensile strength of concrete crack initiated. This is a common phenomenon considered in fracture mechanics (Bhargava et al., 2006; Maaddawy & Soudki, 2003; Pantazopoulou & Papoulia, 2001; Val et al., 2009). But this phenomenon was not perfect for all cover thickness. For a lower cover thickness, the surface of cover concrete heaved and crack initiated due to bending effect. In this chapter, this phenomenon different from the conventional theory would be investigated.

4.2 Experimental Program

An experimental program was furnished by accelerated corrosion test with an applied current to measure the level of corrosion. In order to find the mechanism of crack initiation, an experimental setup was prepared to have two deformation dial gauge. The width of crack was measured by image analysis. The images were captured on the top surface of the specimen using USB digital microscope at different time intervals. Mass loss was measured by gravimetric loss method which is characterized as the difference of the masses of reinforcing steel measured before and after the accelerated corrosion test. After the test, the reinforcing steel was cleaned by a steel wire brush and then the mass was measured.
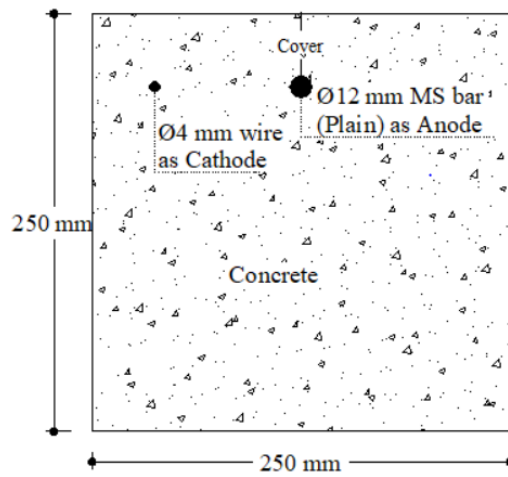
4.2.1 Specimen

A C30 grade concrete was also used for this experiment. The mix proportion was designed according to ACI 211.1 and is shown in Table 4.1. A w/c of 0.45 was selected to implement the codal restriction due to exposure condition of concrete in a saline environment. ASTM Type-I (Ordinary Portland Cement) was used as a binding material, 19 mm downgrade stone chips was used as coarse aggregate and river sand with fineness modulus of 2.8 was used as fine aggregate in concrete. The water used in this study was tap water having a chloride ion concentration of 1200 mg/L. The compressive strength and tensile strength of concrete were tested according to ASTM C39 and ASTM C426, respectively. The studied average compressive strength and tensile strength of concrete were found as 30 MPa and 2.9 MPa respectively. Two types of steel reinforcement were used in this research. A 12 mm diameter Grade 60 MS plain bar was used to represent as an anode and a 4 mm diameter wire was used as a cathode. Length of each bar was 380 mm for beam specimens and 75 mm for plates.

Two types of specimens were used in this study; beam specimen and plate of circular in cross section. The crack initiation phenomenon observed in the beam specimen was verified through plates. The dimension of the beams was 200 mm x 200 mm x 300 mm. Cylindrical plates were 100 mm in diameter and 50 mm in thickness. Plain bar was embedded in four beam specimens with a clear cover of 20 mm, 37.5 mm, 50 mm and 75 mm, respectively. A schematic diagram of the test specimen is shown in Figure 4.1. The uncovered portion of bar in beam specimens was coated by cement paste for a length of 25 mm to avoid pitting. In cylindrical plates, the 12 mm diameter bar (anode) was placed in the center and three 4 mm diameter wires (cathode) were placed equidistant from each other as well as from central anode bar. The test specimens are shown in Figure 4.2. Specimens were cured for 28 days.

Table 4.1: Mix Proportions for the Concrete

Materials (kg/m^3)					w/c
Water	Cement	Fine Aggregate	Coarse Aggregate	Fresh density	ratio
190	422	677	1056	2345	0.45

(a)
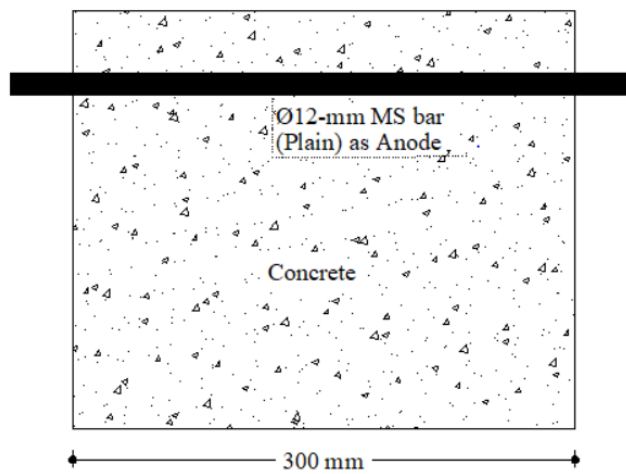
(b)

Figure 4.1: Details of Beam specimen (a) Cross Section (b) Longitudinal Section
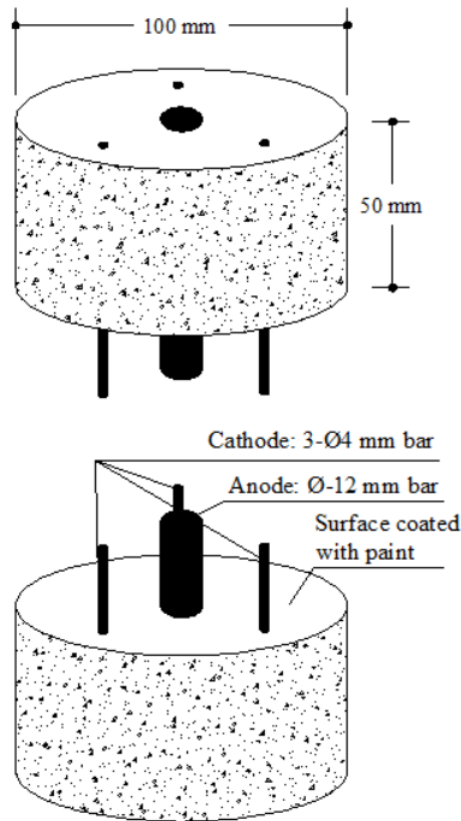
Figure 4.2: Details of Cylindrical Plates (a) Top View (b) Bottom View

4.2.2 Test Setup

In real time corrosion, a microcell is formed after the steel has depassivated and a potential difference is created between the corroding bar and the surrounding corrosion products and continued to corrode. To replicate this phenomenon in a short time, an external DC power supply was used to supply a direct current between the anode (steel reinforcement) and cathode. Capacity of power supply was 30 V, 6 A. A constant voltage of 30 V was applied through the circuit and the voltage drop across a fixed resistor was measured. From which the current supply was calculated by Ohm's law ($I = V/R$). The specimens were ponded partially with 3.5% NaCl solution for at least one day before starting the test since in the preceding chapter it was investigated that the current efficiency in accelerated corrosion test was 100% when the specimens were ponded in 3.5% NaCl solution for one day.

4.2.2.1 Beam Specimen

Two deformation dial gauges were set on the top surface of the beam specimen along the longitudinal reinforcement to measure the heaving due to corrosion. The setup was shown in

Figure 4.3. Crack width was measured by a magnifying USB digital Microscope (Manufacturer: TQC, Model: LD6184, Resolution: 1 microne), shown in Figure 4.4.
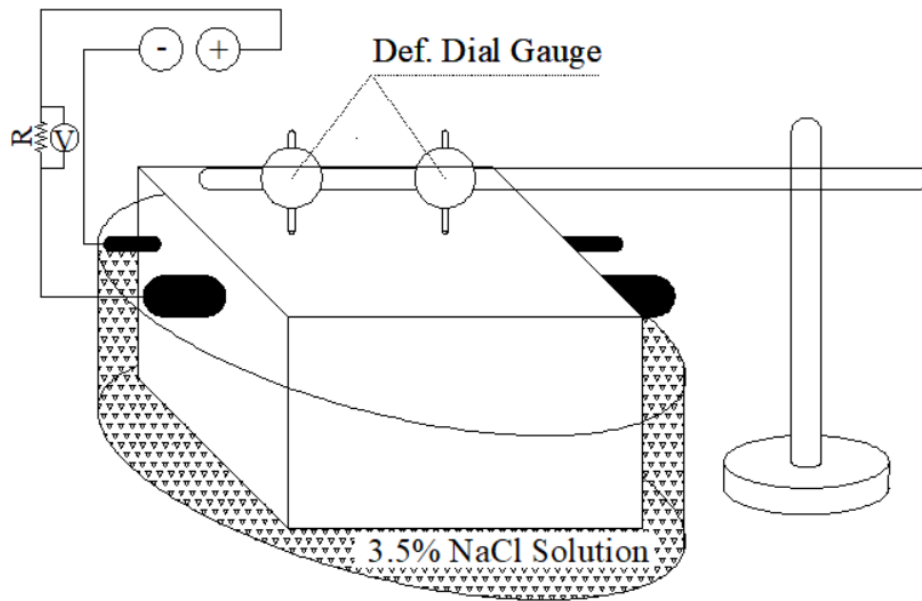
(a)

(b)

Figure 4.3: Details of Test Setup for Beam Specimen (a) Schematic Diagram (b) Onside View

Figure 4.4: USB Digital Microscope

4.2.2.2 Plates

The top surface of the cylindrical plates were polished and smoothened with grade 400 sand paper and then cleaned with air blower and duster cloth. The bottom side of the specimen was sealed with paint before ponding it in 3.5% NaCl solution in a manner that the chloride ions penetrate only through the side surface. The setup was shown in Figure 4.5. The specimens were immersed partially at 3.5% NaCl solution for at least one day before starting the test. Every time the top surface of the specimens was dried and cleaned before taking any photograph.
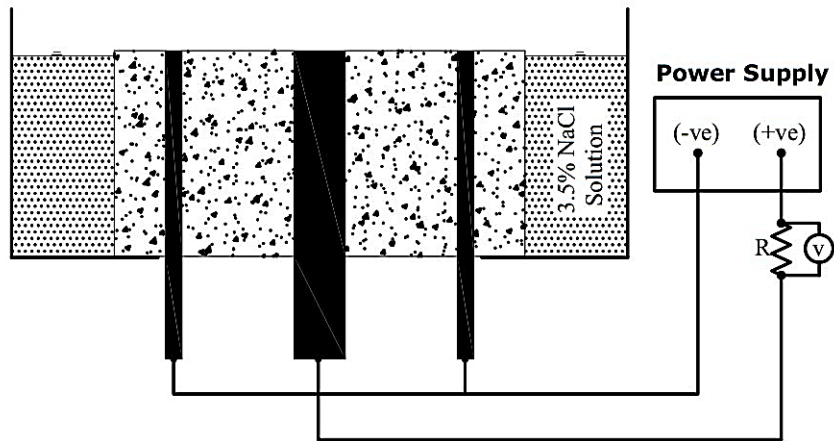
(a)

(b)

Figure 4.5: Details of Test Setup for Plates (a) Schematic Diagram of Setup (b) Onside View

4.3 Results of Beam Specimens

4.3.1 Mechanism of Crack Initiation

There is an increase in volume due to formation of corrosion products. The corrosion products with increased volume creates pressure outward on the concrete surface in steel concrete interface. The mechanism of crack formation depends on the cover thickness. Heaving of surface was observed due to internal expansive pressure for a cover thickness of 20 and 37.5

mm. Whereas no heaving was observed for cover of 50 and 75 mm. When heaving occurred, the tensile stress reached maximum on the cover surface just above the rebar. On the other hand when there was no heaving, circumferential tensile stress reached maximum in the steel concrete interface. For this reason a crack was initiated at the cover surface for a cover of 20 mm as well as 37.5 mm. And crack initiation occurred from steel concrete interface for a cover of 50 mm and 75 mm. A schematic diagram of the mechanism is illustrated in Figure 4.6. Figure 4.6 (a) showed that the surface heaved due to the expansive corrosion products. That is why a bending stress was developed. When this bending stress exceeded the tensile strength of concrete, crack initiated at the outer face and propagated towards the reinforcement. This phenomenon was also observed by Tran et al. (2011). However, with the increase in cover thickness to 50 mm, larger confinement occurred and crack initiated internally around the rebar and propagated towards cover surface. The phenomenon is shown in Figure 4.6 (b). This phenomenon occurred when circumferential stress exceeded the tensile strength of concrete crack initiated. However, a large amount of micro pores were present in concrete. So that it was easier to release energy through the internal micro pores instead of bending the surface of concrete cover. On the other hand, a local bending might occur due to the expansive corrosion products.
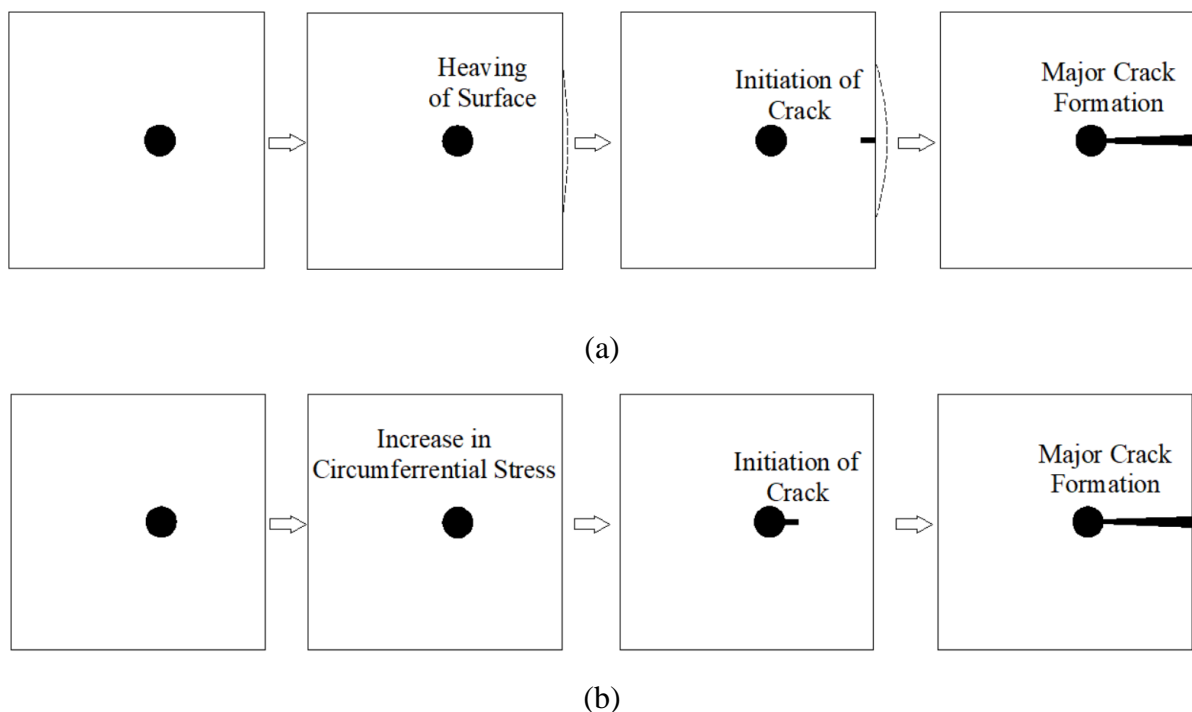

(a)

(b)

Figure 4.6: Initiation and Propagation of Crack (a) for Cover 20 mm and 37.5 mm and (b) for Cover 50 mm and 75 mm

4.3.2 Heaving of Surface

In order to understand the relation between corrosion level and heaving of the concrete surface, the heaving of cover surface was measured during the accelerated corrosion test using two deformation dial gauges having an accuracy of 1 μm (Figure 4.3). The deformation dial gauges were set up at 100 mm from end on the surface of the specimen along the reinforcement. The heaving of surface is plotted with respect to the level of corrosion which was previously calculated by Faraday's law and are shown in Figure 4.7 and Figure 4.8.

Figure 4.7 showed a gradual increase in surface deformations with level of corrosion for a clear cover 20 mm. From Figure 4.7 it was observed that the surface started to heave after a certain corrosion level of 3.2 mg/cm^2. The surface deformed gradually and at a deformation of 125 to 173 μm crack appeared on the surface, at a level of corrosion 22.7 to 24.7 mg/cm^2. Whereas for cover thickness of 37.5 mm, level of corrosion at which heaving started could not identified as shown in Figure 4.8. With an increase in cover to 37.5 mm as shown in Figure 4.8 the deformation at which cover cracked was 50 to 62.5 μm at a corrosion level of 21.2 to 22.6 mg/cm^2 respectively. Comparing Figure 4.7 and 4.8, it is also apparent that the lower the cover thickness the higher the curvature of the heaving of surface.

Thus for further increase in cover thickness to 50 mm as well as 75 mm the curvature of the heaving of surface might be so little that no heaving of surface was observed prior to cracking of surface. There was a linear relationship between the decreases in surface deformation with increasing the cover surface up to 50 mm which is shown in Figure 4.9.
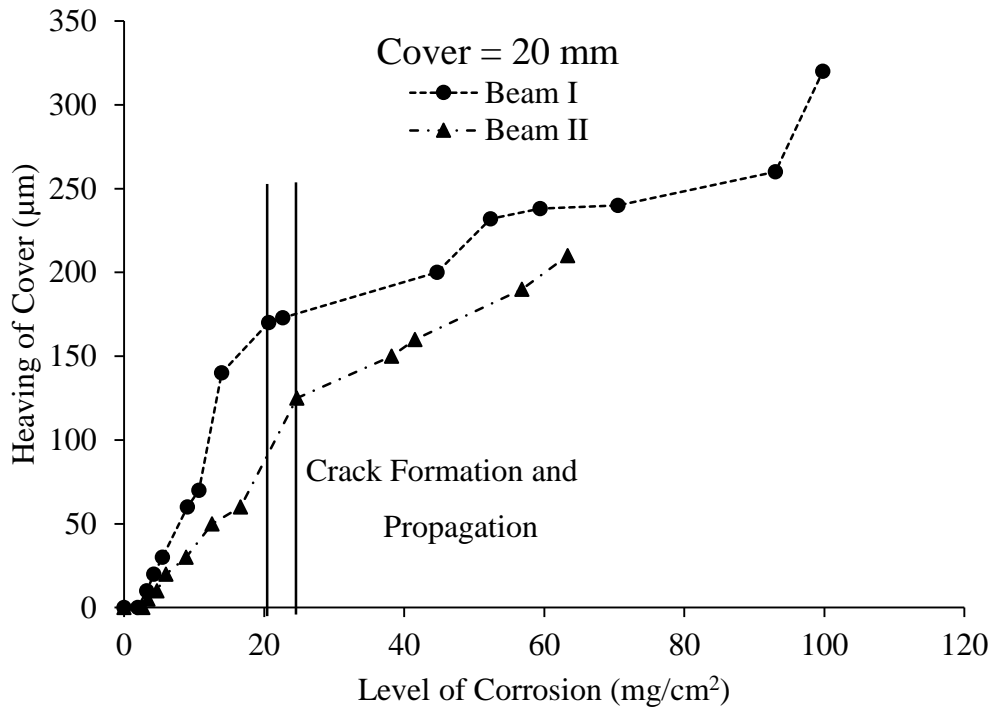
Figure 4.7: Heaving of Surface due to Corrosion of Reinforcement for Cover 20 mm
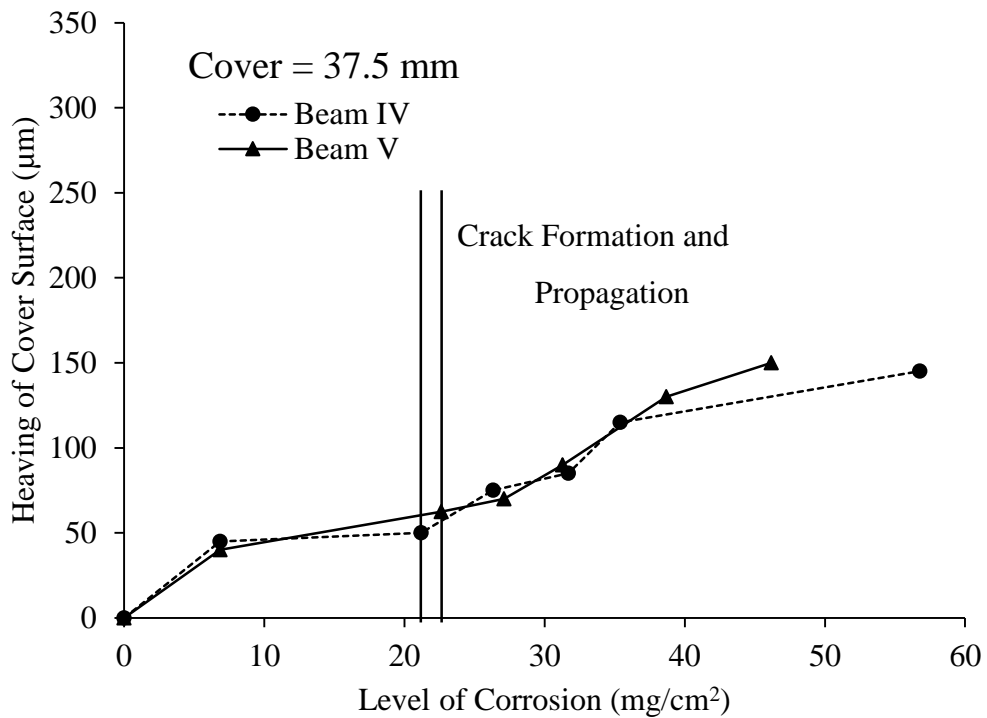
Figure 4.8: Heaving of Surface due to Corrosion of Reinforcement for Cover 37.5 mm
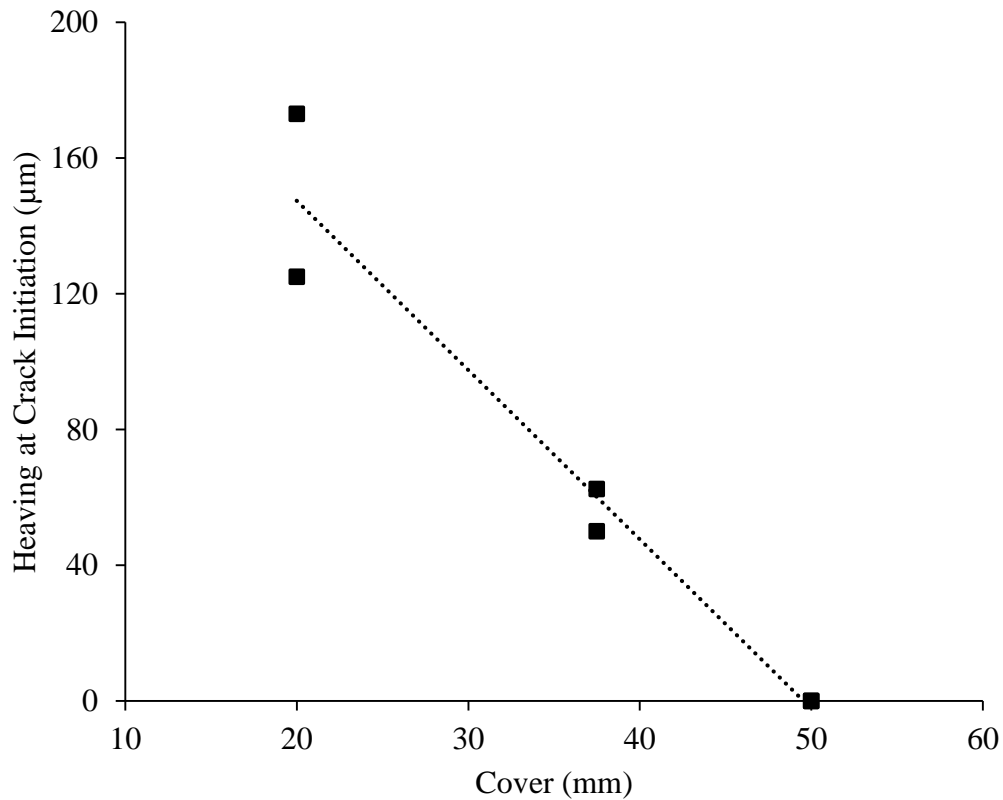
Figure 4.9: Variation of Heaving at Crack Initiation with respect to Cover Thickness

4.3.3 Surface Crack Propagation

In the field of structural health monitoring, the prediction for loss of reinforcement is very important. In order to fulfill the objective, width of surface crack was captured by a digital microscope and a relationship between propagation of crack width and amount of corrosion has been developed which is shown in Figure 4.10 to Figure 4.13. From the figures it is found that there is a linear relationship between crack width and level of corrosion. There were a number of pictures of crack captured at an interval of distance throughout the beam along the crack. At each corrosion level, the variation of crack width along the beam is shown in the Figure 4.10 to Figure 4.13. The previous study showed both linear relations (Vu et al., 2005) as well as nonlinear (Tran et al., 2011). They showed an average crack width but it's quite difficult to find a uniform crack width along the beam. With the time the amount of corrosion products was increased and only soluble part was leached out through the crack. As a result, the pressure induced part was accumulated around the rebar and the opening of the crack was increased as well.
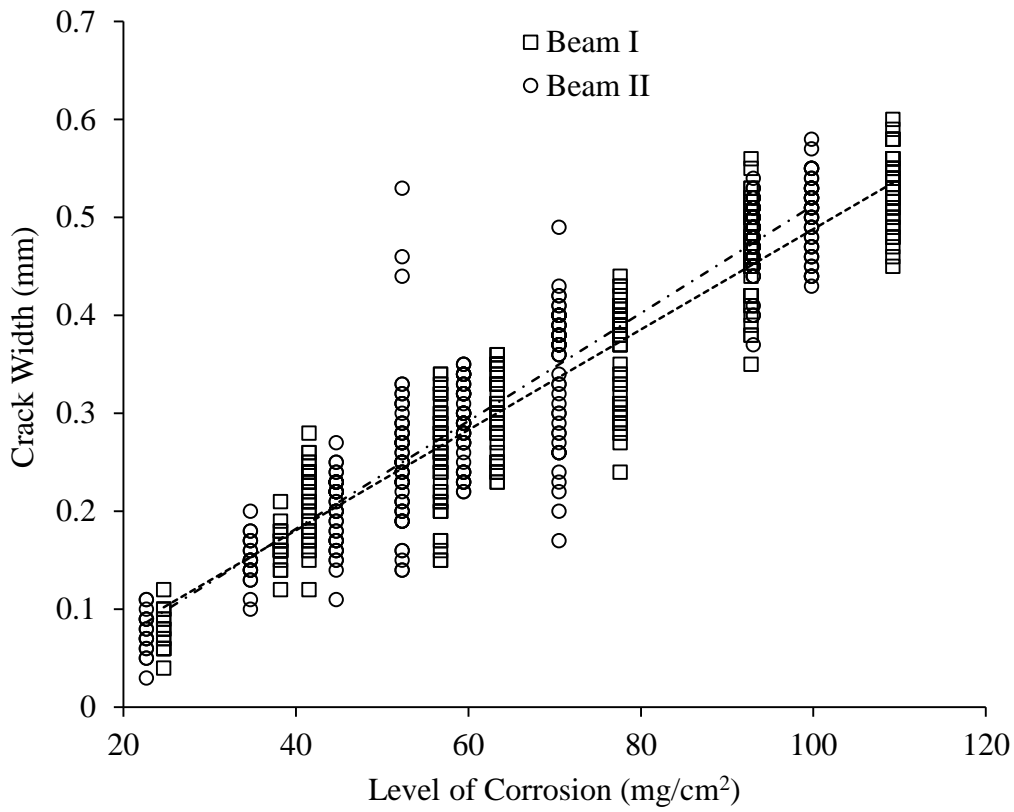
Figure 4.10: Surface Crack Propagation for C = 20 mm
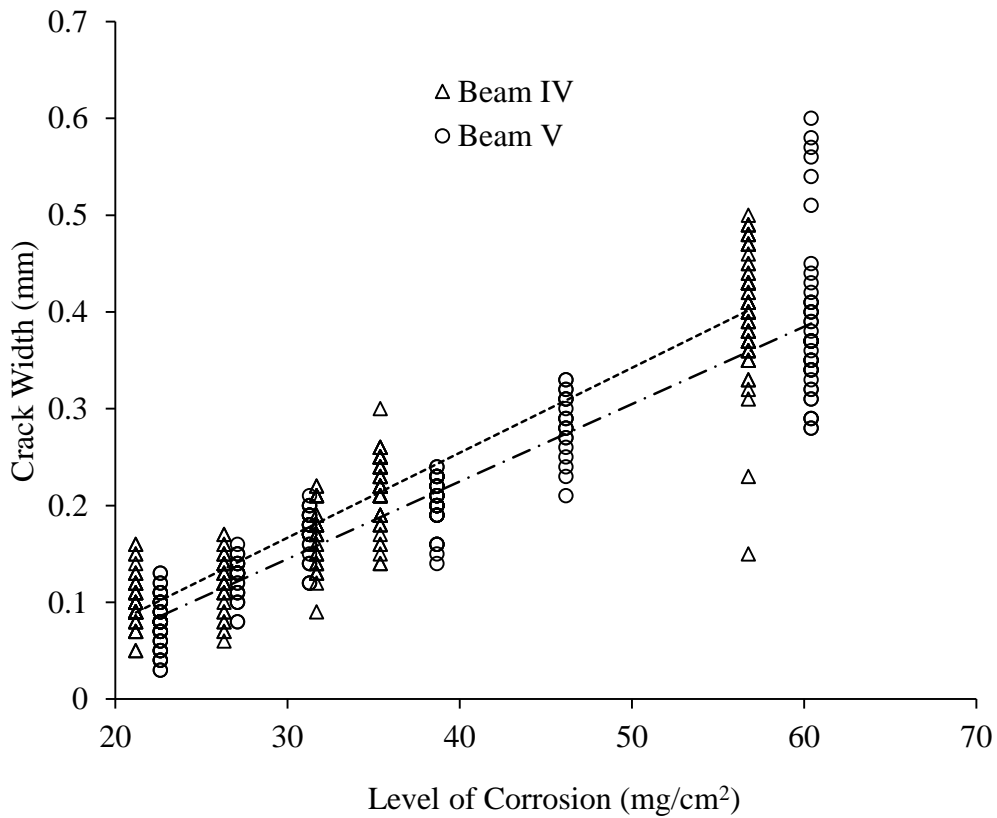
Figure 4.11: Surface Crack Propagation for C = 37.5 mm
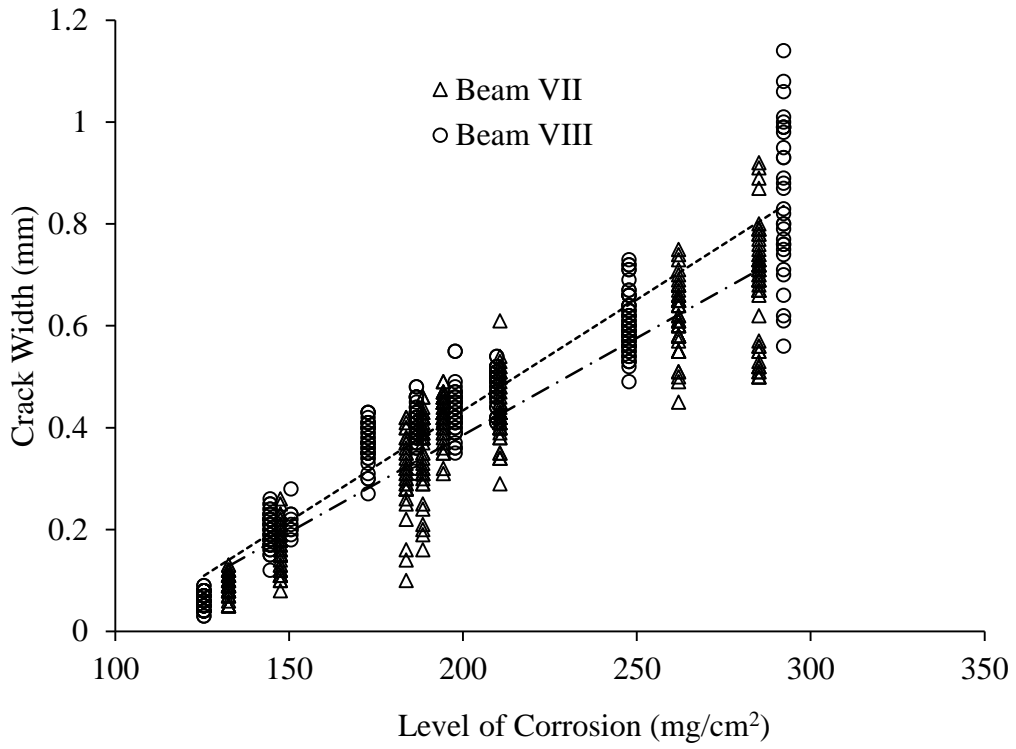
Figure 4.12: Surface Crack Propagation for C = 50 mm
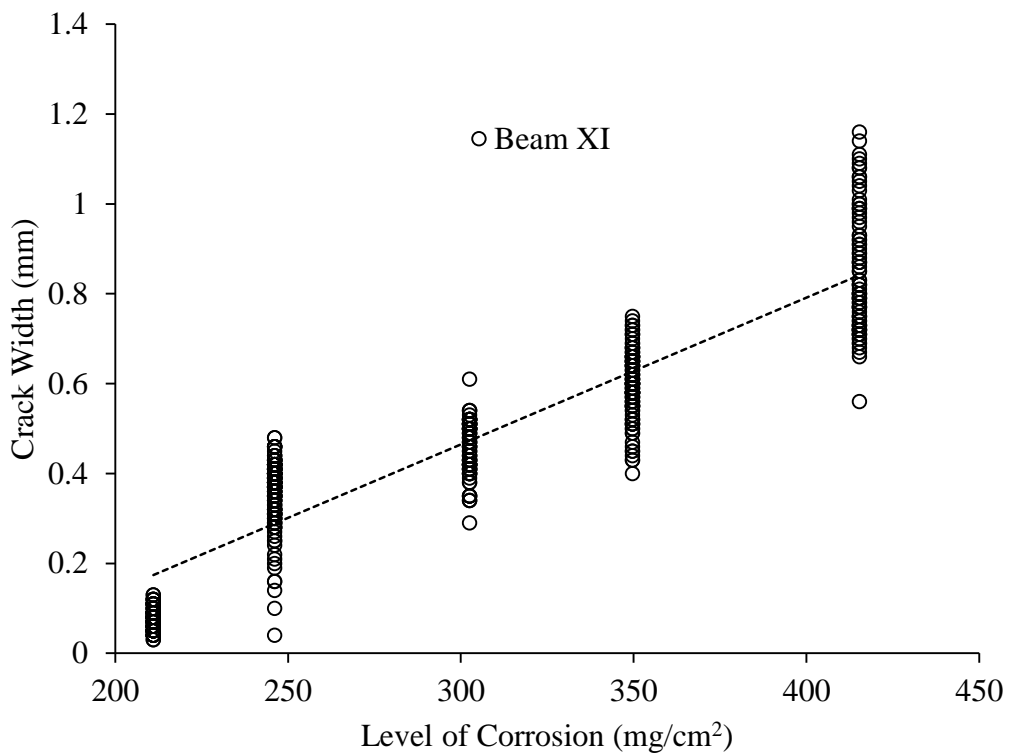
Figure 4.13: Surface Crack Propagation for C = 75 mm

4.3.4 Variation of Critical Corrosion for Cover Cracking

From Figure 4.10 to Figure 4.13 it was found that a certain amount of corrosion is needed for crack formation, which is known as critical corrosion amount. The variation between Critical Corrosion Amount and Cover Thickness is shown in Figure 4.14.
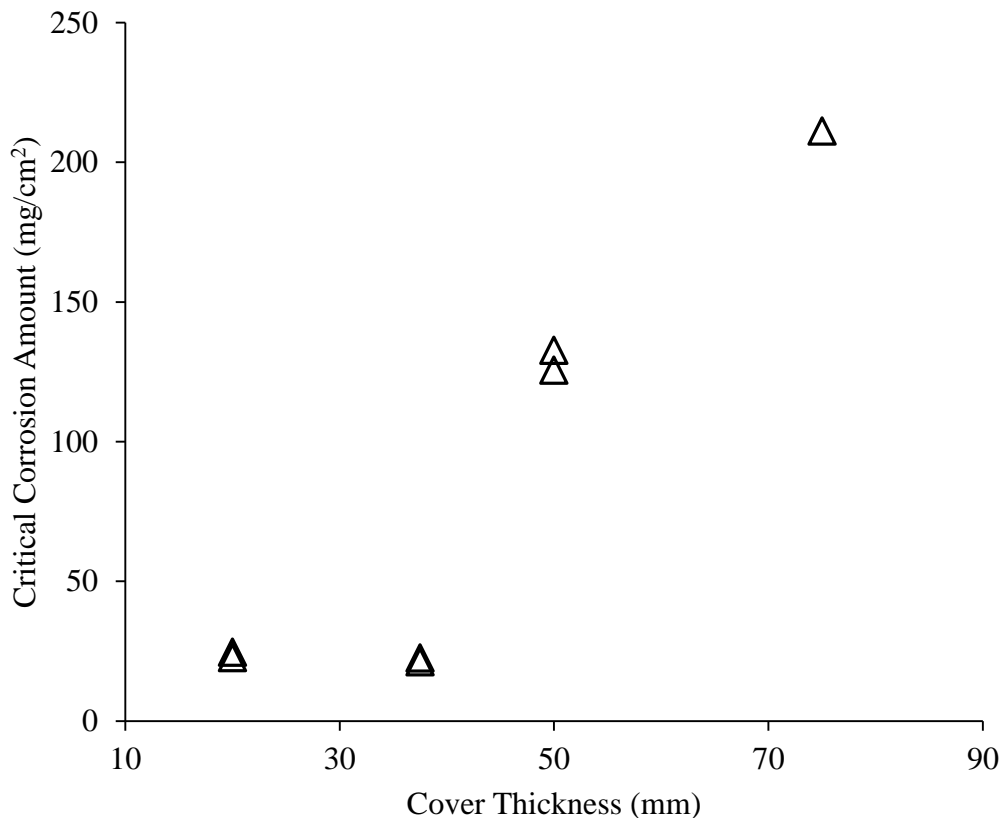
Figure 4.14: Relation between Critical Corrosion Amount and Cover Thickness

From the Figure 4.14 it is seen that mass loss of 22.7 mg/cm^2 and 24.7 mg/cm^2 was needed to initiate the crack for cover thickness 20 mm. For cover thickness 37.5 mm, 21.2 mg/cm^2 and 22.6 mg/cm^2 mass loss was needed to initiate crack. For an increase in cover from 37.5 mm to 50 mm, critical amount of corrosion increased drastically from 22 mg/cm^2 to 129 mg/cm^2. On the other hand for a cover thickness of 75 mm, amount of corrosion needed to initiate cracks was 211 mg/cm^2. The same pattern was found for a definite crack width of 0.3 mm shown in Figure 4.15. This 0.3 mm crack width was used because of the serviceability limit state (Andrade et al., 1993). The serviceability limit state is the controlling factor for evaluating structural repair or replacement due to corrosion (Val et al., 2009). Initiation of corrosion is an indication of serviceability failure (Maage et al., 1996). But it is difficult to identify the time to start the initiation if corrosion. Formation of a first crack in the concrete cover also an indicator

of serviceability limit sate (Liu & Weyers, 1998; Torres-Acosta & Martnez-Madrid, 2003). Since the time between corrosion initiation and the first cracking is usually short (experiment based), cracks formed immediately after their initiation are very small (width less than 0.05 mm). So that these cracks did not cause any danger or serviceability concern for a structure (Val et al., 2009). For this reason, formation of 0.3 mm crack, is considered as the serviceability limit state in this study.
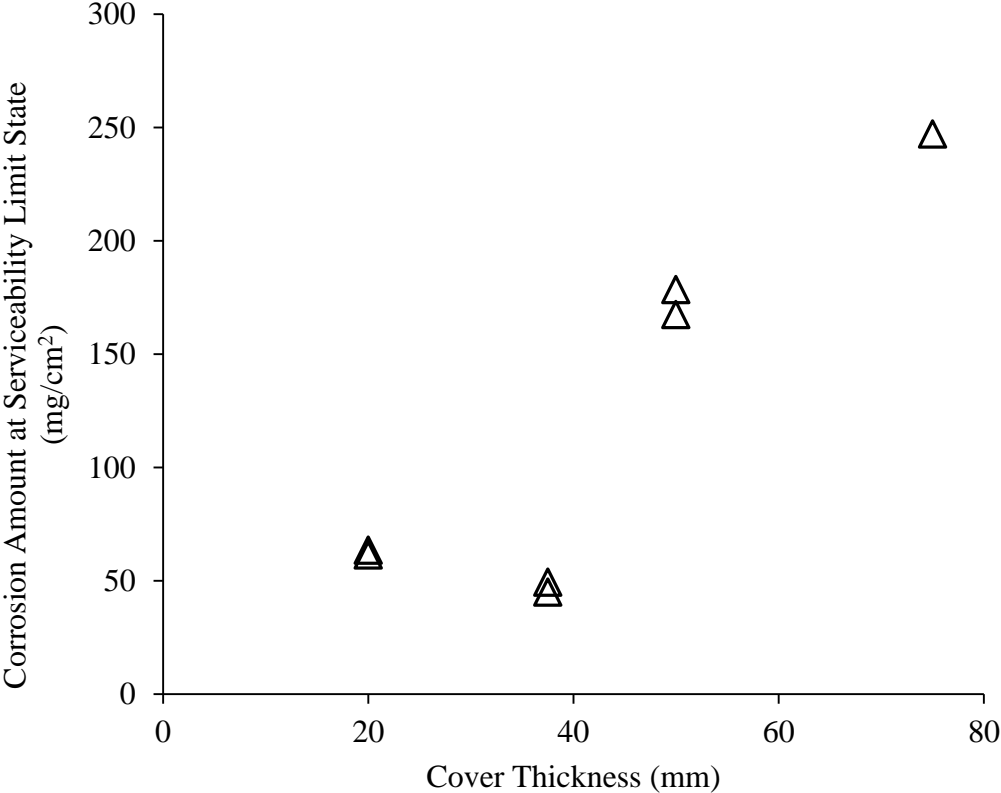
Figure 4.15: Relation between Corrosion Amount at Crack Width 0.3 mm and Cover Thickness

4.3.5 Patterns of Cracks

Cracks were found to be formed on the top surface along the reinforcement. The pattern of cracks are shown in Figure 4.16 to Figure 4.19 and the magnified view of the cracks are shown in Figure A1 to Figure A4, showing the level of corrosion as well as average width of crack. All the cracks were on the perpendicular plane of reinforcement.
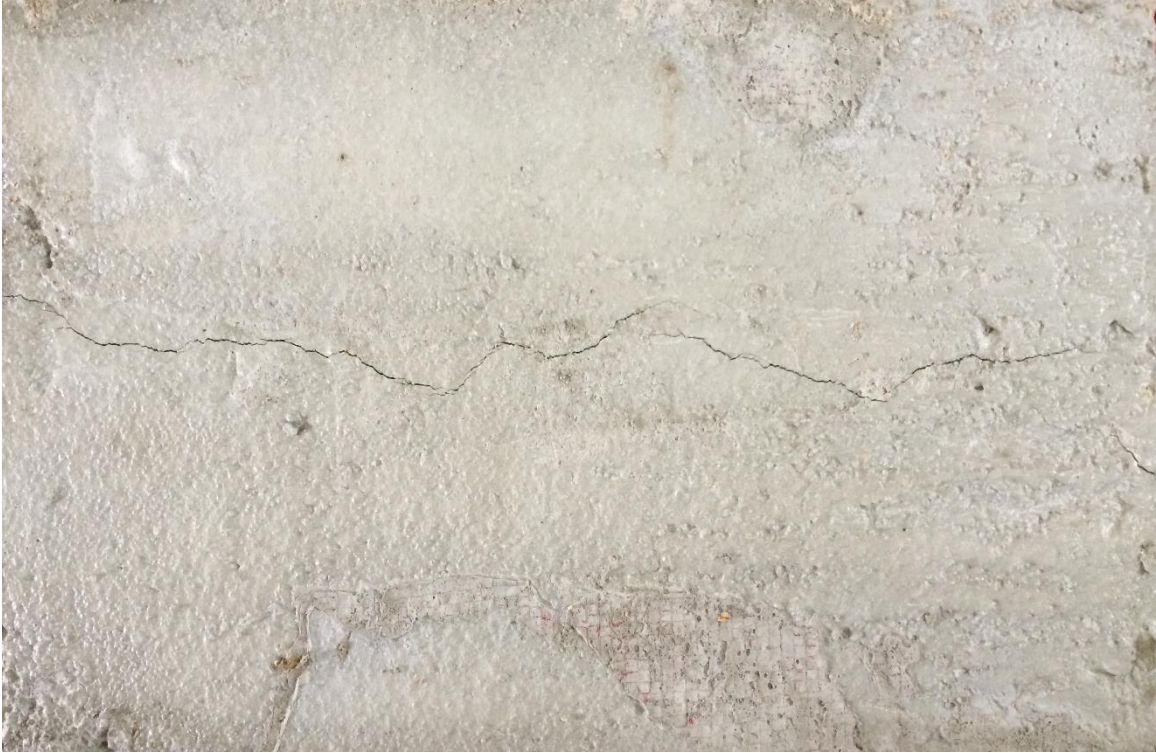
Figure 4.16: Longitudinal Crack Pattern of Beam I (C = 20 mm)

Figure 4.17: Longitudinal Crack Pattern of Beam V (C = 37.5 mm)

Figure 4.18: Longitudinal Crack Pattern of Beam VII (C = 50 mm)
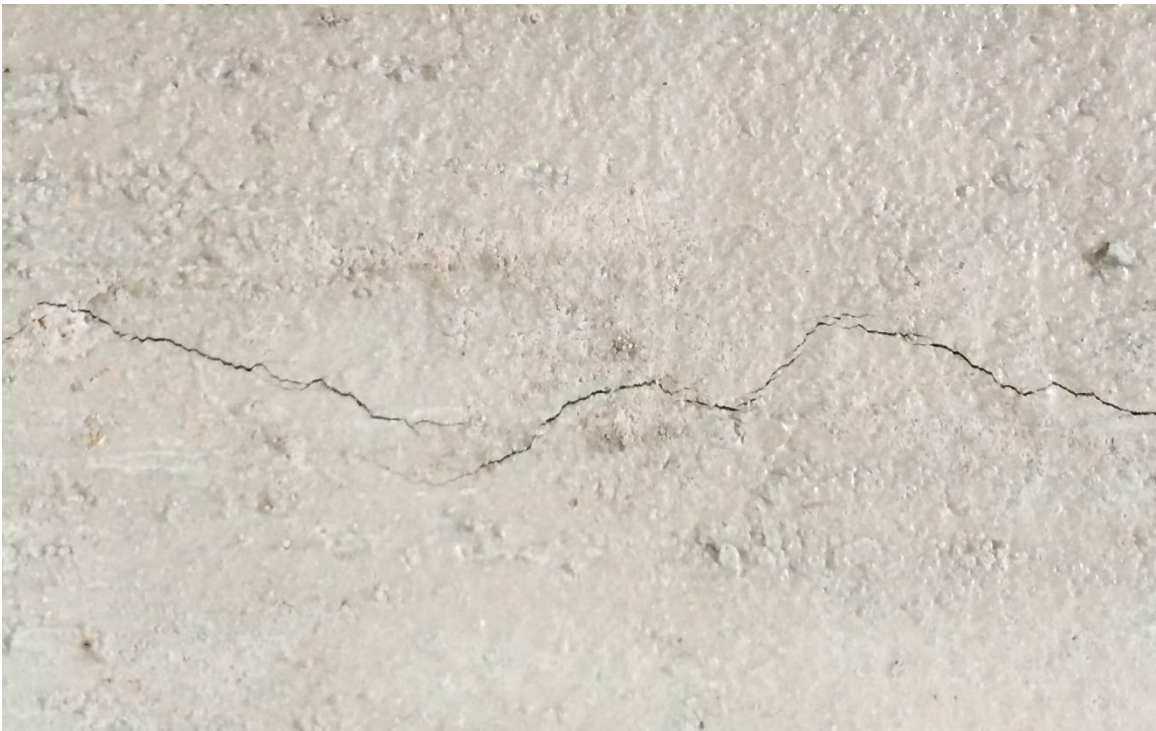
Figure 4.19: Longitudinal Crack Pattern of Beam XII (C = 75 mm)

On the other hand, a vertical crack was formed deep inside the beam as well. This observation is very much alarming, because this would affect the capacity of beam. The pattern of cracks ae shown in Figure 4.20 and Figure 4.21.
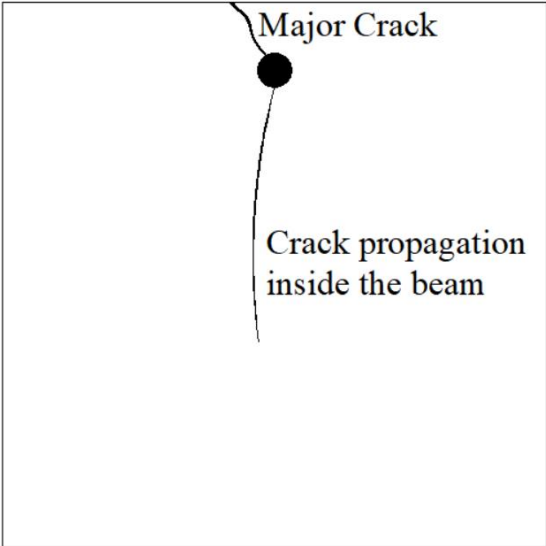
Figure 4.20: Propagation of Cracks inside the Beam (C = 20 mm)
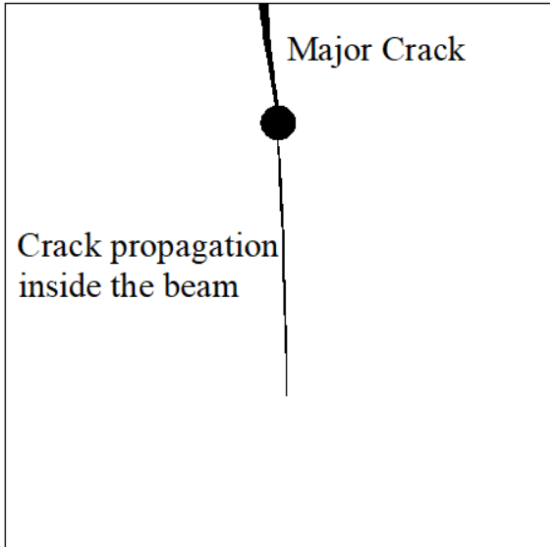
Figure 4.21: Propagation of Cracks inside the Beam (C = 37.5 mm)

4.4 Results of Plate Specimens

4.4.1 Thickness of Corrosion Products

The oxides formed due to corrosion of reinforcement occupy 2 to 6 times larger volume than the parent material. Information regarding the relation between the amount of corrosion and the thickness of corrosion products built up around the reinforcement are still limited. To understand the phenomenon cylindrical specimens were prepared. Color photographs, taken by the magnifying USB digital Microscope, could clearly illustrate the layer of corrosion products and the cracks formed due to expansive nature of corrosion products. The variation of thickness of corrosion products with respect to mass loss is shown in Figure 4.22. It is seen that a gradual increase in thickness of oxides due to increase in mass loss. The thickness was dependent on the type of oxide formed in the reaction.
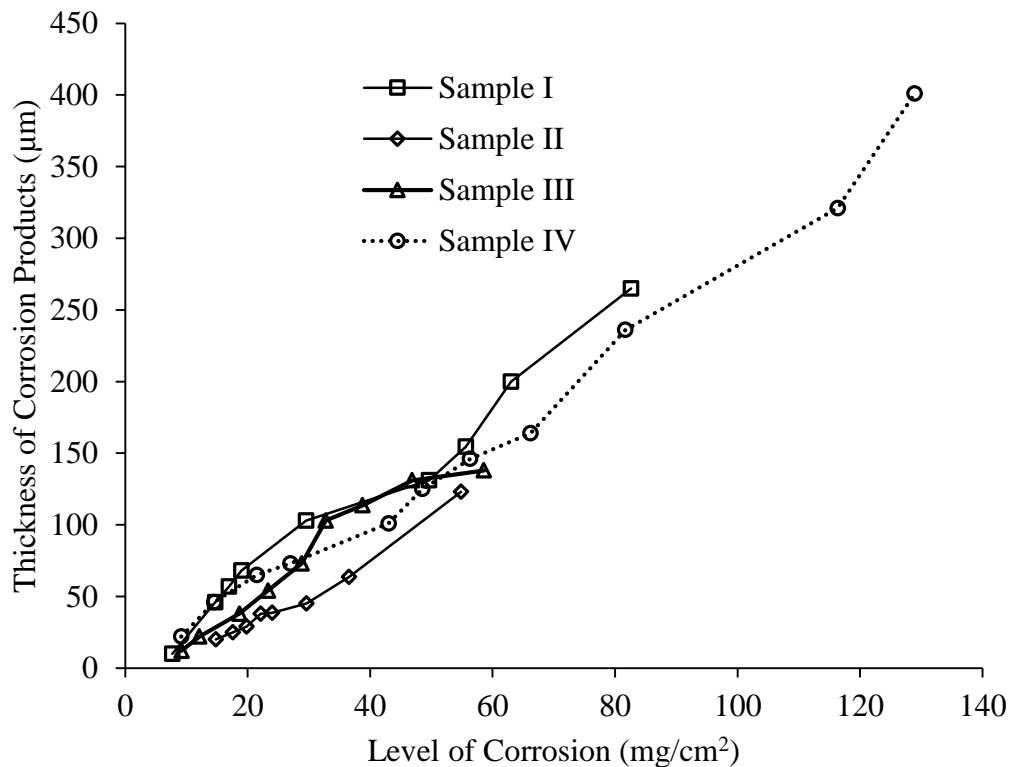
Figure 4.22: Variation of Thickness of Corrosion Products against Level of Corrosion

4.4.2 Cracking of Cover Concrete

With an increase in the amount of corrosion products, a visible crack is initiated from the concrete surface and propagated towards the reinforcement. This phenomenon was also observed in beam specimen for cover of 20 mm and 37.5 mm. The clear cover of cylindrical

plates were 44 mm. This was due to the bending of the surface. The surface crack width with respect to amount of corrosion is shown in Figure 4.27. It is found that the critical amount of corrosion for initiation of crack varied from 18.98 mg/cm^2 to 23.3 mg/cm^2 which was also observed for beam specimens having clear cover 20 mm and 37.5 mm. In addition, a crack of 0.3 mm width was formed for a corrosion level varied from 55 mg/cm^2 to 58 mg/cm^2. Relevant photographs are shown in Figure 4.28 regarding the cracks as well as formation of oxides around the reinforcement captured by digital microscope.
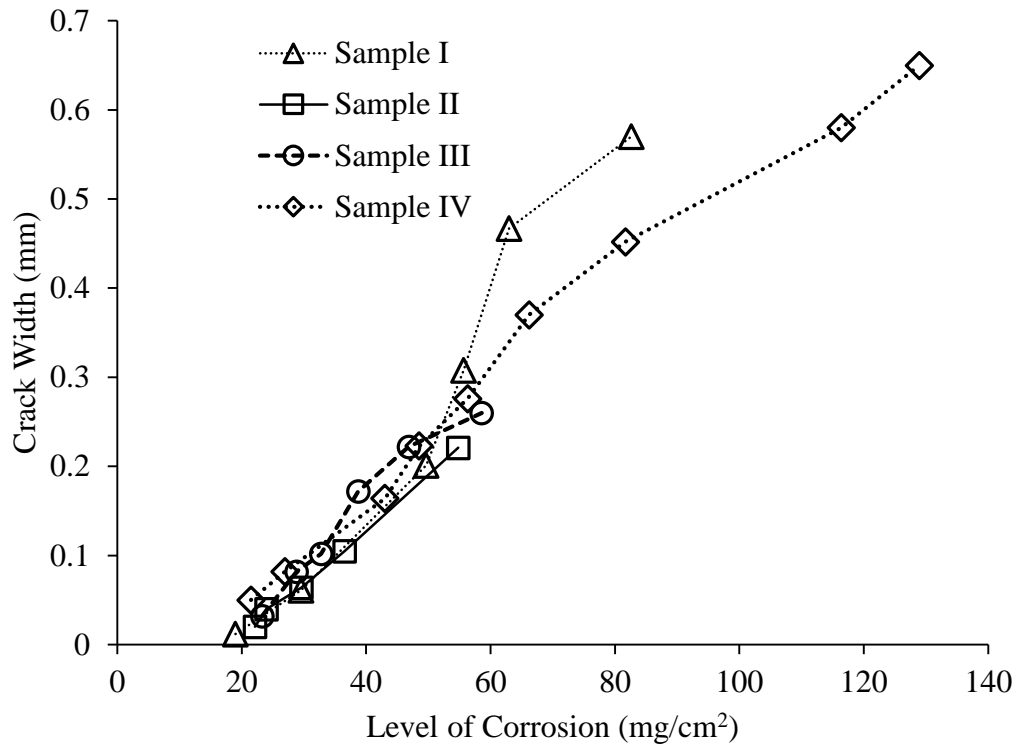
Figure 4.23: Surface Crack Propagation for Cylindrical Plates
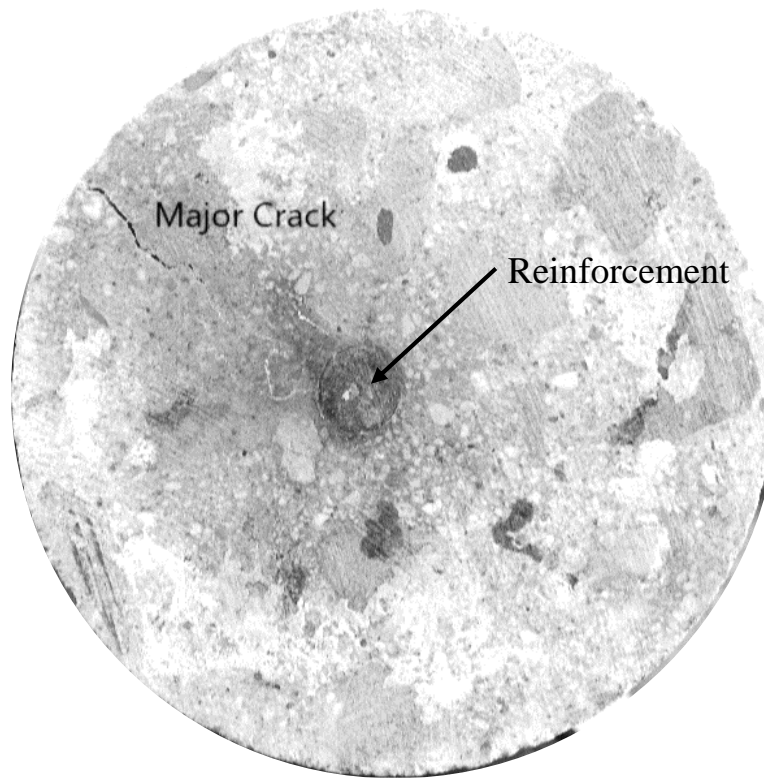
(a)

(b)
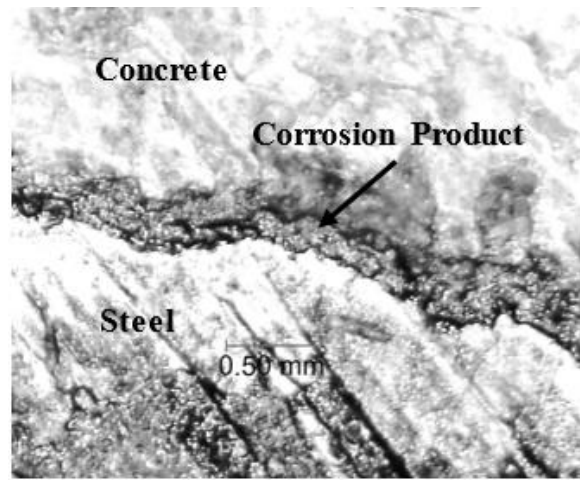
(c)

Figure 4.24: Crack Pattern of the Specimen (a) Cylindrical Plate Specimen (b) Crack Mouth Opening at Cover (c) Corrosion Product Build up at Steel Concrete Interface

4.4.3 Efficiency of Current

Gravimetric losses were measured in order to find out the relationship between actual mass loss and theoretical mass loss. The ratio of actual weight loss and theoretical weight loss is defined as efficiency of current. The results are shown in Table 4.2. The results showed that the current

efficiencies were higher than 100%. As the current efficiency was 100% when the samples were partially immersed in 3.5% NaCl for at least one day before starting test, almost all the samples showed just above 100% current efficiency. This results might be due to two effects. One is the acidification developed by the progressive corrosion and the other was parts of the steel that spalled out from the steel surface when the surrounding material is oxidizing (Alonso et al., 1998a). Few results showed below 100% efficiency. The current might be used to break down the water molecule instead of corrosion of reinforcement. The reason for diversion might be due to presence of insufficient chlorides adjacent to steel. It might also because of continuous generation of heat (Alonso et al., 1998a).

Table 4.2: Comparison of Theoretical and Actual Loss of Specimens

Specimen	Gravimetrical loss (gm)	Theoretical loss (gm)	Current Efficiency	Test time (hours)
Beam I	13.5	11.05	122.17	58.5
Beam II	12.2	12.09	100.91	65
Beam IV	7.7	6.28	122.61	46.5
Beam V	6.9	6.68	103.29	49
Beam VII	29.1	31.56	92.21	95.5
Beam VIII	30.6	32.34	94.62	98
Beam X	47.9	45.97	104.20	159.75
Cyl. Plate I	1.55	1.56	99.36	22.75
Cyl. Plate II	1.12	1.03	108.74	16.4
Cyl. Plate III	1.12	1.1	101.82	21
Cyl. Plate IV	2.45	2.42	101.24	32.2

CHAPTER 5

MODELING OF CORROSION INDUCED EXPANSIVE PRESSURE

5.1 Introduction

Corrosion of reinforcement occurrs due to either carbonation or chlorination. The corrosion products occupy a larger volume than that of parent material. The products that soluble to water, leaches out with water through the capillary pores of the concrete and stain the concrete surface which is the first indication of corrosion activity (Pantazopoulou & Papoulia, 2001) and the insoluble products cause the internal pressure on the concrete perpendicular to the concrete surface. When the tensile stress of concrete developed due to this pressure, exceeds its tensile strength crack would develop (Bhargava et al., 2006; Maaddawy & Soudki, 2003). The appearance of surface cracking is a common limit on the service life of reinforced concrete structures.

Corrosion of steel is a process of chemical reaction in which products consist of various oxides, collectively known as rust (Pantazopoulou & Papoulia, 2001), which expands as much as it's six times its original volume (Liu & Weyers, 1998) depending on the level of oxidation. The corrosion products diffuse into capillary voids in the concrete. If the total amount of corrosion products is less than the porous zone volume, free expansion occurs when there is no additional stress develops in concrete. However, when the products volume exceeds that of the porous zone, expansive stress is developed in concrete surrounding the reinforcing bars. Once the stress exceeds the tensile strength of concrete, cracking initiates (Bhargava et al., 2006). Therefore, RC structures exposed to aggressive environments are prone to fail before reaching the end of their service lives.

A variety of analytical models dealing with corrosion-induced concrete cover cracking is found in the literature (Bazant, 1979; Bhargava et al., 2006; Liu & Weyers, 1998; Pantazopoulou & Papoulia, 2001). Bazant (1979) proposed an analytical model to predict the time of the cover cracking caused by corrosion of embedded reinforcing steel. Another model was developed by Bhargava et al. (2006) to predict the time required for cover cracking and the weight loss of reinforcement.

Dagher and Kulendran (1987) simulated the corrosion-induced fracture of concrete via finite element analysis where the smeared crack approach was employed for fracture analysis. The model considered only the radial expansive deformation around the reinforcing bar induced by corrosion while other loadings, such as dead and live loads, were not included. Du et al. (2006) presented a two-dimensional (2D) finite element (FE) model under a plane strain assumption to idealize three-dimensional physical specimens, tested by the simulated method and investigated the development mechanism of the concrete cracking. The model was then employed to predict test results from reinforced concrete accelerated corrosion. Val et al. (2009), considered crack initiation and propagation as a 2D problem—plain strain formulation. The model was mainly employed to predict the thickness of the concrete porous zone and volume of corrosion product penetrating into the concrete pores before crack initiation.

A schematic diagram of the mechanical process of the corrosion product expansion due to corrosion is shown in Figure 5.1. The steel might be considered as a metal cylinder with an initial radius 'r', immersed in a semi-infinite concrete medium with a cover 'c', and undergoing corrosion. As corrosion progresses, the radius decreases by an amount 'x' (corrosion penetration). However, corrosion products occupy a volume that is larger than the original metal. The final volume increase corresponds to an increase 'dr', over the initial rebar radius, for a total value of, 'r+dr'. The surrounding concrete is stressed by this effective radial expansion and provokes the concrete-cover cracking and spalling. This work contributes to the study of the pressure and deformation needed to crack a certain cover and to confirm a predictive model for corrosion penetration taking into account specimen dimensions and fracture mechanic properties of the concrete. The proposed model has been validated against experimental works.
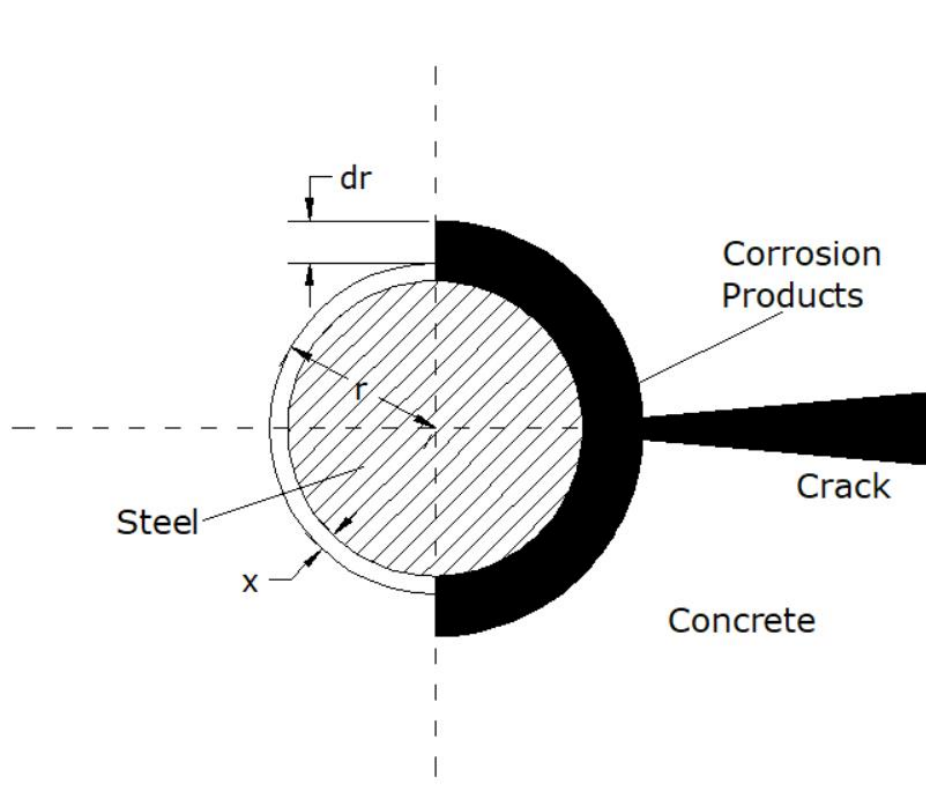
Figure 5.1: Representation of a Cross-Section of a Corroded Rebar with Expansive Oxides

5.2   Constitutive Modeling of Concrete

Commercial software ABAQUS was employed as a modeling platform. The software is capable of simulating the damage using either of the three crack models for reinforced concrete elements: (1) Smeared crack concrete model, (2) Brittle crack concrete model, and (3) Concrete damaged plasticity model. Concrete damaged plasticity is very much appropriate when the concrete is subjected to monotonic, cyclic and dynamic loading under low confining pressure. This method comprises of the combination of non-associated multi-hardening plasticity and scalar damaged elasticity to describe the irreversible damage that occurrs during the fracturing process (ABAQUS Inc., 2010). Due to this vast application and relevancy with the failure mechanism of concrete due to corrosion, the concrete damaged plasticity model was selected in the present study.

The concrete damaged plasticity model assumes two main failure mechanisms in concrete: the tensile cracking and the compressive crushing.   In this model, the uniaxial tensile and compressive behaviour was characterized by damaged plasticity.

In general, the nonlinearity of concrete under compression was modeled by approaches based on the concept of either damage or plasticity, or both (Yu et al., 2010a) which is shown in Figure 5.2. Yu et al., (2010a) defined Plasticity as the unrecoverable deformation after all loads have been removed and Damaged as the reduction of elastic constants. In order to present the inelastic behaviour of concrete, the concrete damaged plasticity model uses concepts of isotropic damage in combination with isotropic tensile and compressive plasticity (Yu et al., 2010a). The key aspects of this model are compressive and tensile behaviour of concrete as well as the hardening/softening rule, the damage function, the yield criterion, and the flow rule, which are summarized as follows.

| (a) | Plasticity Model | (b) | Damage Model | (c) | Plastic Damage Model |
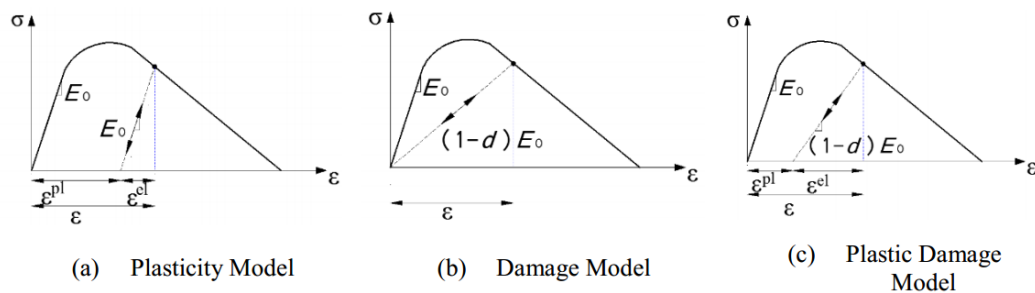
Figure 5.2: Representation of Concrete Damaged Plasticity Model

5.2.1 Compressive and Tensile Behaviour of Concrete

The damaged plasticity was an indication of behaviour of concrete under uniaxial tension and compression, which is shown in Figure 5.3. Under uniaxial tension, the stress-strain response follows a linear elastic relationship until the failure stress, σ_{t0}. There is a formation of microcrack when the maximum in-plane stress has reached the failure stress. Beyond the failure stress, the formation of micro-cracks is represented by a softening stress-strain response, which induces strain localization in the concrete structure. Under uniaxial compression, the response is linear until the value of the initial yield, σ_{c0}. In the plastic regime, the response is typically characterized by stress hardening followed by strain softening beyond the ultimate stress, σ_{cu}.
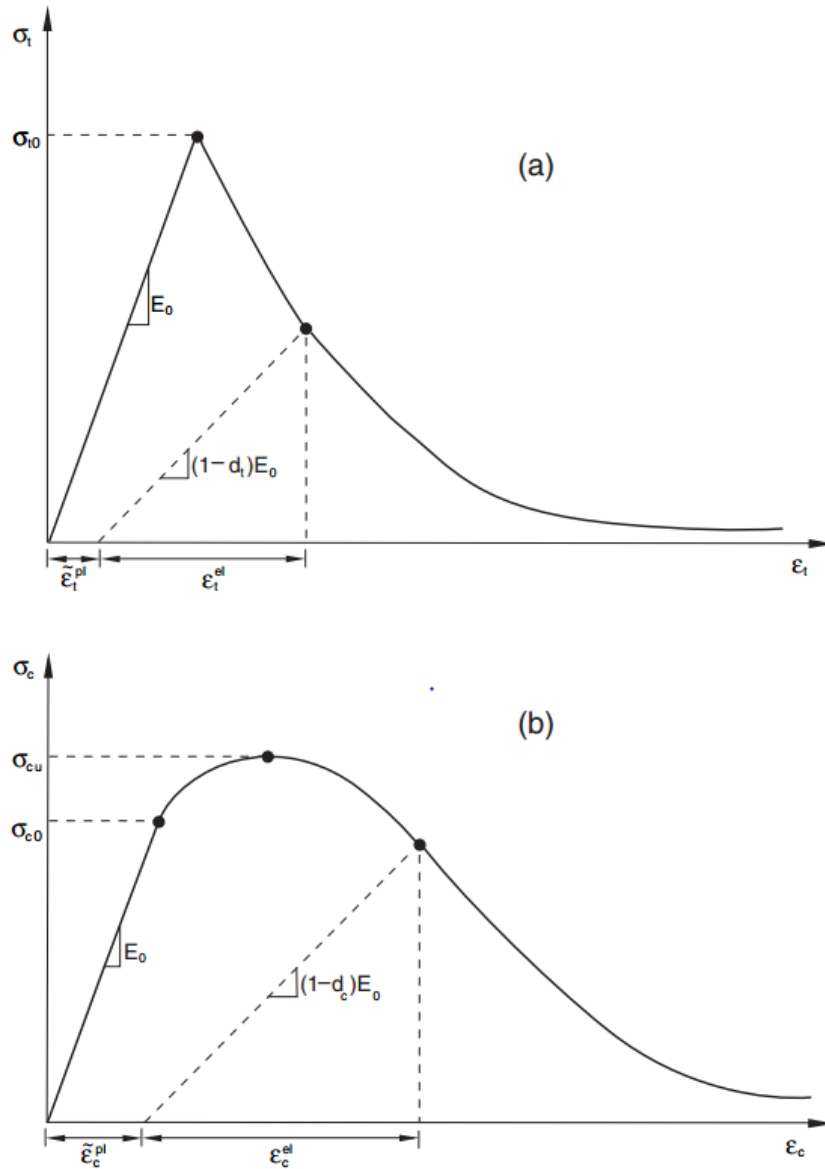
Figure 5.3: Response of Concrete to Uniaxial Loading in (a) Tension and (b) Compression

5.2.2 Damage

As shown in Figure 5.3, when the concrete specimen is unloaded from any point on the strain softening branch of the stress-strain curves, the unloading response is weakened: the elastic stiffness of the material appears to be damaged (or degraded). The degradation of the elastic stiffness is characterized by two damage variables, d_c and d_t, which are assumed to be functions of the plastic strains, temperature, and field variables:

$$d_t = d_t(\tilde{\varepsilon}_t^{pl}, \theta, f_i); \quad 0 \leq d_t \leq 1,$$
$$d_c = d_c(\tilde{\varepsilon}_c^{pl}, \theta, f_i); \quad 0 \leq d_c \leq 1. \quad\ldots\ldots\ldots\ldots\ldots\ldots\ldots\ldots\ldots\ldots\ldots\ldots\ldots\ldots\ldots\ldots\ldots\ldots(5.1)$$

The values of damage variables varies from zero, representing the undamaged material, to one, which represents total loss of strength.

If E_0 is the initial (undamaged) elastic stiffness of the material, the stress-strain relations under uniaxial tension and compression loading are, respectively:

$$\sigma_t = (1 - d_t)E_0(\varepsilon_t - \tilde{\varepsilon}_t^{pl}),$$
$$\sigma_c = (1 - d_c)E_0(\varepsilon_c - \tilde{\varepsilon}_c^{pl}).$$ …..……………………………………....…...……………….....(5.2)

This model assumes that the main two failure mechanisms are tensile cracking and compressive crushing of the concrete material. The evolution of the yield (or failure) surface is controlled by two hardening variables, $\tilde{\varepsilon}_t^{pl}$ and $\tilde{\varepsilon}_c^{pl}$, linked to failure mechanisms under tension and compression loading, respectively. $\tilde{\varepsilon}_t^{pl}$ and $\tilde{\varepsilon}_c^{pl}$ are tensile and compressive equivalent plastic strains, respectively. Abaqus automatically converts the tensile cracking strain ($\tilde{\varepsilon}_t^{ck}$) and compressive inelastic strain ($\tilde{\varepsilon}_c^{in}$) values to plastic strain values using the following relationships,

$$\tilde{\varepsilon}_t^{pl} = \tilde{\varepsilon}_t^{ck} - \frac{d_t}{(1 - d_t)}\frac{\sigma_t}{E_0}.$$

$$\tilde{\varepsilon}_c^{pl} = \tilde{\varepsilon}_c^{in} - \frac{d_c}{(1 - d_c)}\frac{\sigma_c}{E_0}.$$ …..………………………………………...…............................…….(5.3)

The cracking strain is defined as the total strain minus the elastic strain corresponding to the undamaged material; that is $\tilde{\varepsilon}_t^{ck} = \varepsilon_t - \varepsilon_{0t}^{el}$, where, $\varepsilon_{0t}^{el} = \sigma_t/E_0$, the Elastic strain corresponding to the undamaged material, ε_t = total tensile strain which is shown in Figure 5.4(a). The compressive inelastic strain is defined as the total strain minus the elastic strain corresponding to the undamaged material, $\tilde{\varepsilon}_c^{in} = \varepsilon_c - \varepsilon_{0c}^{el}$, where, $\varepsilon_{0c}^{el} = \sigma_c/E_0$, Elastic strain corresponding to the undamaged material and ε_c = Total tensile strain as illustrated in Figure 5.4(b).
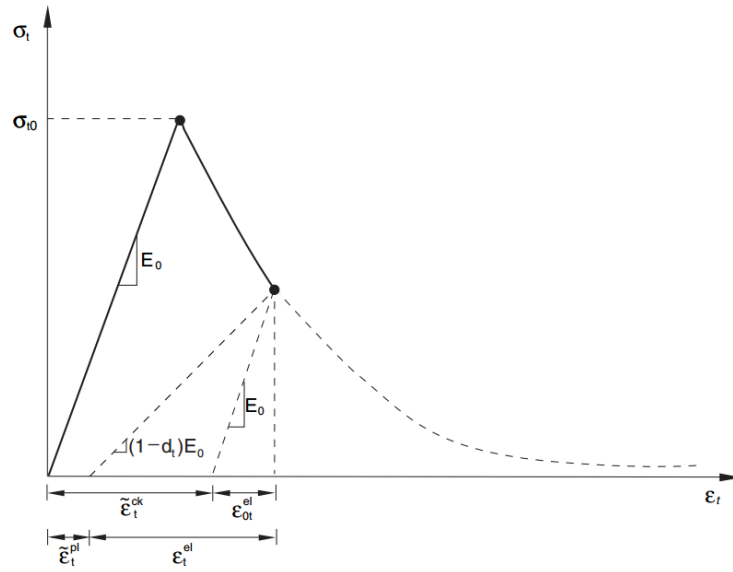
(a)
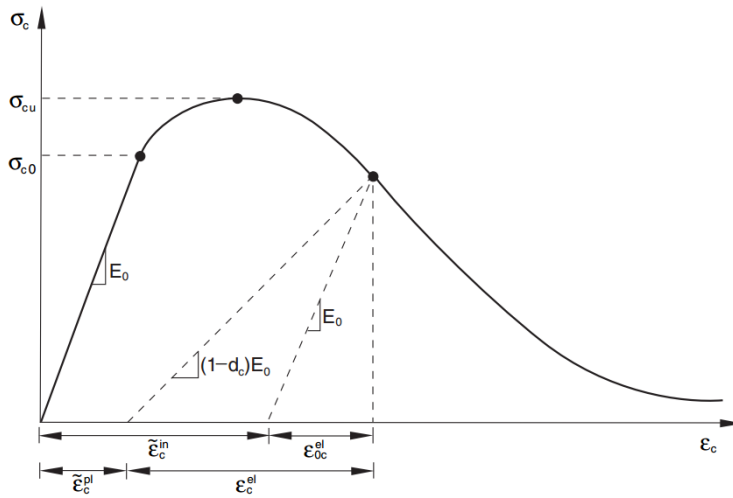
(b)

Figure 5.4: Illustration of (a) Cracking Strain ($\tilde{\varepsilon}_t^{ck}$) and (b) Inelastic Strain ($\tilde{\varepsilon}_c^{in}$)

5.2.3 Yield Function

The model used the yield function of Lubliner et. al. (1989), with the modifications proposed by Lee and Fenves (1998) to account for different evolution of strength under tension and compression. The evolution of the yield surface was controlled by the hardening variables, $\tilde{\varepsilon}_t^{pl}$ and $\tilde{\varepsilon}_c^{pl}$. In terms of effective stresses, the yield function took the form

$$F = \frac{1}{1-\alpha}\left(\bar{q} - 3\alpha\bar{p} + \beta(\tilde{\varepsilon}^{pl})\langle\hat{\bar{\sigma}}_{\max}\rangle - \gamma\langle-\hat{\bar{\sigma}}_{\max}\rangle\right) - \bar{\sigma}_c(\tilde{\varepsilon}_c^{pl}) = 0,$$

................……(5.4)

Where,

$$\alpha = \frac{(\sigma_{b0}/\sigma_{c0}) - 1}{2(\sigma_{b0}/\sigma_{c0}) - 1}; \ 0 \leq \alpha \leq 0.5,$$

$$\beta = \frac{\bar{\sigma}_c(\tilde{\varepsilon}_c^{pl})}{\bar{\sigma}_t(\tilde{\varepsilon}_t^{pl})}(1 - \alpha) - (1 + \alpha),$$

$$\gamma = \frac{3(1 - K_c)}{2K_c - 1}.$$

Where, $\hat{\bar{\sigma}}_{max}$ was the maximum principal effective stress; σ_{b0}/σ_{c0} was the ratio of initial equibiaxial compressive yield stress to initial uniaxial compressive yield stress (the default value is 1.16); K_c was the ratio of the second stress invariant on the tensile meridian, $q_{(TM)}$, to that on the compressive meridian $q_{(CM)}$. It must satisfy the condition $0<K_c\leq1$ (the default value is 2/3); $\bar{\sigma}_t(\tilde{\varepsilon}_t^{pl})$ and $\bar{\sigma}_c(\tilde{\varepsilon}_c^{pl})$ were the effective tensile and compressive cohesion stresses respectively. Typical yield surfaces in the deviatoric plane are shown in Figure 5.5 for different values of K.
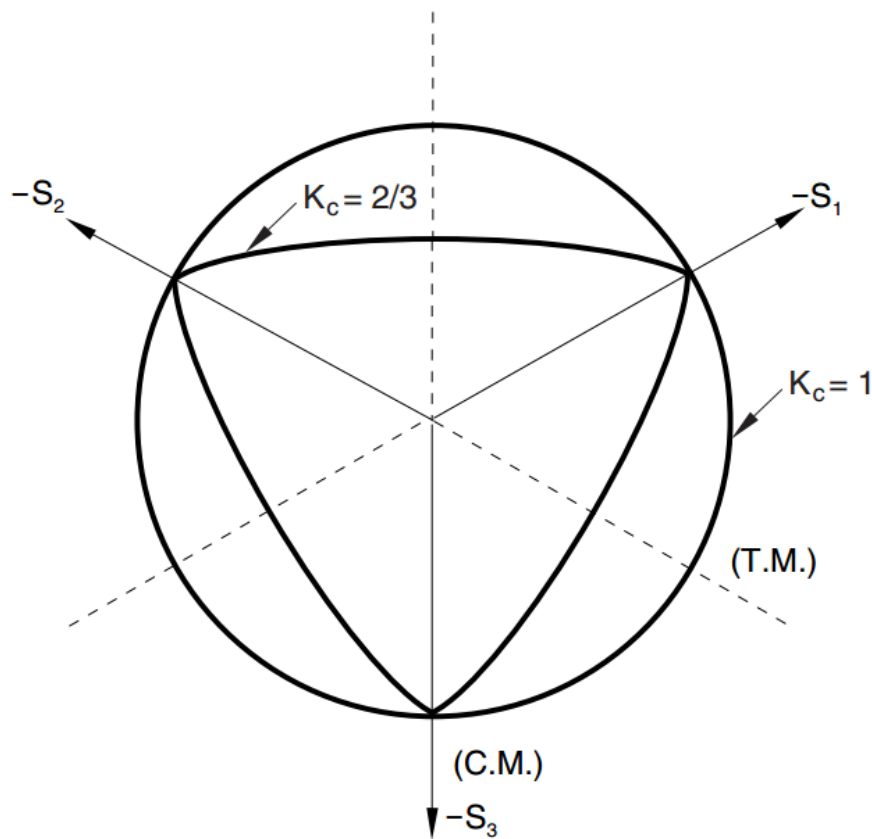

Figure 5.5: Yield Surfaces in the Deviatoric Plane, corresponding to Different Values of K_c (ABAQUS Inc., 2010)

5.2.4 Flow Rule

The concrete damaged plasticity model assumed non-associated potential plastic flow. The flow potential G used for this model was the Drucker-Prager hyperbolic function:

$$G = \sqrt{(\epsilon\sigma_{t0} \tan \psi)^2 + \bar{q}^2} - \bar{p} \tan \psi,$$

....……(5.5)

Where, ψ, was the dilation angle measured in the p–q plane at high confining pressure; σ_{t0}, was the uniaxial tensile stress at failure; ϵ, was a parameter, referred to as the eccentricity, that defined the rate at which the function approaches the asymptote (the flow potential tends to a straight line as the eccentricity tends to zero). The default value was 0.1.

5.3 Numerical Model Inputs of Concrete

To define the elastic part of concrete there were two values to be input, the modulus of elasticity and the poisons ratio. The change in volume of concrete controlled by the Poisson's ratio for the stresses below the critical value. After reaching the critical stress the concrete exhibited an increase in plastic volume. Generally Poisson's ratio ranges from 0.14 to 0.26 for normal weight concrete and 0.20 is applicable to take into consideration the influence of crack formation at the ultimate limit state (ULS) (FIP Model Code, 2010). The elastic modulus was estimated based on compressive strength by the equation given by, ACI 318-02., 2002,

$E_c = 57000\sqrt{f'c}$ psi...……(5.6)

The Concrete Damaged Plasticity Model required concrete compressive and tensile constitutive relationship, cracking and crushing damage parameters and special parameters such as dilation angle, eccentricity, biaxial loading ratio, the coefficient K_c and viscosity parameter to input. The value of the eccentricity of potential surface was used as 0.1 which is default value in Abaqus. The ratio of initial biaxial compressive yield stress to initial uniaxial compressive yield stress, σ_{b0}/σ_{c0} and the ratio of the second stress invariant on the tensile meridian to compressive meridian at initial yield, K_c should be defined based on the biaxial and triaxial tests respectively. In this study the default values of σ_{b0}/σ_{c0} and K_c was used and the default values were 1.16 and 0.667 respectively. The viscosity was an important parameter to solve the convergence problem. A low viscosity parameter helped to improve the convergence rate in the softening regime of concrete stress-strain curve. In this study it was determined with sensitivity analysis.

In the literature there were numerous analytical constitutive models suggested for concrete material (Ernst & Sohn, 2010; Lee & Fenves, 1998; Yang & Chen, 2005; Yu et al., 2010b). In this study, the unconfined stress-strain relationship model for concrete proposed by Popovics (1973) was used. According to this model, the relation between compressive strain (ε_c) and stress (fc) is given by

$$\frac{f_c}{f_c'} = \frac{n\left(\dfrac{\varepsilon_c}{\varepsilon_{co}}\right)}{(n-1)+\left(\dfrac{\varepsilon_c}{\varepsilon_{co}}\right)^n}$$ ....……….(5.7)

where f'$_c$, ε_{co} are the compressive strength in psi and strain corresponding to the maximum stress, respectively. The 'n' is defined by,

$$n = 0.4 \times 10^{-3} f_c'(\text{psi}) + 1.0$$ ....……………….….(5.8)

Tensile stress-strain (σ-ε) relationship was assumed to be linear up to the uniaxial tensile strength and then was determined using the exponential function (Dere & Koroglu, 2017)

$$\sigma = f_t\left(\frac{\varepsilon_t}{\varepsilon}\right)^{(0.7+1000\varepsilon)} , \quad \varepsilon_t = \frac{f_t}{E_c}$$ ....……….(5.9)

Where f$_t$ is the tensile strength of concrete in psi which was measured experimentally in accordance with the ASTM C426 and in case of inability to measure f$_t$ experimentally, the value was estimated by the following equation (Oluokun et al., 1991)

$$f_t = 1.38\,(f'_c)^{0.69}$$...………….(5.10)

5.4 Model Geometry and Validation

In this study crack initiation and propagation are considered as a 2D problem—plain strain formulation. Since this study focuses on the analysis of RC beams subject to accelerated corrosion tests, in which uniformity of corrosion is considered along the beam length, the 2D simplification is suitable. For modelling natural corrosion, which may not be uniform along the length of RC elements, the use of a 3D formulation could be more appropriate. The model was implemented in ABAQUS—a commercial software package for nonlinear FE analysis. A 3-node linear plane strain triangle was used to represent concrete. A sensitivity analysis was done

to find out the optimum mesh size. A 0.05 mm and 0.01 mm mesh showed similar results and for this reason 0.05 mm mesh size was used in this study as optimized mesh to reduce time consumption. To represent the condition of real beam, one edge of the model was restrained by implying a hinge support as shown in Figure 5.6 (d).

The two-dimensional (2D) finite element model was verified through comparison of critical pressure required to crack the concrete cover by numerical analysis with the experimental values. The test specimens were cubes with edge length 150 mm and a cylindrical hole located at one corner with diameter of 16 mm, as shown in Figure 5.6. The concrete cover thicknesses of the specimens were selected as 37.5 mm, 48 mm and 64 mm. A uniform and gradually increasing outward deformation was applied into the holes to simulate the expansion induced by corrosion of steel bars.
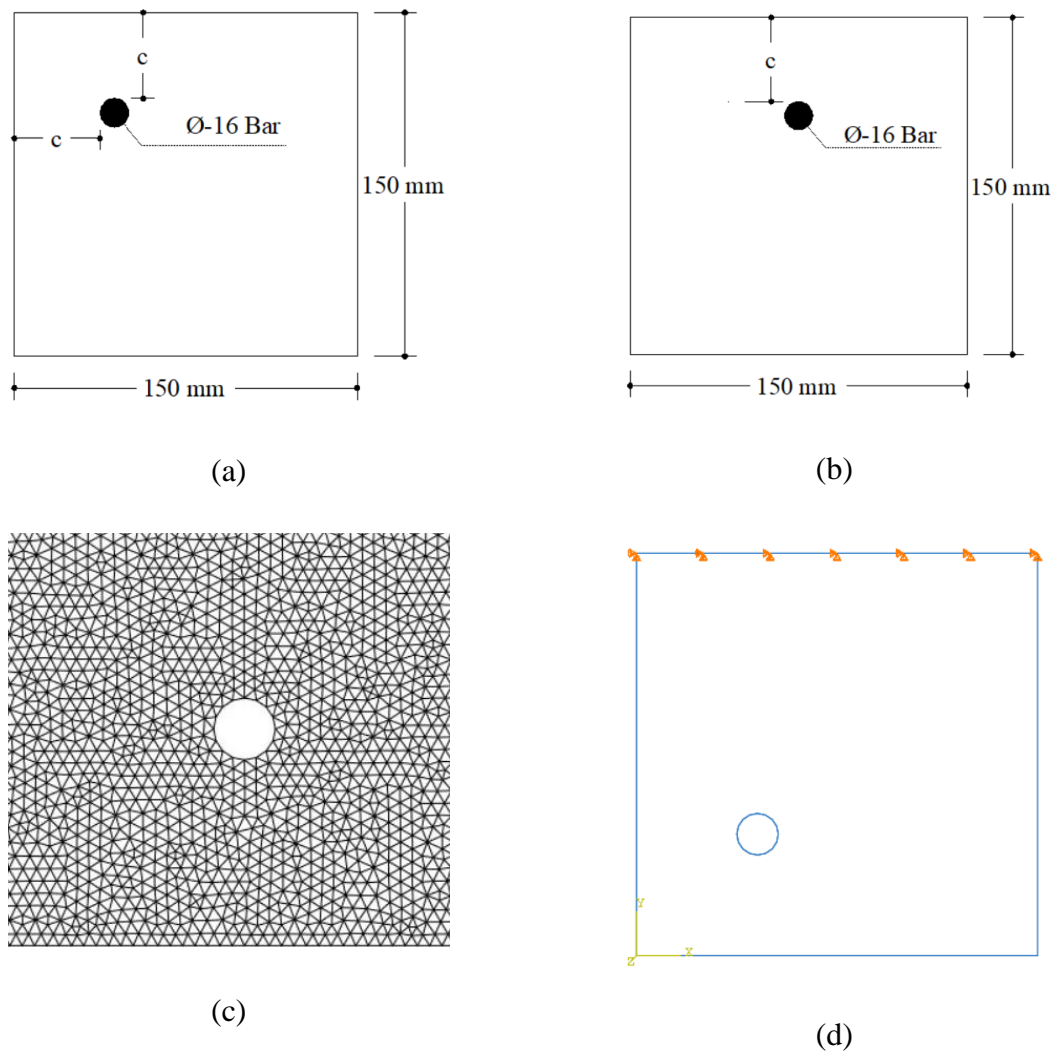

Figure 5.6: Specimens' Dimensions (a) Specimens for Corner Bar (b) Specimens for Side Bar (c) Meshing & (d) Boundary Condition Applied

In order to validate the model it was necessary to compare it with experimental results. However, a quantitative comparison with actual corrosion tests was difficult. Corrosion-induced cracking occurred because corrosion products had a larger volume than the original iron compound of a corroding reinforcing bar. Thus, as corrosion progresses the volume occupied by the corrosion products accumulating around the reinforcing bar increases. This creates increasing pressure on the surrounding concrete, which eventually lead to the concrete cracking. An investigation was done to measure the critical pressure for which the cover concrete began to crack. A cylindrical hole was created to represent as a reinforcement and hydraulic pressure was applied to simulate the pressure exerted due to corrosion of reinforcement. The critical pressure so found was used to validate the numerical model.

5.4.1 Experimental Program

5.4.1.1 Sample Preparation

Three types of concrete were used in this investigation, C12, C16, C20. ASTM Type I (Ordinary Portland Cement) was used as binder material. River sand having FM of 2.80 was used as fine aggregate and crushed stone of 19 mm downgrade was used as coarse aggregate. The compressive strength of concrete was tested according to ASTM C39 and the splitting tensile strength test (ASTM C426) was used to measure the tensile strength of concrete. All the specimens were 150 mm cubes. Schematic diagram of specimen is shown in Figure 5.7. The location of the bars was confirmed by fabricating a 16 mm diameter plain bar and firmly lubricated so that it can be removed easily leaving a cylindrical hole which was used to simulate corrosion pressure. For the purpose of providing barrier against leakage through the contact surface of cylindrical hole and the plate at the bottom surface of the specimens, the hole was 100 mm in length and a 25 mm cover was provided. The detailed test program is shown in Table 5.1. There were two locations of reinforcement chosen to simulate corrosion, one was side bar with various clear covers and the other was corner reinforcement with the same clear cover on both side. All the specimens were wet cured and tested after 28 days.

Table 5.1: Test Specimens

| Bar size (mm)	Bar Location	c/d	Concrete types
16	corner	2.34, 3, 4	C12, C16, C20
	side	2.34, 3, 4	C12, C16
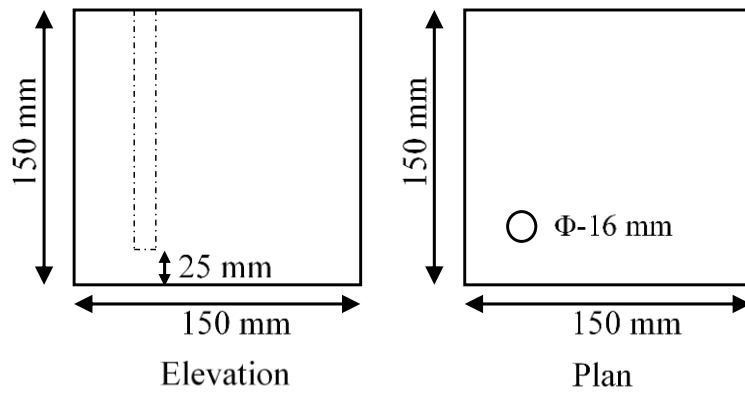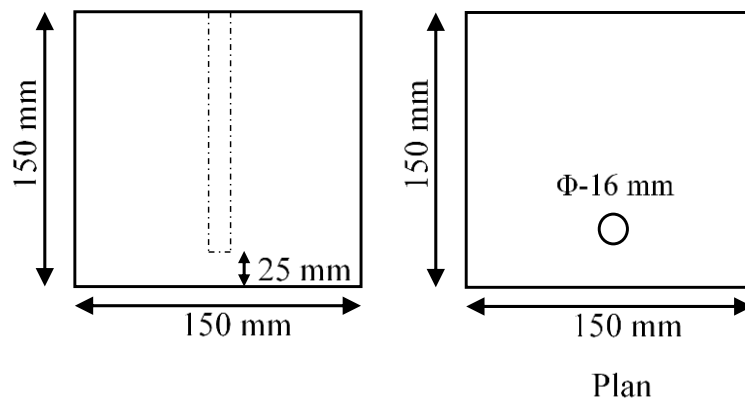
Figure 5.7: Schematic Diagrams of Specimens (a) for Corner Bars (b) for Side Bars (c) Casted Samples

5.4.1.2 Experimental set up

The pressure induced due to the corrosion of reinforcement was characterized by applying a hydraulic pressure through the hole of the specimens and the pressure at which failure of concrete occurred was identified as the critical pressure. The pressure was applied by using a hand pump. A uniform corrosion was modelled by pressurizing through the cylindrical hole. The schematic diagram of the setup is shown in figure 5.8. The end plates were fastened by steel bolt and to resist the longitudinal expansion. The loading rate of the hand pump with mounted pressure gauge was maintained at 0.5 MPa/sec. The maximum pressure sustained by the specimens was the critical load which criteria was also used by Williamson and Clark (2000a). At the time at failure, the liquid came out through the cracks.
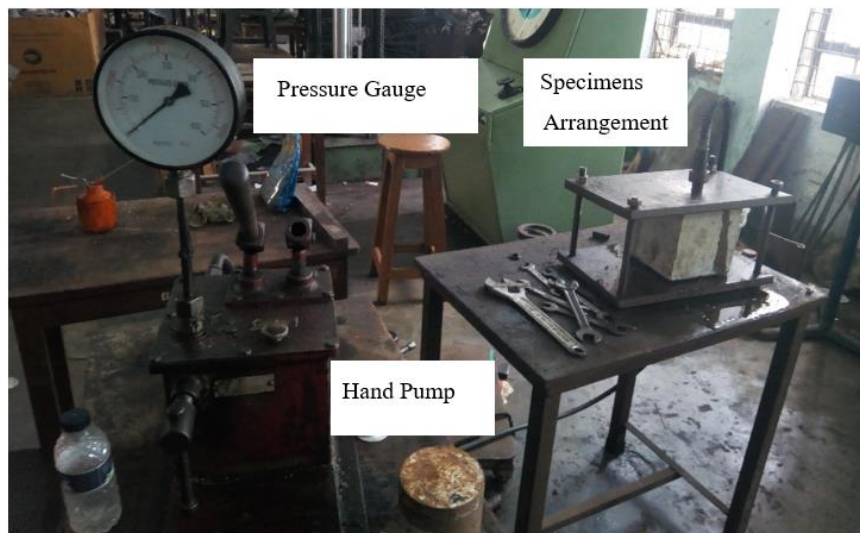
(a)

(b)

(c)

Figure 5.8: Experimental Setup (a) Full Setup (b) Specimen Fastened with End Plates (c) Pressure Gauge

5.4.2 Experimental Results and Validation of Numerical Results

The results of experiment and the variation with the numerical ones are shown in Figure 5.9 and Figure 5.10. Figure 5.9 shows the results for side bars and Figure 5.10 shows the results for corner bars. The pressure needed to initiate crack, known as critical pressure, was increased for increasing both the clear cover and grade of concrete. Numerical results showed the same patterns. The agreement of numerical results with the experimental ones are given in Table 5.2. The percent variation of critical pressure differed from 12 to 30%. The cracking of concrete was mainly dependent on the tensile strength of concrete. Tensile strength of concrete very much dependent on the method of testing (Val et al., 2009). In the experimental works, the splitting tensile strength was used and the results was also employed in the Finite Element analysis. Whereas in the Finite Element analysis, based on Rankine's criteria, the direct tensile strength was appropriate (Val et al., 2009). The variation of the results might be due to the differences in the boundary conditions between the experiment and numerical model. In the experimental investigations, only plain strain condition was maintained and the edges were kept in free. Whereas in the modeling, single edge was restrained against horizontal and vertical movement which is similar to that of real beams. On the other hand, from the model the pressure needed to initiate crack was recorded. Whereas, it was not possible to track the pressure at crack initiation point in the experimental investigation.
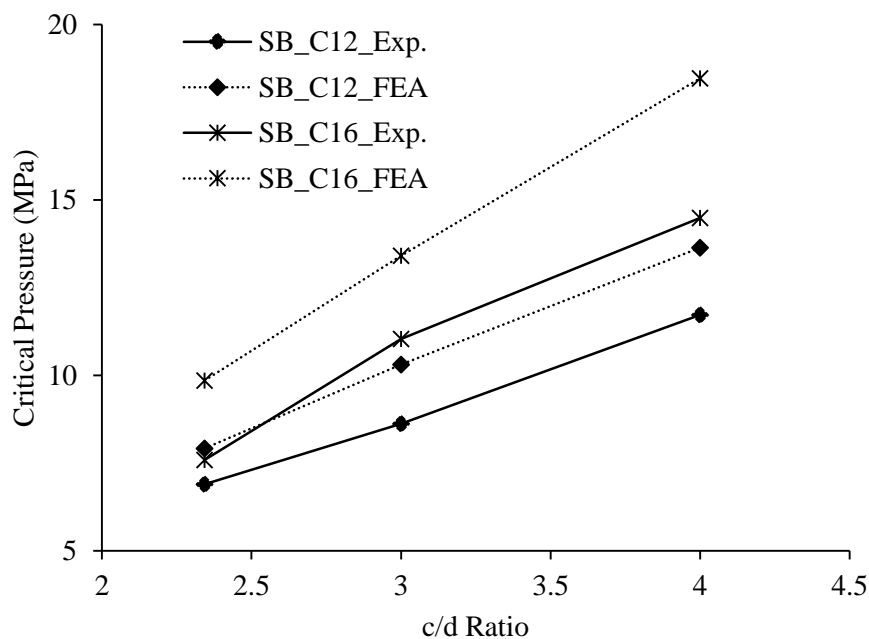

Figure 5.9: Comparison of Failure Pressures Obtained from Experiment and Finite Element Analysis for Side Bars
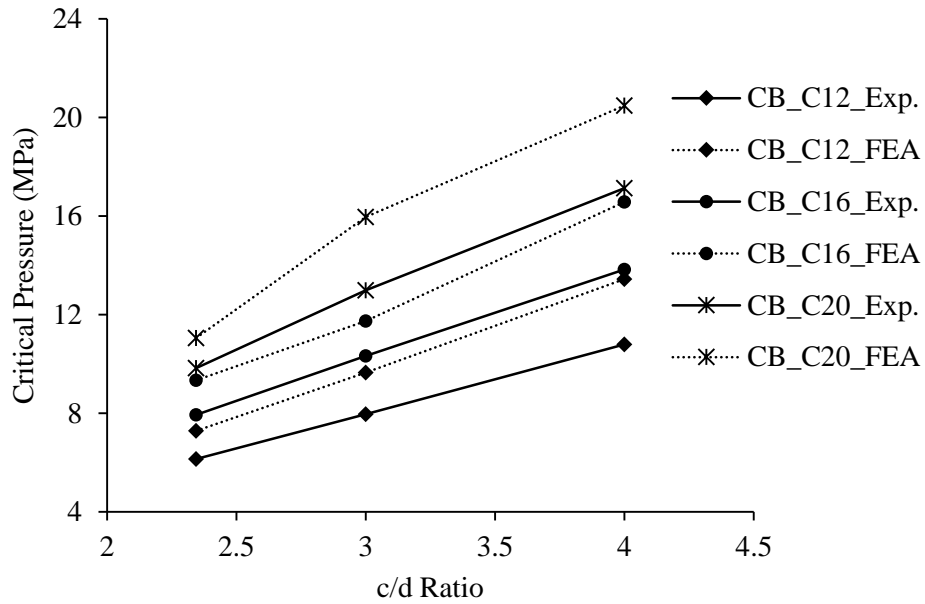
Figure 5.10: Comparison of Failure Pressures Obtained from Experiment and Finite Element Analysis for Corner Bars

both the experimental and the finite element results showed a gradual increase in critical pressure with the increase in strength of concrete which is contradictory to that of Williamson & Clark (2000b) where there was no dependency of the critical pressure on the grade of concrete.

Table 5.2: Percent Variation of Critical Pressure from Finite Element Analysis (FEA) With the Experimental Ones

Clear cover (mm)	For Corner Bar (CB)			For Side Bar (SB)	
	C12	C16	C20	C12	C16
37.5	18.8	17.8	12.4	14.8	29.8
48	21.1	13.7	22.9	19.6	21.6
64	24.6	19.9	19.6	16.4	27.5

5.5 Finite Element Results

5.5.1 Pressure Development due to the Expansive Corrosion Products

There are mainly two ways of extending the service life of the reinforced concrete structures prone to salinity zone. One was employment of protecting measures like cathodic protection, epoxy paint etc. and the other is by providing clear cover or by the material property. In corrosion induced failure, there is a gradual increase in volume of the corrosion products around

the reinforcement. Due to this radial deformation, a gradual increase in pressure occurred. The gradual increase in pressure around the bar due to the corrosion products are shown in Figure 5.11 to Figure 5.16.

Figure 5.11: Gradual Increase in Pressure with the Increase in Corrosion Products for Side Bar

Figure 5.12: Gradual Increase in Pressure with the Increase in Corrosion Products for Side Bar
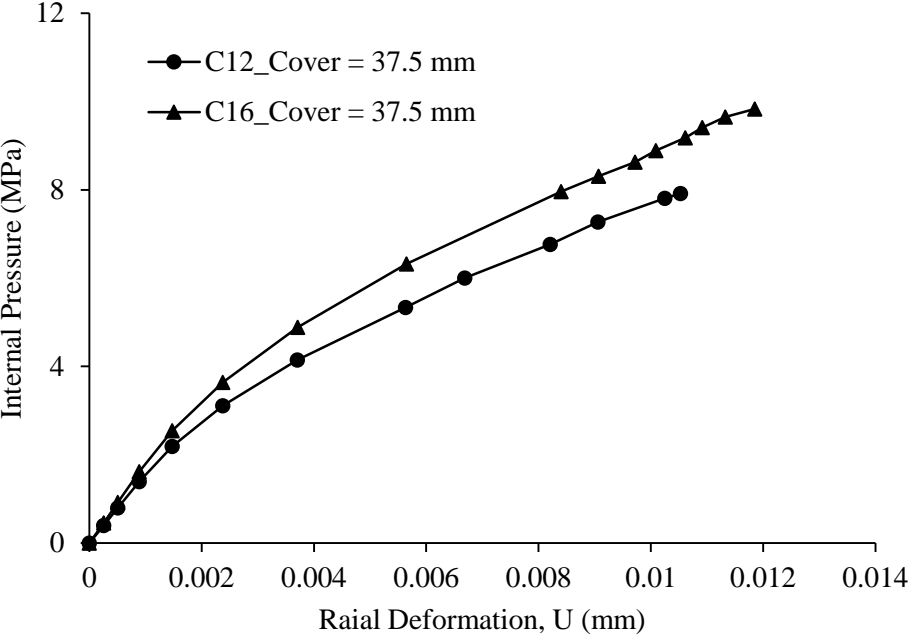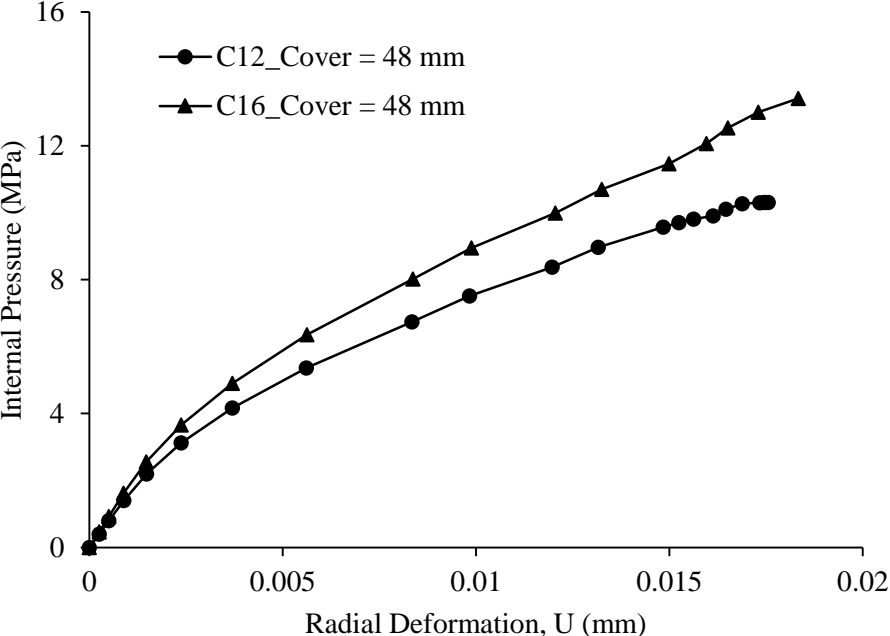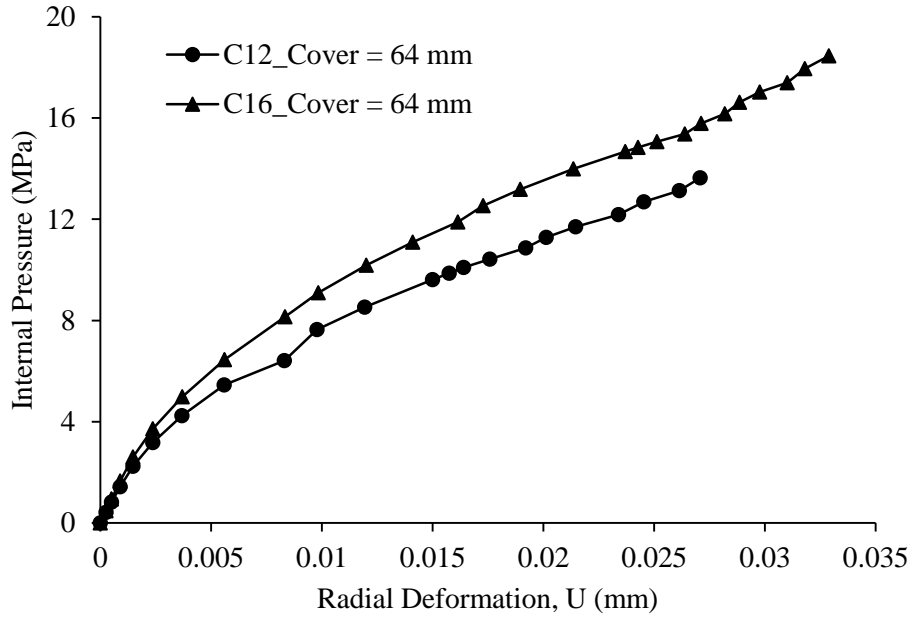
Figure 5.13: Gradual Increase in Pressure with the Increase in Corrosion Products for Side Bar
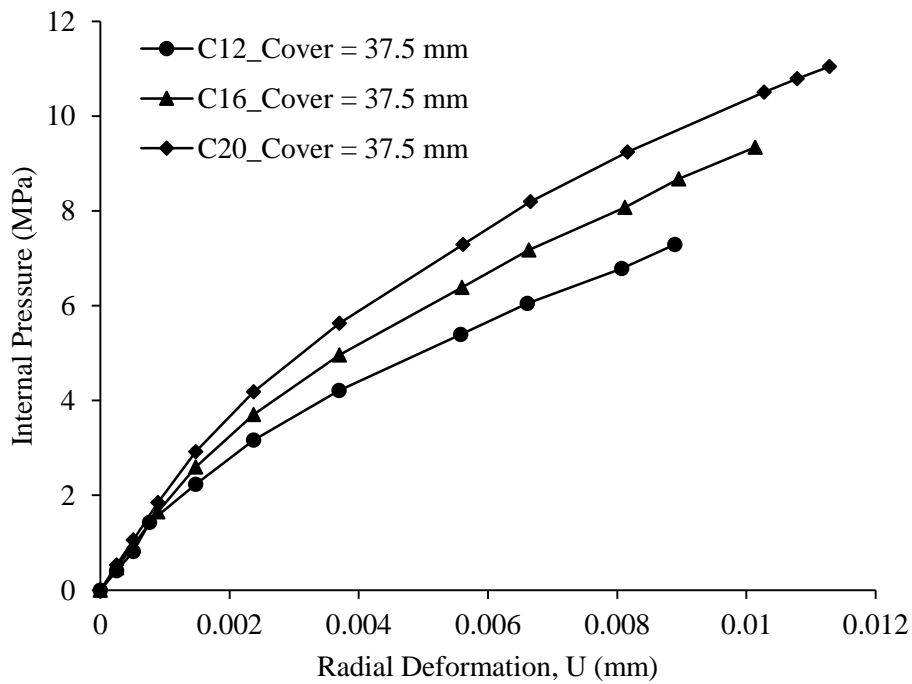
Figure 5.14: Gradual Increase in Pressure with the Increase in Corrosion Products for Corner Bar
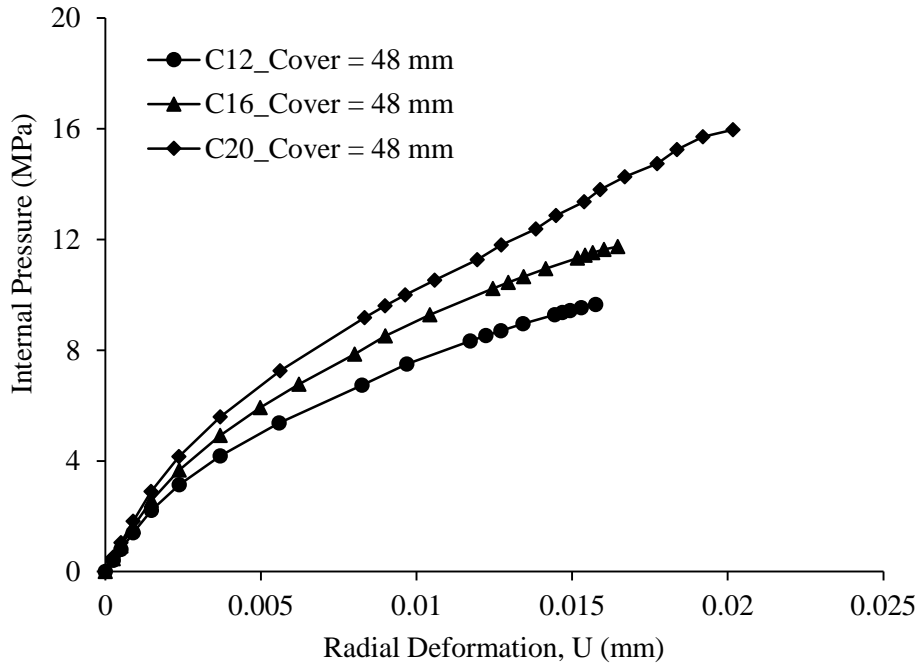
Figure 5.15: Gradual Increase in Pressure with the Increase in Corrosion Products for Corner Bar
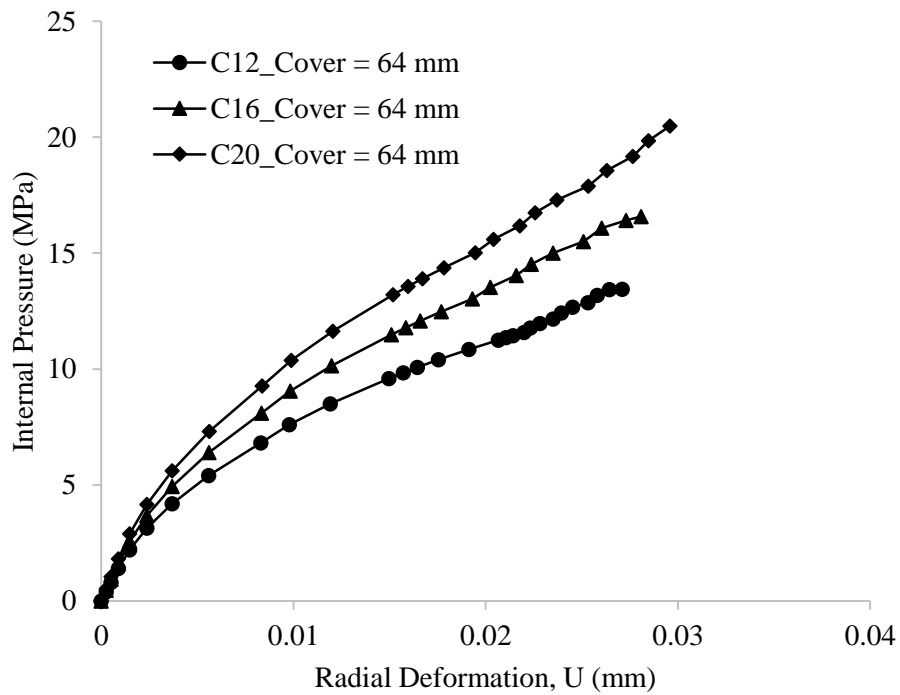
Figure 5.16: Gradual Increase in Pressure with the Increase in Corrosion Products for Corner Bar

5.5.2 Corrosion Products Needed to Initiate Crack
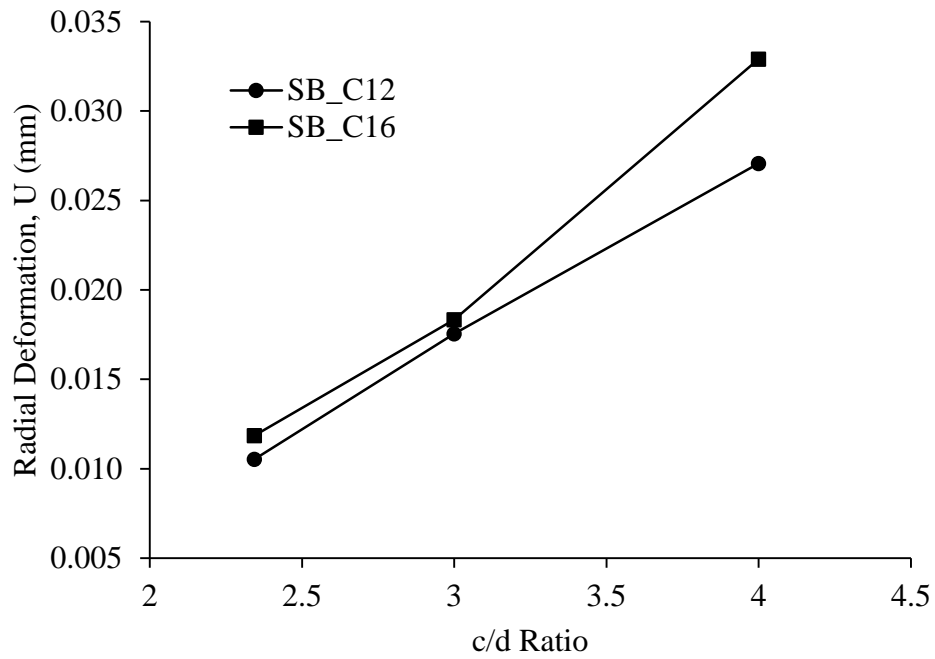
(a)
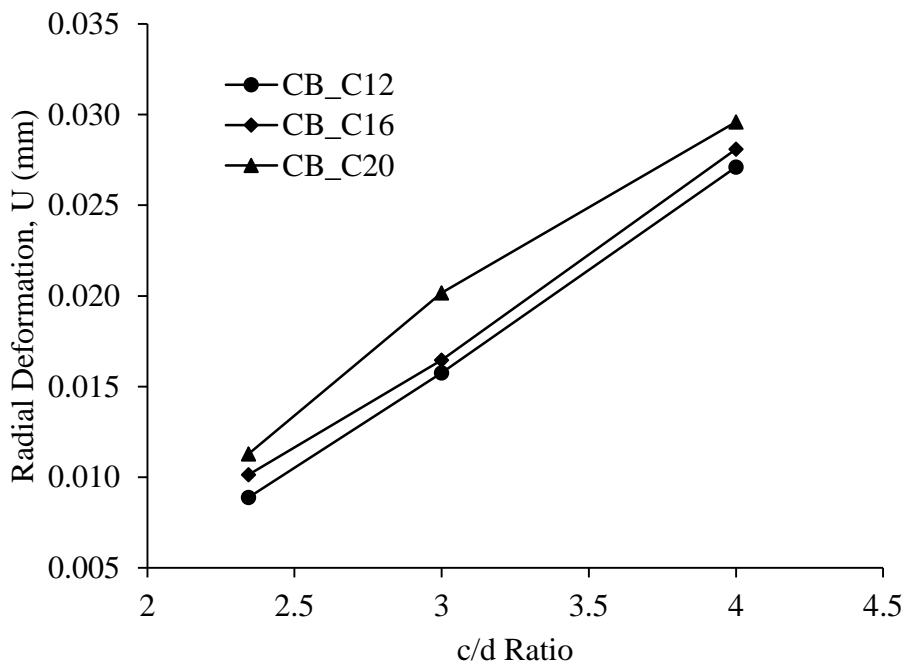
(b)

Figure 5.17: Variation of Radial Deformation with respect to c/d ratio for (a) Side Bars (b) Corner Bars

The variation of radial deformations due to the corrosion products causing the concrete to be cracked is shown in Figure 5.17 (a) in case of side bars and Figure 5.18 (b) in case of corner

bars. Figures shows that there is about 60 to 78% increase in radial deformation to cause the cracking of concrete cover by increasing the clear cover from 37.5 mm to 48 mm and this value was 45 to 78% for an increase in cover from 48 mm to 64 mm. A possible explanation of this phenomenon was the stiffness of cover concrete for c = 64 mm was larger than that for c = 48 mm, whereas due to increase in grade of concrete from C12 to C16, the deformations were increased but the amount was about 4.5 to 22%.

5.5.3 Effect of Bar Location

In Figure 5.18 the critical pressures for corner bars were plotted with respect to that of side bars to evaluate the effect of bar location. Figure 5.18 shows that the experimental results were very close to the line of equality for all grade of concrete whereas the results from finite element results for the higher grade of concrete shows a lower critical pressure for corner bars. And this effect prolonged for higher c/d ratio. This might be due to as larger the diameter of bar, cover concrete for corner reinforcement was more fragile than an equal thickness of cover for a side bar (Williamson & Clark, 2000b). A similar pattern was also found in past studies which showed that several specimens with corner reinforcement failed at lower pressures than the specimens with side bar (Allan & Cherry, 1992).
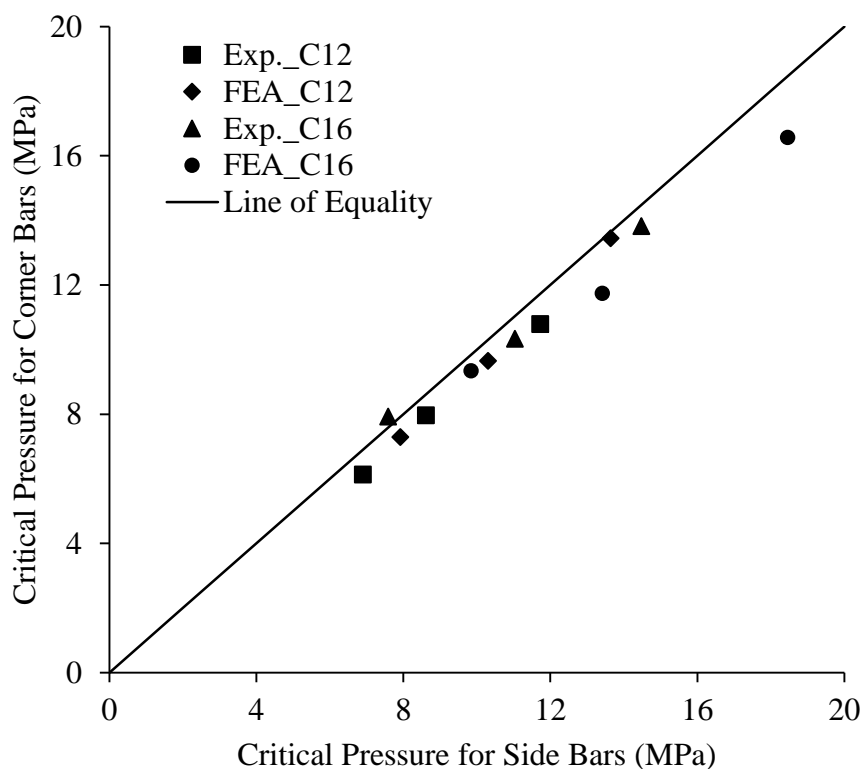

Figure 5.18: Effect of Bar Location on Failure Pressure

The radial deformations needed to crack the concrete cover is plotted in Figure 5.19 to evaluate the effect of bar location. The figure showed a similar pattern as for pressure shown in Figure 5.18. For higher cover to diameter ratio a lower expansion was needed for corner bar.
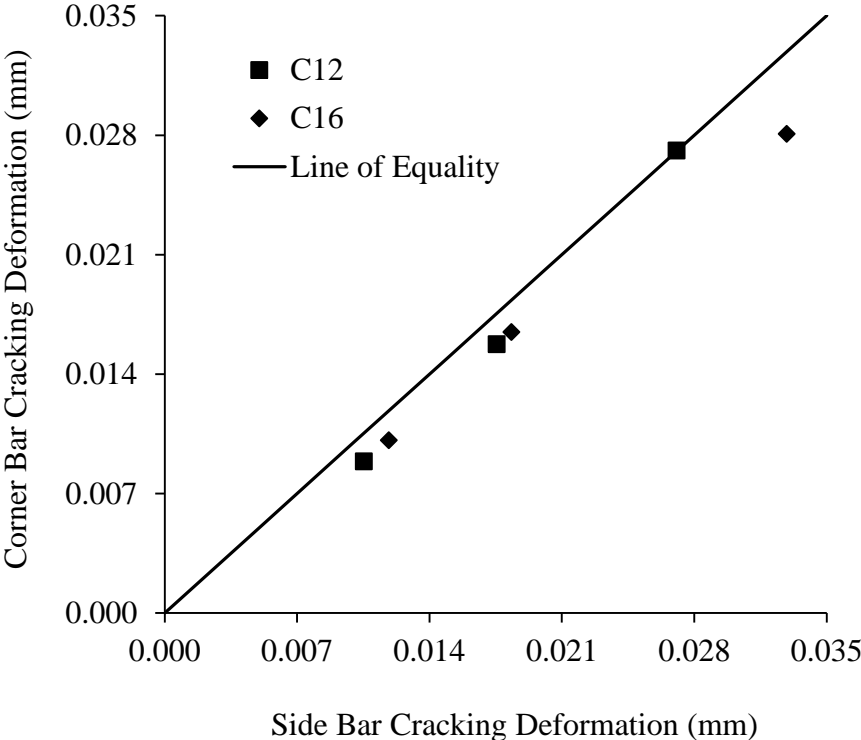
Figure 5.19: Effect of Bar Location on Radial Expansion

5.5.4 Effect of Bar Size

Five finite element models were developed with varying hole diameters (d), from 10 mm to 25 mm, where all other geometric and material properties were kept constant (C = 48 mm, Grade of concrete, C20). The pressure required for cracking of the concrete cover for each model is shown in Figure 5.21. Figure 5.20 shows that the expansive pressure decreased with the increase in bar diameter. By increasing the bar diameter, the lateral surface of the hole increased which results in higher outward force and consequently lower required pressure for the cracking. On the other hand for the same cover thickness, if the bar diameter was increased, the cover of smaller diameter was stiffer than that of larger diameter (Williamson & Clark, 2000b). It is obvious that the greater the bar diameter, the larger the loading surface area so that there is more probability to find a weak point in the larger diameter. Williamson & Clark

(2000b) also found a reduction of about 20% in pressure for doubling the bar diameter from 8 mm to 16 mm.
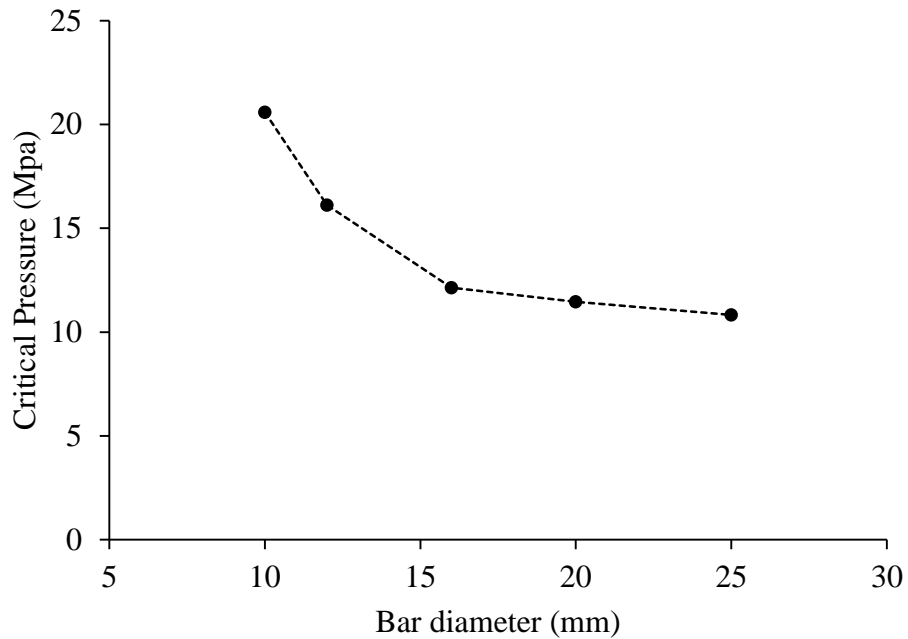
Figure 5.20: Effect of Bar Diameter on the Required Pressure for Cracking

5.5.5 Patterns of Crack

To compare the patterns of cracks, the geometry of the models were selected similar to that of the beam specimens (Experimental specimens shown in Figure 4.1). The mechanism of initiation of cracks were similar to that of experimental one shown in Figure 5.21 and Figure 5.22.

(a)   (b)
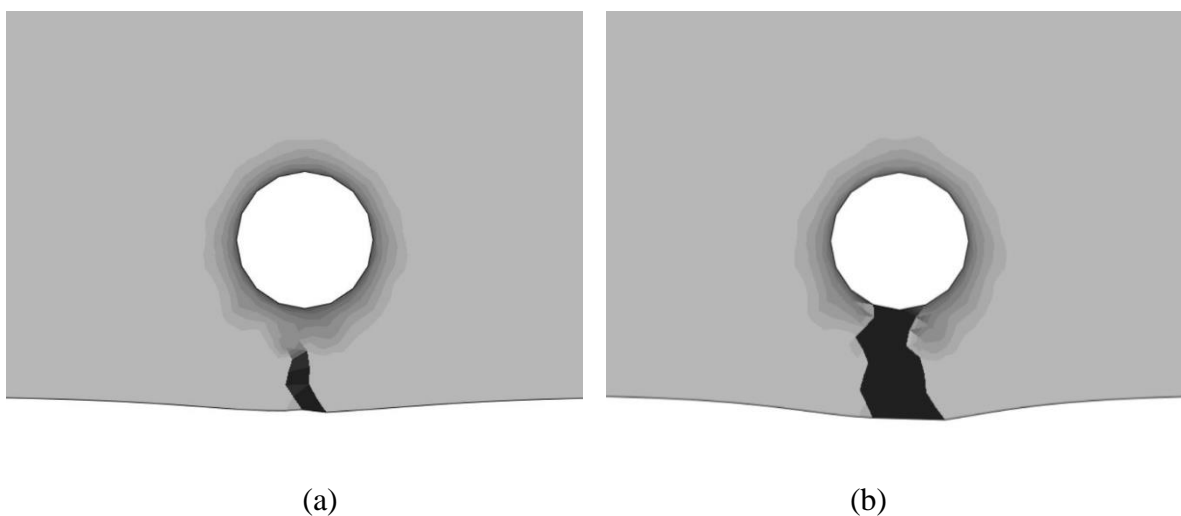
Figure 5.21: Initiation and Propagation of Crack for C = 20 mm

(a)   (b)
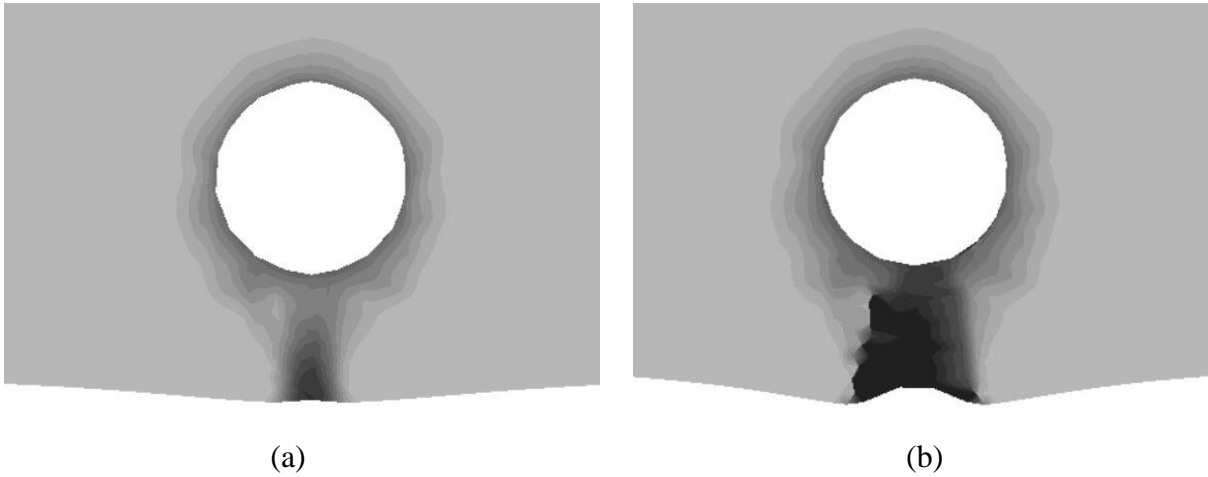
Figure 5.22: Initiation and Propagation of Crack for C = 37.5 mm

Figure 5.21 and Figure 5.22 showed that a heaving of concrete surface occurred and the crack was initiated from the outer edge of cover for cover of 20 mm and 37.5 mm respectively. Whereas in case of 50 mm and 75 mm cover, crack was initiated from steel concrete interface and propagated towards the surface as shown in Figure 5.23 and Figure 5.24.

(a)   (b)
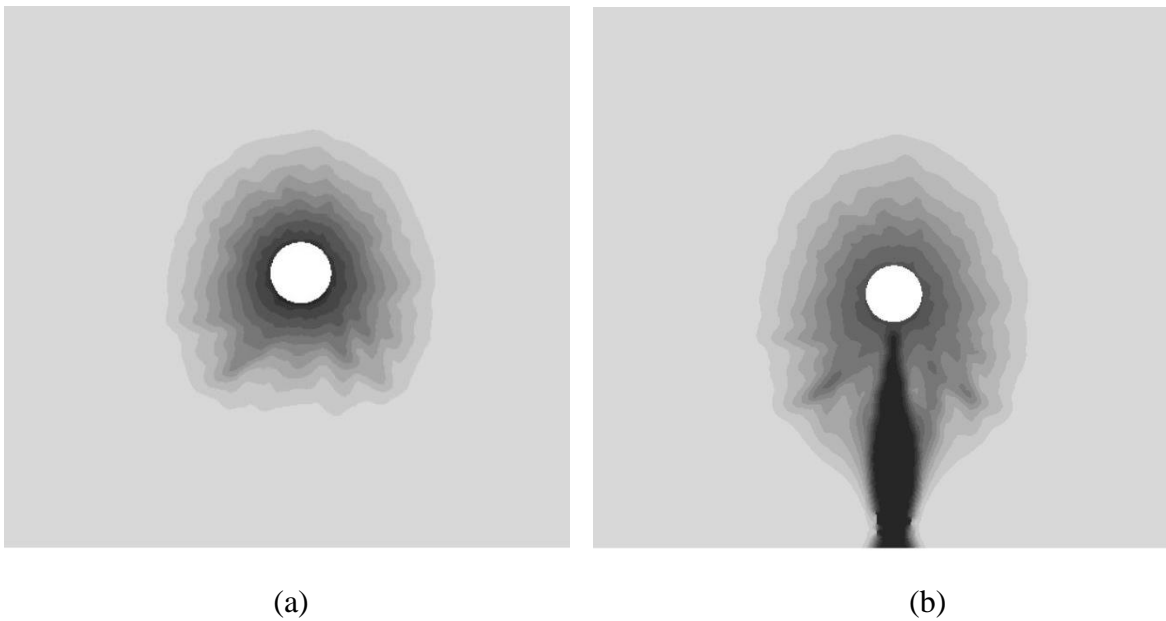
Figure 5.23: Initiation and Propagation of Crack for C = 50 mm

<div align="center">(a)</div>
<div align="center">(b)</div>
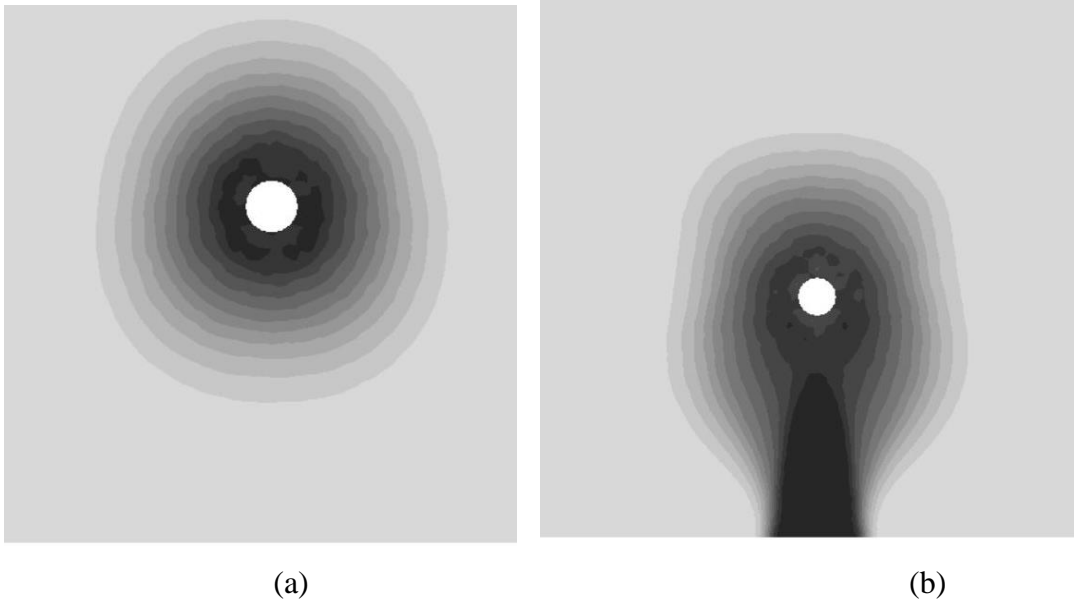
<div align="center">Figure 5.24: Initiation and Propagation of Crack for C = 75 mm</div>

5.5.6 Application of Models to Real Beams

The model was applied to predict the cracking of cover concrete in a real beam specimen having a cross section of 300 mm x 500 mm. Reinforcement bars were arranged in different configuration for a cover thickness (C) of 37.5 mm.

<div align="center">(a)</div>

<div align="center">(b)</div>
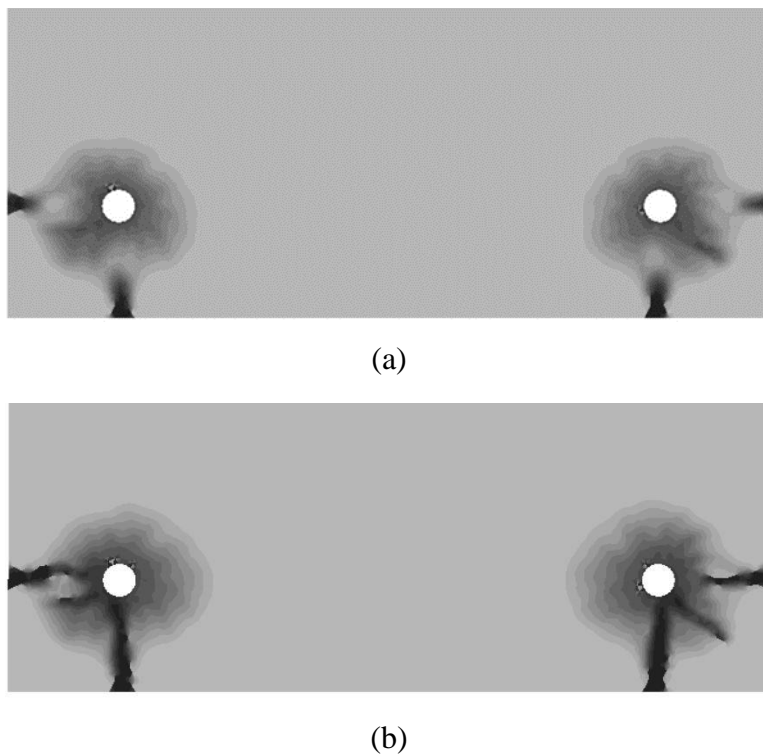
<div align="center">Figure 5.25: (a) Initiation and (b) Propagation of Crack for 2-12 mm bar</div>
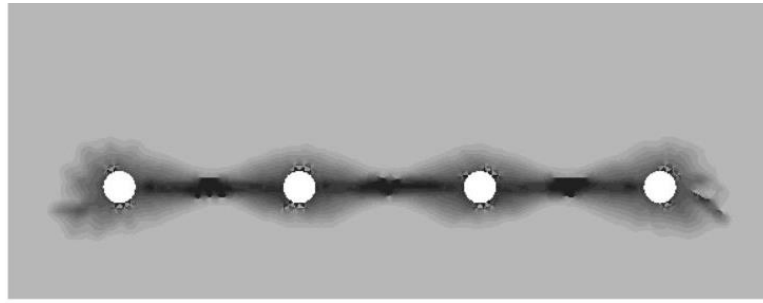
(a)
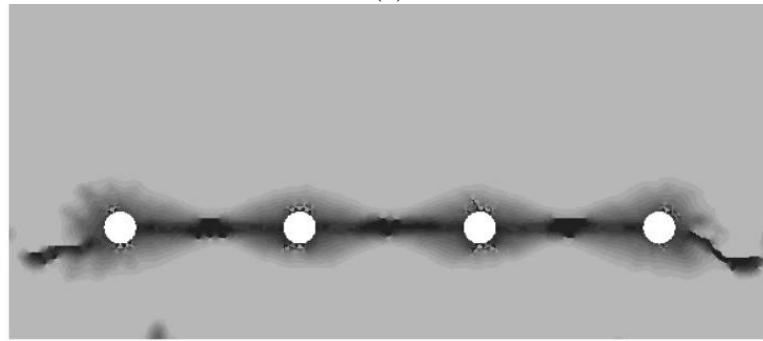
(b)

Figure 5.26: (a) Initiation and (b) Propagation of Crack for 4-12 mm bar
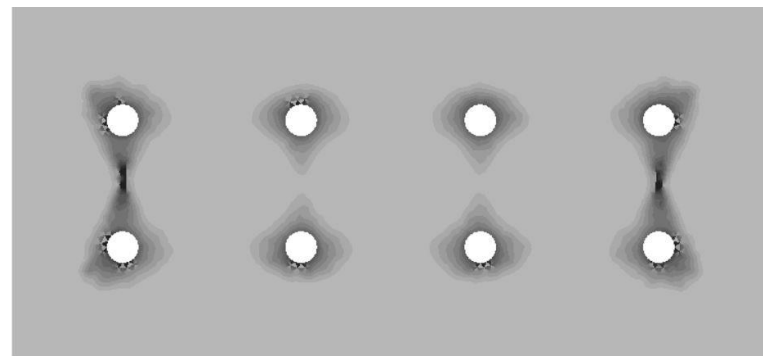
(a)
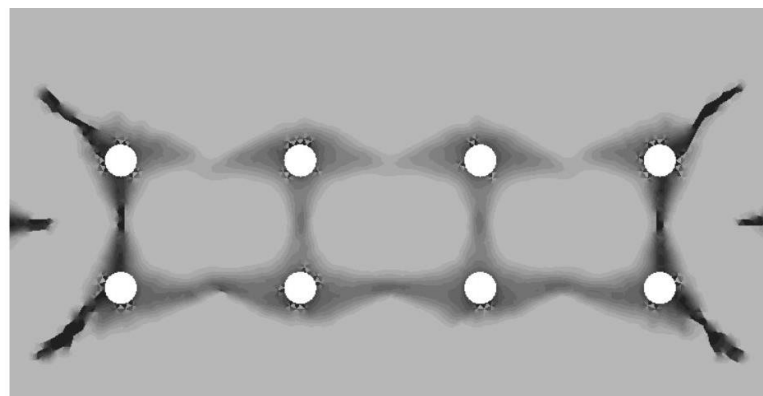
(b)

Figure 5.27: (a) Initiation and (b) Propagation of Crack for 8-12 mm bar

Cracking initiation and propagation pattern of different configurations with 2, 4 & 8-12 mm diameter plain bar are shown in Figure 5.25 to Figure 5.27. When number of bars were two, then cracking at corner and spalling was occurred which is shown in Figure 5.25. Whereas for number of bars increased to four, spalling had found which is shown in Figure 5.26.

CHAPTER 6

CORROSION PROTECTION BY SACRIFICIAL ANODE

6.1 Introduction

Cathodic protection can be used to control corrosion of reinforcement in two ways: one is impressed current system and the other is a sacrificial anode system. In impressed current system, an anode is connected with the target reinforcement to be protected and an external current is applied so that the corrosion reaction of reinforcement is forced to stop. Whereas in sacrificial anode system a galvanic anode, a piece of a more electrochemically "active" metal, is attached to the surface of reinforcement. Zinc is used as a sacrificial anode in reinforced concrete structures due to its availability and low cost, however researches regarding the effectiveness of zinc as a sacrificial anode is very scarce. In this study, a comprehensive study was done on the effectiveness of zinc as a sacrificial anode.

6.2 Materials Used

Two 10 mm in diameter deformed mild steel bars were used as anode and cathode in this investigation. The length of each bar was 76 mm. The bars were cleaned with steel wire brush. Pallets of NaOH, $Ca(OH)_2$, and KOH was used to prepare the high pH solution. A piece of Zinc was tied up with the anode bar by steel wire. The piece of zinc is shown in Figure 6.1. The sacrificial anode was tied up with the protecting bar. The setup of the experimental program is shown in Figure 6.2.

Figure 6.1: Preparation of Zinc Anode
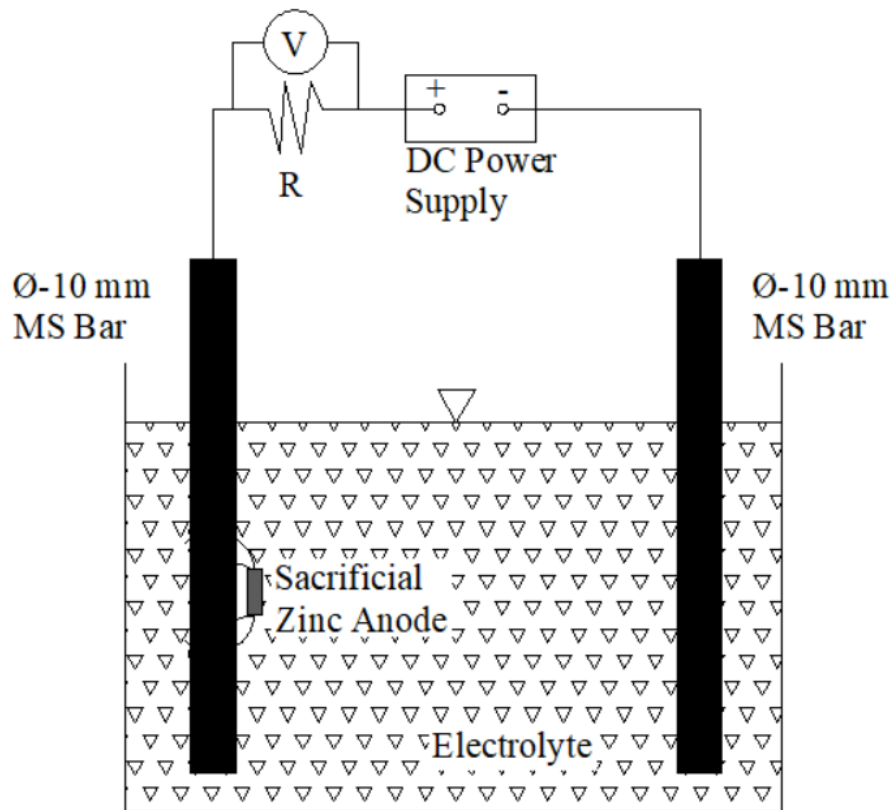
Figure 6.2: Test Setup in Solution

6.3 Experimental Programs

Two different tests were conducted to evaluate the effectiveness of Zinc anode as a sacrificial material. The accelerated corrosion test was done firstly in solutions of high pH similar to concrete pore solution and then in concrete. The procedure for both in solution and in concrete was characterized in chapter 3. In this methodology, the optimum chloride content was found as 3.5%. Similar solutions were used in this study and 3.5% NaCl was used to improve electrical conductivity. The solution properties are shown in Table 6.1.

Table 6.1: Solution properties

	$[OH^-]$ (mMol/L)	$[Na^+]$ (mMol/L)	$[K^+]$ (mMol/L)	$[Ca^{2+}]$ (mMol/L)	Calculated pH
Solution 1	470	130	380	1.0	13.7
Solution 2	834	271	629	1.0	13.9
Solution 3	288	85	228	0	13.5

For the test in concrete, a concrete with w/c ratio 0.45 was used. To keep the consistency of work, similar mix proportion to the previous study was used which is shown in Table 6.2. The specimens were 50 mm x 50 mm x 50 mm in size. Zinc anode was attached with the target bar

as well. The setup is shown in Figure 6.3. The samples were tested after 7-days curing. The samples were immersed in 3.5% NaCl solution for 24 hours before starting the test. For both cases, target bar and the zinc anode were cleaned after test by steel wire brush.

Table 6.2: Mix proportions for the concrete

| Materials (kg/m³) | | | | | w/c |
Water	Cement	Fine Aggregate	Coarse Aggregate	Fresh density	ratio
190	422	677	1056	2345	0.45

Figure 6.3: Test Setup in Concrete

6.4 Results and Discussion

The effect of using Zinc as cathodic protection is summarized in Table 6.3. Where the theoretical mass loss for both iron and zinc was calculated based on the full current used to

corrode. For all the tests, a constant ratio between the surface area of steel and weight of zinc was maintained. The surface area was 1570 ± 10 mm^2 and the weight of zinc was 12 ± 0.5 gm. The results showed that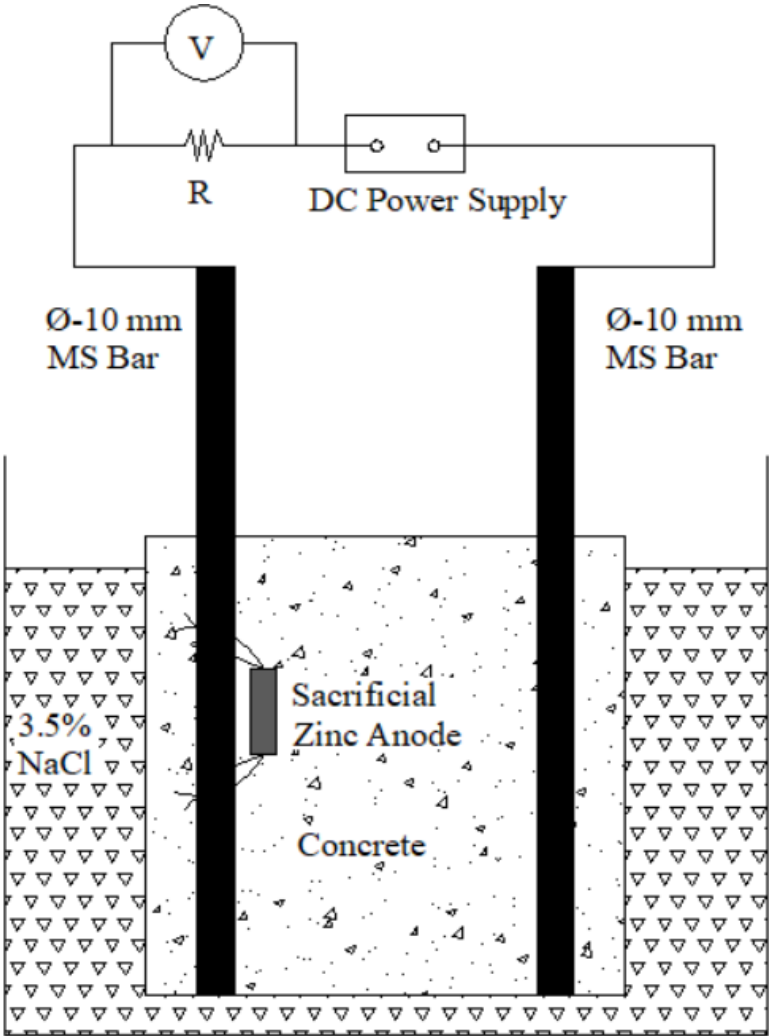 total current was divided into corrode steel, zinc and splitting the water. A partial amount of current was used to oxidize the steel in all the solutions as well as in concrete. 30 to 50% current was active to oxidize the steel bar diverting 50 to 70% of current. Whereas this 50 to 70% diverted current was active not only for oxidizing zinc but also for splitting the water. This value was up to 80% in only 3.5% NaCl solution, about 57% in solution 2 & 3 and 9% in solution 1. In the concrete environment, this value was 64%. When only zinc metal was used as an anode and a 10 mm-Ø bar, it was found that about 100% efficiency as an anode in all solutions. In another case, the surface area was raised to 11300 ± 10 mm^2 and the weight of zinc was 66 ± 0.5 gm, the diverted current was about 25%. If diverted current was considered in the calculation of mass loss it was about 94% efficient to corrode zinc.

Table 6.3: Results of the Tests

	Solution 1	Solution 2	Solution 3	Only 3.5% NaCl in Distilled water	In Concrete
Duration of test (min)	30	30	30	30	1000
Actual wt loss of Fe (gm)	0.553	0.523	0.473	0.922	3.337
Theoretical wt loss of Fe (gm)	1.599	1.042	1.188	1.459	8.312
Actual wt loss of Zn (gm)	0.107	0.346	0.474	0.506	2.506
Theoretical wt loss of Zn (gm)	1.872	1.22	1.39	1.708	9.705
Current efficiency of Fe	35	50	40	63	40
Current efficiency of Zn considering total current	6	28	34	30	26
Current efficiency of Zn considering diverted current	9	57	57	81	64
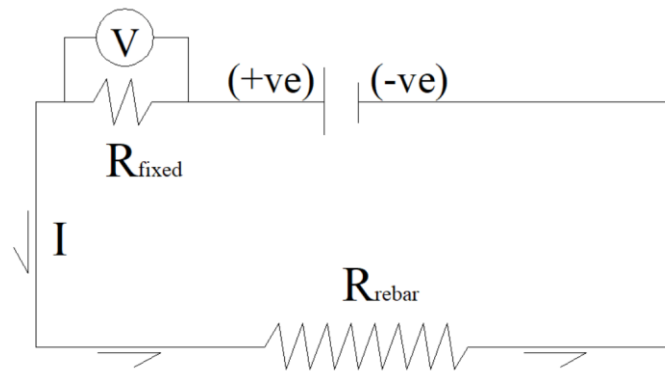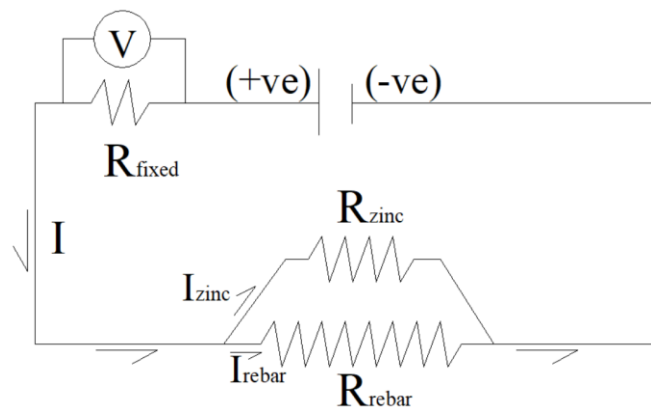
Figure 6.4: Proposed Circuit Diagram of Accelerated Corrosion Cell (a) Without Cathodic
Protection (b) With Cathodic Protection

The diversion mechanism may be explained by electric circuit diagram of the corrosion cell as shown in Figure 6.4. General circuit diagram of accelerated corrosion test setup is shown in Figure 6.4 (a). Where the anode is represented as a resistor. In this circuit the total voltage applied is dropped in a fixed resistor and the resistor due to rebar. Same current is passed through the resistors as they are connected in series connection. When a sacrificial anode was connected with the protecting rebar, it was also represented as a resistor. But it seems, the resistor due to sacrificial anode is connected parallel to the resistor due to rebar. For this reason the current was divided.

The phenomenon of diversion of current may also be explained by pourbiax diagram of zinc. From the pourbiax diagram of zinc as shown in Figure 6.5, it is seen that a passive state occurred at pH between 7.0 and 12.0 and above 12.0 an active state found. But pure zinc in air, forms a layer of hydrated oxide which combines with the carbon dioxide forming zinc carbonate ($ZnCO_3$) layer that protects the metal from corrosion. In this study, there was a possibility to

form a protective zinc carbonate layer because the zinc bar was stored in air before tests. On the other hand, the behavior of zinc in concrete is different. Zinc reacts with the hydroxyl ions in concrete to form zinc oxide and hydrogen gas. Zinc oxide reacts with the calcium ions to form calcium hydroxyzincate which forms stable coating at a pH less than 13.3 that passivate the zinc (Das, 2015). In this study, if the pH value of the concrete pore solution didn't remain above 13.3, it could not protect steel from corrosion.
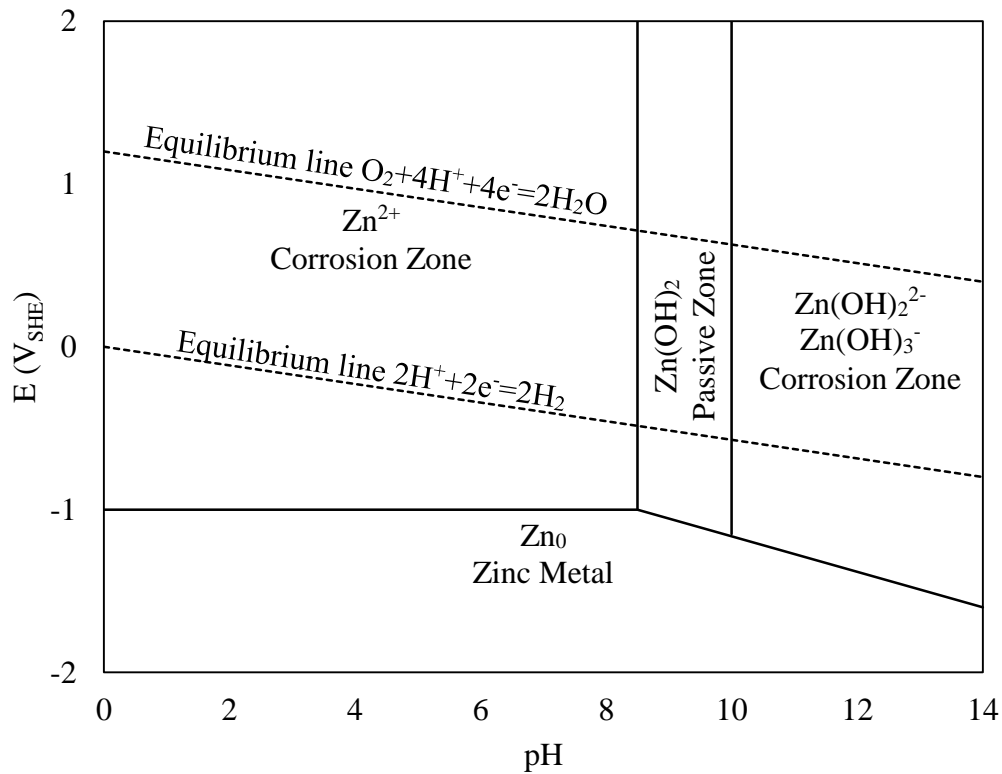
Figure 6.5: Pourbiax Diagram of Zinc

The condition of steel and zinc anode after test was shown in Figure 6.6. This Figure shows that both the rebar and zinc was corroded. In the investigation it was found that the surface in contact with the zinc was not corroded. The distribution of corrosion products over the surface area is shown in Figure 6.6.

Figure 6.6: Steel and Zinc Anode after Test

Figure 6.7: Steel and Zinc Anode after Test for Corroding Surface Area of 11300 mm^2

CHAPTER 7
CONCLUSIONS AND RECOMMENDATIONS

7.1 Conclusions

This thesis focused on the experimental investigation and numerical analysis of the corrosion induced pressure to initiate and propagate the concrete cover crack. Based on the results of the comprehensive study the following conclusions were drawn.

(a) In impressed current technique, amount of chloride ions is an important factor affecting the corrosion of steel. In solutions similar to that of concrete pore solution an experimental investigation was carried out to find the optimum chloride content. It was found that at a high chloride concentration of 3.5% by mass of mixing water, the actual mass loss met the theoretical one. In concrete, the chloride ions are to be transported through the pore space need to be saturated with the chlorides adjacent to the steel-concrete interface for 100% current efficiency. An investigation was carried out regarding this point. The cubical specimens were immersed in 3.5% chloride solution for different period of time and it was found that an immersion for at least one day before starting the tests was needed to saturate.

(b) For cover thickness of 20 mm and 37.5 mm the major crack was initiated from the surface of the cover due to surface heaving and propagated towards steel concrete interface. For cover thickness of 50 mm and 75 mm the major crack was initiated from the steel concrete interface and propagated towards the surface of the cover. There was no significant variation of the critical amount of corrosion for cover 20 mm and 37.5 mm. For an increase in cover from 37.5 mm to 50 mm, critical amount of corrosion increased drastically from 22 mg/cm^2 to 129 mg/cm^2. Further increase in cover to 75 mm amount of corrosion needed to initiate cracks was 211 mg/cm^2. From this results it is recommended to provide at least 50 mm clear cover to prolong the service life of reinforced concrete structures exposed to marine environment. There was a linear relation between crack width and level of corrosion found which may help to predict the corrosion level in existing structures.

(c) From the experimental simulation of the critical pressure for cover cracking it was found that the critical pressure was very much dependent on the cover thickness, grade of concrete and location of the bar. The greater the cover thickness the greater the cracking pressure. It was also found that, a greater pressure was needed when a higher grade of concrete was

used. On the other hand, for corner bars a lower pressure was needed to crack with respect to the side bars.

(d) A numerical model was developed to predict the pressure and radial expansion induced due to corrosion products. The model predicted the patterns of cracks due to uniform corrosion. Critical pressure and the radial expansion induced due to expansive corrosion products were found to be affected by cover thickness, grade of concrete, location of bar and diameter of bar. With the increase in cover thickness the pressure as well as the radial expansion needed to initiate crack was increased. On the other hand, with the increase in bar diameter a decrease in critical pressure was observed.

(e) Zinc sacrificial anode was found to protect the corroding reinforcement partially instead of full protection. This result was found for two environment: i) in solution similar to concrete pore solution and ii) in concrete. The total current supplied through the circuit was divided through the rebar and sacrificial anode instead of total current flowed through the sacrificial anode.

7.2 Limitations and Recommendations

In this study an experimental study was performed as well as a finite element model was developed to predict the corrosion induced cracking and the associated expansive pressure. The limitations and the recommendations are shown below

➢ In this research, characterization of accelerated corrosion test was done considering only two factors: critical chloride content and immersion time before testing. Effects of other factors like grade of concrete, density of concrete, clear cover etc should also be investigated.

➢ The finite element model was developed considering a uniform corrosion but in actual case the corrosion is highly non uniform.

➢ The properties of corrosion products are dependent on the environmental conditions like wetting and drying cycle, continuous wetting, loading conditions. Continuous wetting condition was followed in this research. The other environmental conditions should also be investigated.

References

ABAQUS Inc. (2010). ABAQUS Theory Manual. In *ABAQUS Documentation* (p. 1176).

Ahmed, S. F. U., Maalej, M., & Mihashi, H. (2007). Cover cracking of reinforced concrete beams due to corrosion of steel. *ACI Materials Journal*, *104*(2), 153–161.

Allan, M. L., & Cherry, B. W. (1992). Factors controlling the amount of corrosion for cracking in reinforced concrete ☆. *Concrete*, (May), 426–430.

Alonso, C., Andrade, C., Rodriguez, J., & Diez, J. M. (1998a). Factors controlling cracking of concrete affected by reinforcement corrosion. *Materials and Structures*, *31*(7), 435–441.

Alonso, C., Andrade, C., Rodriguez, J., & Diez, J. M. (1998b). Factors controlling cracking of concrete affected by reinforcement corrosion. *Materials and Structures*, *31*(7), 435–441.

Andrade, C., Alonso, C., & Molina, F. J. (1993). Cover cracking as a function of bar corrosion: Part I-Experimental test. *Materials and Structures*, *26*(8), 453–464.

Austin, S. A., Lyons, R., & Ing, M. J. (2004). Electrochemical behavior of steel-reinforced concrete during accelerated corrosion testing, *60*(2), 203–212.

Bazant, Z. P. (1979). Physical model for steel corrosion in concrete sea structures - theory. *Journal of the Structural Division-ASCE*, *105*(6), 1137–1153.

Bertolini, L., Elsener, B., Pedeferri, P., Redaelli, E., & Polder, R. B. (2013). Corrosion of steel in concrete. Weinheim, Germany: Wiley-VCH Verlag GmbH & Co. KGaA.

Bertolini, L., & John Wiley & Sons. (2013). Corrosion of steel in concrete : prevention, diagnosis, repair. Wiley-VCH.

Bhargava, K., Ghosh, A. K., Mori, Y., & Ramanujam, S. (2006). Model for cover cracking due to rebar corrosion in RC structures. *Engineering Structures*, *28*(8), 1093–1109.

Broomfield, J. P. (2006). Corrosion of steel in concrete: understanding, investigation and repair*, Second Edition*.

Dagher, H. J., & Kulendran, S. (1987). Finite element modeling of corrosion damage in concrete. *ACI Structural Journal*, *89*(6).

Das, S. C. (2015). Zinc rich paint as anode system for cathodic protection (CP) of reinforced concrete structures and development of corrosion / CP monitoring probes Zinc Rich Paint as Anode System for Cathodic Protection (CP) of Reinforced Concrete Structures.

Das, S. C., Pouya, H. S., & Ganjian, E. (2015). Zinc-rich paint as anode for cathodic protection of steel in concrete, 1–9.

Dere, Y., & Koroglu, M. A. (2017). Nonlinear fe modeling of reinforced concrete. *International Journal of Structural and Civil Engineering Research J. Struct. Civ. Eng. Res*, *6*(1).

Du, Y. G., Chan, A. H. C., & Clark, L. A. (2006). Finite element analysis of the effects of radial expansion of corroded reinforcement. *Computers & Structures*, *84*(13–14), 917–929.

El-Maaddawy, T., Bouchair, A., El-Dieb, A. S., & Biddah, A. (2015). Corrosion aging of reinforced concrete t-girders strengthened with near-surface-mounted composites. *Journal of Composites for Construction*, *19*(3), 04014053.

El Maaddawy, T. A., & Soudki, K. A. (2003). Effectiveness of impressed current technique to simulate corrosion of steel reinforcement in concrete. *Journal of Materials in Civil Engineering*, *15*(1), 41–47.

Ernst, & Sohn. (2010). *fib* model code for concrete structures *2010*.

Hausmann, D. A. (1967). Steel corrosion in concrete -- how does it occur? *Materials Protection*.

He, J., Zhou, Y., Guan, X., Zhang, W., Wang, Y., & Zhang, W. (2016). An integrated health monitoring method for structural fatigue life evaluation using limited sensor data. *Materials (Basel, Switzerland)*, *9*(11).

Honda, M., Kobayashi, Y., & Tamada, A. (1992). Stress corrosion cracking of stainless alloys in alkaline sulfide solutions. *Corrosion*, *48*(10), 822–829.

Kassir, M. K., & Ghosn, M. (2002). Chloride-induced corrosion of reinforced concrete bridge decks. *Cement and Concrete Research*, *32*(1), 139–143.

Kulkarni, S. S., & Achenbach, J. D. (2008). Structural health monitoring and damage prognosis in fatigue. *Structural Health Monitoring: An International Journal*, *7*(1), 37–49.

Lee, J., & Fenves, G. L. (1998). Plastic-damage model for cyclic loading of concrete structures. *Journal of Engineering Mechanics*, *124*(8), 892–900.

Liu, Y., & Weyers, R. E. (1998). Modeling the time-to-corrosion cracking in chloride contaminated reinforced concrete structures. *ACI Materials Journal*, *95*(6), 675–680.

Lubliner, J., Oliver, J., Oller, S., & Oñate, E. (1989). A plastic-damage model for concrete. *International Journal of Solids and Structures*, *25*(3), 299–326.

Magne Maage, Steinar Helland, Ervin Poulsen, Øystein Vennesland, and J. E. C. (1996). Service life prediction of existing concrete structures exposed to marine environment. *ACI Materials Journal*, *93*(6).

Mindess, S., Young, J. F., & Darwin, D. (2003). *Concrete*. Prentice Hall.

Molina, F. J., Alonso, C., & Andrade, C. (1993). Cover cracking as a function of rebar corrosion: Part 2—Numerical model. *Materials and Structures*, *26*(9), 532–548.

Nossoni, G. (2010). Holistic electrochemical and mechanical modeling of corrosion-induced cracking in concrete structures.

Nossoni, G., & Harichandran, R. (2012). Current efficiency in accelerated corrosion testing of

concrete, *68*(9), 801–809.

Nossoni, G., & Harichandran, R. S. (2014). Electrochemical-mechanistic model for concrete cover cracking due to corrosion initiated by chloride diffusion. *Journal of Materials in Civil Engineering*, *26*(6), 04014001.

Oluokun, F. A., Burdette, E. G., & Deatherage, J. H. (1991). Splitting tensile strength and compressive strength relationships at early ages. *ACI Materials Journal*, *88*(2), 115–121.

Ouglova, A., Berthaud, Y., François, M., & Foct, F. (2006). Mechanical properties of an iron oxide formed by corrosion in reinforced concrete structures. *Corrosion Science*, *48*(12), 3988–4000.

Pantazopoulou, S. J., & Papoulia, K. D. (2001). Modeling cover-cracking due to reinforcement corrosion in rc structures. *Journal of Engineering Mechanics*, *127*(4), 342–351.

Popovics, S. (1973). A numerical approach to the complete stress-strain curve of concrete. *Cement and Concrete Research*, *3*(5), 583–599.

Shao, K. (2016). Experimental investigation of non-uniform corrosion of the steel bars in concrete.

Song, H., & Saraswathy, V. (2007). Corrosion monitoring of reinforced concrete structures - a review, *2*, 1–28.

Torres-Acosta, A. A., & Martnez-Madrid, M. (2003). Residual life of corroding reinforced concrete structures in marine environment. *Journal of Materials in Civil Engineering*, *15*(4), 344–353.

Tran, K. K., Nakamura, H., Kawamura, K., & Kunieda, M. (2011). Analysis of crack propagation due to rebar corrosion using RBSM. *Cement and Concrete Composites*, *33*(9), 906–917.

Val, D. V., Chernin, L., & Stewart, M. G. (2009). Experimental and numerical investigation of corrosion-induced cover cracking in reinforced concrete structures. *Journal of Structural Engineering*, *135*(4), 376–385.

Vrable, J. B., & B., J. (1977). Cathodic protection for reinforced concrete bridge decks: Laboratory phase. *Final Report Transportation Research Board, Washington, DC.*

Vu, K., Stewart, M. G., & Mullard, J. (2005). Corrosion-induced cracking: experimental data and predictive models. *ACI Structural Journal*, *102*(5), 719–726.

Williamson, S. J., & Clark, L. A. (2000a). Pressure required to cause cover cracking of concrete due to reinforcement corrosion. *Magazine of Concrete Research*, *52*(6), 455–467.

Williamson, S. J., & Clark, L. A. (2000b). Pressure required to cause cover cracking of concrete due to reinforcement corrosion. *Magazine of Concrete Research*, *52*(6), 455–467.

Yang, Z. J., & Chen, J. (2005). Finite element modelling of multiple cohesive discrete crack propagation in reinforced concrete beams. *Engineering Fracture Mechanics*, *72*(14), 2280–2297.

Yu, T., Teng, J. G., Wong, Y. L., & Dong, S. L. (2010a). Finite element modeling of confined concrete-II: Plastic-damage model. *Engineering Structures*, *32*(3), 680–691.

Yu, T., Teng, J. G., Wong, Y. L., & Dong, S. L. (2010b). Finite element modeling of confined concrete-II: Plastic-damage model. *Engineering Structures*, *32*(3), 680–691.

Zhang, Y., & Poursaee, A. (2014). Study the passivation and corrosion activity of carbon steel in concrete simulated pore solution under tensile and compressive stresses. *ASCE Journal of Materials in Civil Engineering*, 4014234.

Zhao, X., Gong, P., Qiao, G., Lu, J., Lv, X., & Ou, J. (2011). Brillouin corrosion expansion sensors for steel reinforced concrete structures using a fiber optic coil winding method. *Sensors*, *11*(11), 10798–10819.

Zhao, Y., & Jin, W. (2016). Steel corrosion-induced concrete cracking. Butterworth-Heinemann is an imprint of Elsevier.

Appendix A

Table A1: Summary of Some Previous Accelerated Corrosion Tests

Study	Specimen type	Applied current(mA)	Current density	Cathode type	Corrosion environment
Uomoto et al. (1984)	Beams	167	200-630	External copper plate	Constant immersion, 5% NaCl solution
Tachibana et al. (1990)	Beams	1,000[a]	500	External copper plate	Constant immersion, 3.5% NaCl solution
AlSulaimani et al. (1990)	Beams	Varies	2,000	External stainless steel plate	Constant immersion, salted solution[c]
Lee et al. (1996)	Beams	1,000	2,000[a]	External copper plate	Constant immersion, 3% NaCl solution
Lee et al. (1997)	Beams	672	230[a]	External copper plate	Constant immersion, 3% NaCl solution
Phillips (1991)[b]	Slabs	1800(average)	600(average)	External steel mesh	Constant immersion, 3% NaCl solution
Almusallam et al. (1996a)	Slabs	2,000	3,000	External stainless steel plate	Specimen soffits in contact with 5% NaCl solution

Tachibana et al. (1990)	Bond pull-out	32	500	External copper plate	Constant immersion, 3.3% NaCl solution
AlSulaimani et al. (1990)	Bond pull-out	Varies	2,000	External stainless steel plate	Constant immersion salted solution[c]
Almusallam et al. (1996b)	Bond pull-out	400	10,400[a]	External stainless steel plate	Constant immersion, 3% NaCl solution
Bonacci et al. (1998) [b]	Columns	150(average)	45(average)[a]	Internal stainless steel bar	2.5 day dry, 1 day immersion cycle in 3% NaCl solution. Concrete cast with 2% NaCl by weight of cement
Tamer A. El Maaddawy et al. (2003)	Columns		100-500	Internal stainless steel bar	1 week curing, 1 week air dry cycle .Concrete cast with 5% NaCl by weight of cement

[a] Not reported. Estimated using reported reinforcement sizes and dimensions.

[b] Phillips (1991) and Bonacci et al. (1998) used constant applied voltage of 6V and 6–12V, respectively, with variable applied current. Listed currents are averages for whole corrosion process.

[c] NaCl percentage not reported.

Table A2: Ionic concentration (mmol/L) measured in pore solution

Cement	Age (days)	Sample	[OH⁻]	[Na⁺]	[K⁺]	[Ca²⁺]	[Cl⁻]	[SO₄²⁻]
OPC	28	Paste	470	130	380	1	n. a.	n. a.
OPC	28	Mortar	391	90	288	<1	3	<0.3
OPC	28	Paste	834	271	629	1	n. a.	31
OPC	192	Mortar	251	38	241	<1	n. a.	8
OPC	--	Paste	288	85	228	n. a.	1	n. a.
OPC	84	Paste	589	n. a.	n. a.	n. a.	2	n. a.
OPC	84	Paste	479	n. a.	n. a.	n. a.	3	n. a.

Note: n. a. = concentration not available

Average crack width = 0.076 mm

Level of corrosion = 22.69 mg/cm^2

Average crack width = 0.151 mm

Level of corrosion = 34.73 mg/cm^2
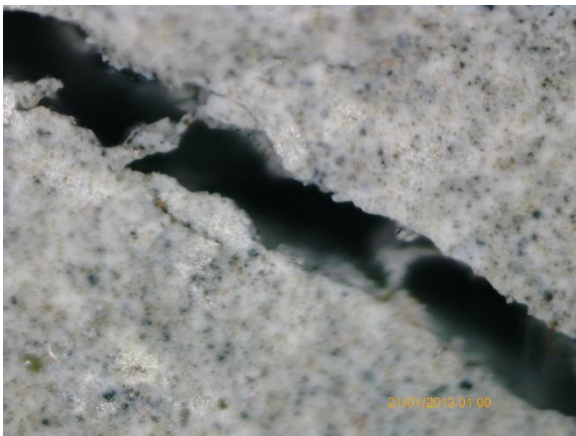
Average crack width = 0.202 mm

Level of corrosion = 44.7 mg/cm^2

Average crack width = 0.293 mm

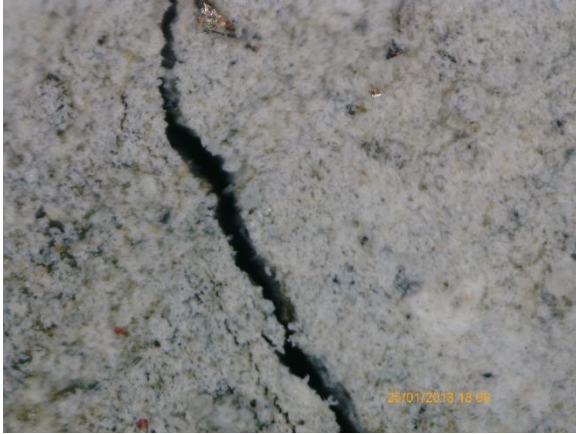Level of corrosion = 59.4 mg/cm^2

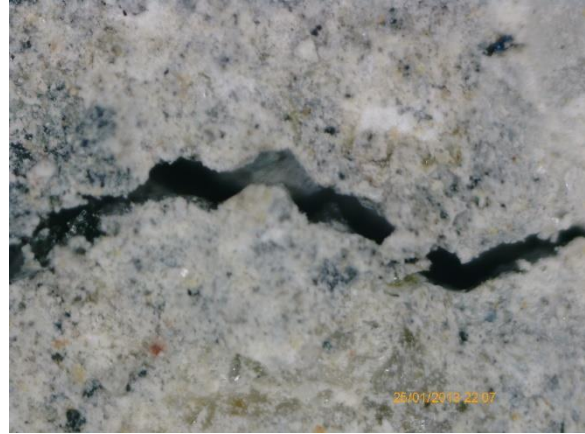Average crack width = 0.35 mm

Level of corrosion = 70.5 mg/cm^2

Average crack width = 0.503 mm

Level of corrosion = 99.8 mg/cm^2

Figure A1: Magnified View (Magnification Factor = 200-230) of Cracks Captured by Digital Microscope (C = 20 mm)

Average crack width = 0.102 mm

Level of corrosion = 21.2 mg/cm^2
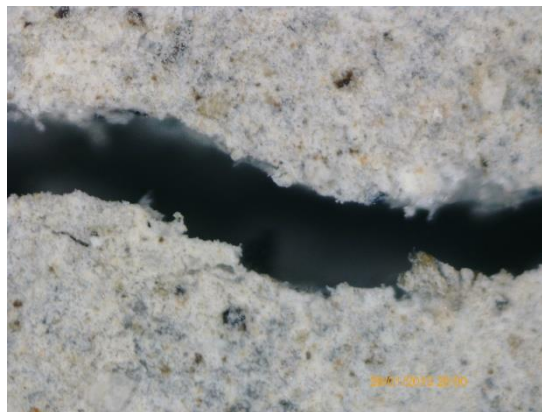
Average crack width = 0.121 mm

Level of corrosion = 26.3 mg/cm^2

Average crack width = 0.168 mm

Level of corrosion = 31.7 mg/cm^2

Average crack width = 0.216 mm
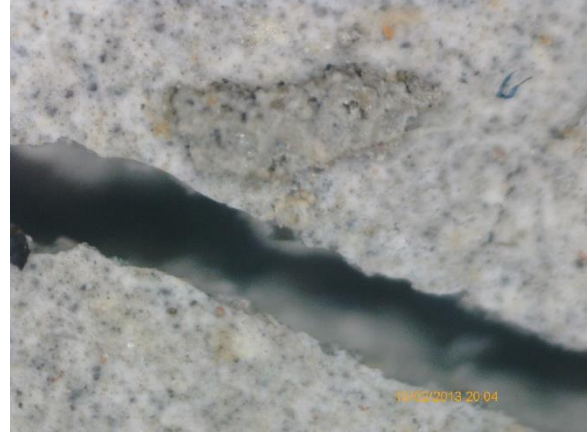
Level of corrosion = 35.4 mg/cm^2

Average crack width = 0.403 mm

Level of corrosion = 56.8 mg/cm^2

Figure A2: Magnified View (Magnification Factor = 200-230) of Cracks Captured by Digital Microscope (C = 37.5 mm)
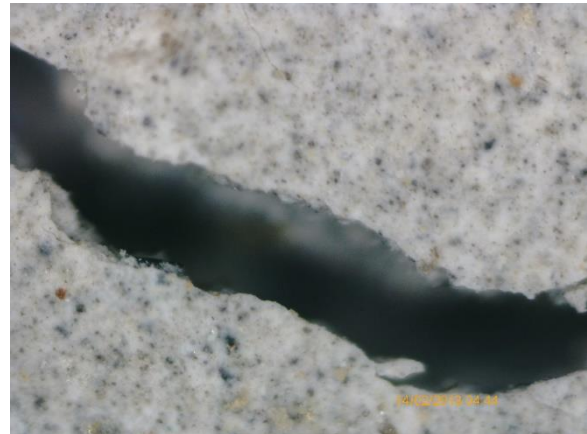
Average crack width = 0.092 mm

Level of corrosion = 132.6 mg/cm^2

Average crack width = 0.312 mm

Level of corrosion = 183.7 mg/cm^2

Average crack width = 0.355 mm

Level of corrosion = 188.5 mg/cm^2

Average crack width = 0.437 mm

Level of corrosion = 210.7 mg/cm^2

Average crack width = 0.619 mm

Level of corrosion = 261.9 mg/cm^2

Average crack width = 0.684 mm

Level of corrosion = 285.1 mg/cm^2

Figure A3: Magnified View (Magnification Factor = 200-230)of Cracks Captured by Digital Microscope (C = 50 mm)

Average crack width = 0.076 mm

Level of corrosion = 211.1 mg/cm^2

Average crack width = 0.363 mm

Level of corrosion = 246.1 mg/cm^2

Average crack width = 0.455 mm

Level of corrosion = 302.5 mg/cm^2

Average crack width = 0.598 mm

Level of corrosion = 349.7 mg/cm^2

Average crack width = 0.85 mm

Level of corrosion = 415.4 mg/cm^2

Figure A4: Magnified View (Magnification Factor = 200-230) of Cracks Captured by Digital Microscope (C = 75 mm)

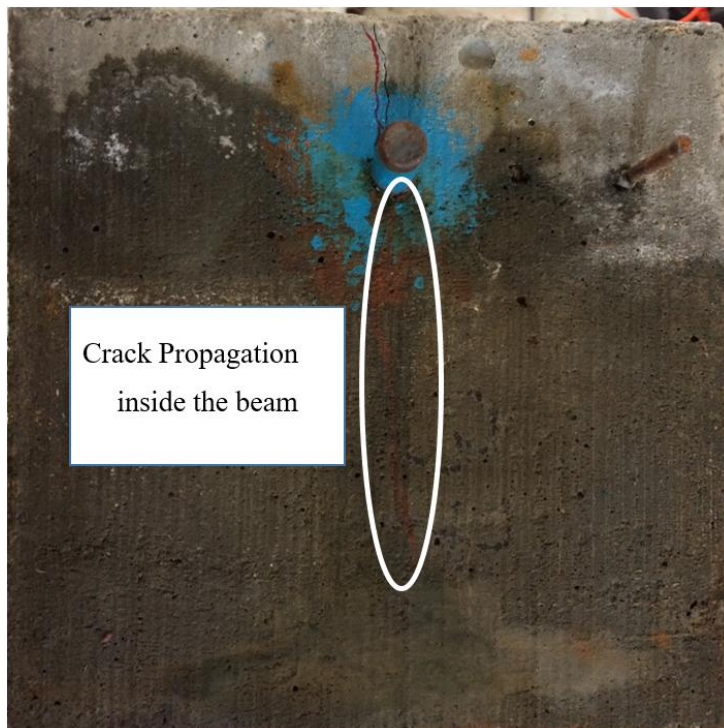Figure A5: Propagation of Cracks inside the Beam (C = 20 mm)

Figure A6: Propagation of Cracks inside the Beam (C = 37.5 mm)